Thèse présentée pour obtenir le grade de

DOCTEUR DE L'ECOLE POLYTECHNIQUE

Domaine : Mathémathiques Appliquées

Specialité: Neurosciences Théoriques

par

Geoffroy Hermann

Quelques équations de champ moyen en neuroscience

(Some mean field equations in neuroscience)

Directeur de Thèse: Olivier Faugeras

Codirecteur de Thèse: Jonathan Touboul

Thèse préparée à l'INRIA Sophia Antipolis, dans l'équipe NeuroMathComp

et soutenue à l'Ecole Polytechnique le 15 Décembre 2011 devant le jury composé de

M. Olivier Faugeras	*Directeur de Thèse*	INRIA Sophia/ENS Paris
M. Jonathan Touboul	*Co-directeur de Thèse*	INRIA Paris/Collège de France
M. Alain Destexhe	*Rapporteur*	UNIC (CNRS)
M. Eric Shea-Brown	*Rapporteur*	University of Washington
M. Carl Graham	*Examinateur*	Ecole Polytechnique
M. Khashayar Pakdaman	*Examinateur*	Université Paris VII
M. Jean Petitot	*Examinateur*	CREA/EHESS


INVENTEURS DU MONDE NUMÉRIQUE


ÉCOLE
POLYTECHNIQUE

Abstracts

French Abstract

La thèse porte sur l'étude des propriétés dynamiques de grands réseaux de neurones. Nous étudions des neurones à taux de décharge, dotés d'une dynamique intrinsèque linéaire, et prenons en compte différents types de bruit microscopique affectant le comportement des neurones individuels. L'approche "champ moyen" consiste à étudier la limite du système d'équations différentielles stochastiques décrivant le réseau, lorsque le nombre de neurones tend vers l'infini. Le bruit est soit additif, soit multiplicatif s'il affecte les poids synaptiques, et ceux-ci sont soit figés au début de l'évolution, soit dynamiques. Nous obtenons donc trois types d'équations qui sont étudiées dans cette thèse. Un résultat important est qu' à chaque fois la propriété de propagation du chaos est vérifiée. Nous analysons tout particulièrement l'influence du bruit sur la dynamique (en montrant par exemple le rôle de celui-ci dans la création de cycles) et discutons des implications en neurosciences.

English Abstract

This thesis deals with the study of the dynamical properties of large neuronal networks. We study neurons described by their firing rate with a linear intrinsic dynamics, and take into account several types of microscopic noise impacting the behavior of individual neurons. The "mean field" approach consists in studying the limit of the system of stochastic differential equations describing the network, when the number of neurons tends to infinity. The noise is either additive, or multiplicative if it affects the synaptic weights, and these ones are either fixed at the beginning, or dynamic. Therefore we obtain three types of equations that we study in this thesis. One of the main result is that in each case the propagation of chaos property holds. We analyze particularly the influence of the noise on the dynamics (we show for example its role in the creation of cycles) and we discuss the implications in neuroscience.

Acknowledgments and dedication

Je dédie ce travail à mon grand-père, Louis Capronnier, qui m'a appris, jeune, à dessiner un pentagone régulier à la règle et au compas.

Contents

Part I

Introduction

Chapter 0

Epistemological introduction

The work presented here pertains to the field of **mathematical neuroscience**. We may define neuroscience as the scientific study of the structure and functioning of the nervous system at all scales (from the molecular level up to the level of organs). As such neuroscience, initially almost identified with neurobiology, has become more and more interdisciplinary to include specific contributions from chemistry, physics, computer science and mathematics. We may make a slight distinction between mathematical neuroscience and computational neuroscience. Computational neuroscience focuses on the information processing properties of the nervous system, it emphasizes realistic descriptions of the neurons and often makes extensive use of computer simulations. On the contrary, for example in the work of Jean Petitot on **neurogeometry** [Petitot, 2008], mathematical structures play an essential role in unravelling the functioning of the brain; they are not used only as a tool. But whatever the ultimate epistemic value granted to mathematics it remains that building mathematical models seems necessary to discover functioning principles in the midst of an increasing amount of biological data. As René Thom [Thom, 2009] put it, science exists only insofar as scientists are able to build a virtual and controlled theoretical framework.

One of the early advocate of the use of mathematics to understand the brain was Michael Arbib in a book [Arbib, 1964] dating back to 1964. In his preface he explains the benefits of using the mathematicodeductive method in neuroscience. First, though the neurophysiological theories evolve and become more and more intricate, it is possible, starting from a grossly simplified view of the brain, to demonstrate that purely electrochemical mechanisms possess a wide range of interesting properties (pattern recognition in the case of the perceptron, reliability despite component malfunction in the Cowan-Winograd theory of reliable automata). As Arbib explains: "We may not *yet* have modeled *the* mechanisms that the brain employs, but we have at least modeled *possible* mechanisms." Second a comparison may be made with physics: in the modern era the physical sciences have developed thanks to the dialog between the mathematicodeductive method and the experimental method, and reciprocally mathematics (even pure mathematics) has vastly developed from the needs of physics. We may hope that a similar dialog between mathematics and biology will benefit both fields, and that *biological* mathematics, in its very infancy, will one day bear as many fruits as mathematical physics.

In this thesis, we will mainly **apply** mathematical results to derive properties of models based on neurophysiological data. The two basic theories that we will use are the bifurcation theory, to study qualitative changes in dynamical systems, and the theory of stochastic differential equations, to include

the effect of randomness. In the debate opposing realistic to abstract models (bottom-up vs top-down), we will be closer to realistic biological models, since we will take descriptions of biological neurons as our elementary building bricks, but we will make simplification assumptions to allow an analytical mathematical treatment. Our main object of analysis will indeed be models of neural networks, whose characteristics are derived from neurophysiology and whose dynamical properties are studied mathematically.

Cognitive science is an interdisciplinary field studying mind and its processes. Neuroscience is just a subfield of cognitive science along with, for example, artificial intelligence, linguistics or psychology. In its attempt to naturalize the mind, cognitive science has developed many approaches, based on two main conflicting paradigms[1]. For the first one, cognitivism, the cognition comes under information processing: it is the manipulation of symbols, based on rules. The second one, termed connectionism, defines cognition as the emergence of global states in a network of simple elements. Though the perspective of information processing has permeated most of neurobiology (so that the brain is often seen as an aggregate of cells receiving information, working it out and perceiving it in order to take decisions) without questioning the origins and presuppositions of such perspective, we may say that connectionism is the natural framework for the study of neural networks. This is particularly true in our case, since we will be interested in this thesis in the global behavior of neural populations emerging from the interactions of many individual neurons.

[1]For a detailed analysis of these paradigms and the proposal of a third one called *enaction* see the book [Varela et al., 1993] by Francisco Varela, Evan Thompson and Eleanor Rosch.

Chapter 1

Introduction to computational neuroscience

Overview

In this chapter we give a very brief introduction to some concepts used in theoretical neuroscience, focusing first on neurobiology, then on rate models and eventually on the concept of noise. The main reference books that we have used are the ones by Dayan and Abbot [Dayan and Abbott, 2001], Gerstner and Kistler [Gerstner and Kistler, 2002], Petitot [Petitot, 2008], and Ermentrout and Terman [Ermentrout and Terman, 2010].

Contents

1.1 Neurobiology

1.1.1 The neuron and the brain

The brain is the center of the nervous system for all vertebrates and most invertebrates and only primitive animals like jellyfish and starfish have no brain, their nervous system being decentralized. Since the pioneering work of the Spanish anatomist Ramón y Cajal (see one of his drawing in Figure 1.1) at the beginning of the twentieth century, the neuron is seen as the main functional unit of the nervous system. Note anyhow that glial cells that were thought for over a century to assume only supporting functions for neurons (keeping them in place, maintaining homeostasis and providing them energy) are now believed to affect neurotransmission though the exact mechanism is poorly understood [Gourine et al., 2010]. Most animals possess neurons and only sponges and a few other simpler animals have no neurons. As cells, neurons are very diverse and there may be exceptions to nearly every rule.

We will focus here on a schematic description of the structure and function of a "typical" neuron. Neurons are cells that generate characteristic electrical pulses, called action potentials or spikes, that propagate along nerve fibers. An anatomical description of a neuron is presented in the figure 1.2. As a cell the neuron has a nucleus located in the soma. Dendrites may be seen as constituting a very fine filamentary bush. The stereotypical impulse called spike propagates down along the axon through the movement of ions across the cell membrane. The axon splits at the end in a fine arborization. Each branch then almost makes contact with the dendrites of another neuron at a place called the synapse. The transmission of the signal in the synaptic cleft is either electrical in nature or chemical in nature. In the electrical case, a gap junction channel allows a ionic current flow initiated by the arrival of the spike. However chemical synapses are more widely represented and they involve neurotransmitters.

Depending on the type of the neurotransmitters in the synapse, each impulse may either facilitate or hinder the firing of the postsynaptic neuron. Indeed the arrival of a spike at a synapse triggers the release of neurotransmitters that will diffuse across the synaptic cleft, bind to receptors on the postsynaptic neuron and elicit either a depolarizing voltage pulse, increasing the probability of spikes in the postsynaptic neuron, or a hyperpolarizing voltage pulse decreasing this probability. In this schematic view the neuron is seen as an integrator of its inputs with a crucial distinction between excitatory and inhibitory neurons. Actually the Dale's Principle (as rephrased by Eccles in

1976) states that at all the axonal branches of a neuron, there is liberation of the same transmitter substance or substances. This allows the liberation of more than one type of neurotransmitter (co-release) but states that the same set is liberated at all synapses[1]. In the following we will make the assumption that a neuron is either excitatory or inhibitory.

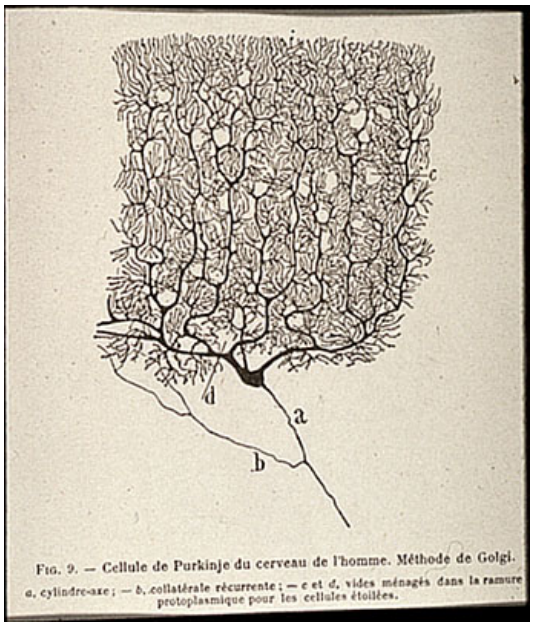

Figure 1.1: Anatomical drawing of a Purkinje cell by Ramón y Cajal. These cells found in the cerebellum are characterized by an intricate dendritic tree presenting many dendritic spines.

1.1.2 Action potentials and channel noise

Let us explain in more details the formation of action potentials. The relevant signal is the difference in electrical potential between the interior and the exterior of the neuron. At rest the potential inside is about -70 mV if we set by convention the extracellular environment at 0 mV. Ion channels, embedded in the membrane, control the flux of ions and therefore, thanks to this gradient, the difference in electrical potential between the inside and the outside. These channels are voltage-gated: some ion channels begin to open more and more when the value of the membrane potential increases in

[1]There are exceptions to this rule: for example dopamine neurons may also release glutamate as a neurotransmitter, but at separate release sites [Sulzer and Rayport, 2000]

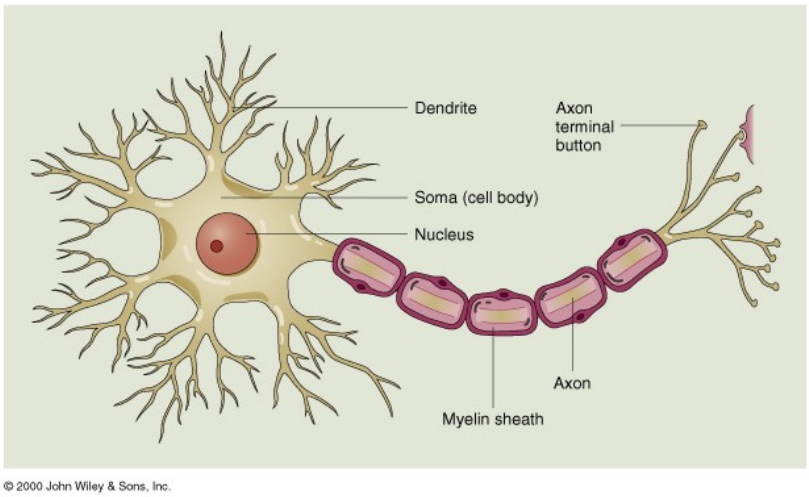

Figure 1.2: Anatomical drawing of a typical neuron. We see the respective arborization of the dendrites and of the axon.

response to a sufficiently large input current, which causes the membrane potential to increase: this is called depolarization. If this positive feedback is strong enough the neuron generates an action potential, i.e a positive impulse of about 100 mV lasting about 1 ms and able to propagate across long distances. Smaller fluctuations are in fact too much attenuated to propagate whereas action potentials are regenerated along axons. When the voltage is high enough competitive channels open so that the membrane potential begins to hyperpolarize until it goes back approximately to its rest value. Just after the emission of a spike it is impossible to initiate another one: this delay is called the absolute refractory period. There is also a longer time during which it is harder to initiate a new spike: this is the relative refractory period.

What will be of central interest for us is that ion channels are macromolecules whose conformational changes are subject to thermal noise. Hence one of the main intrinsic stochasticity in spike generation is due to the fluctuations of the membrane potential induced by the random opening and closing of ion channels. This source of noise is called **channel noise**. One of the goal of our thesis will be to understand the resulting dynamics in large scale population of neurons of this type of microscopic noise.

1.1.3 Cortical columns and the mesoscopic scale

The number of neurons in the brain varies of course dramatically from species to species. A recent study [Azevedol et al., 2009] in comparative neurology asserts that the human brain contains approximately 86 billion neurons, with 17 billion in the cerebral cortex and 69 billion in the cerebellum. As each neuron may be synaptically connected up to 10000 other neurons, the human brain forms a very complex system. The biophysical understanding of individual neurons and synapses has made considerable progress, but it is way harder to understand the global picture emerging from so many interactions. **Mean field approaches** in neuroscience are precisely an attempt at deciphering this problem.

The models introduced in this thesis depict idealized and simplified neuronal networks that can encompass a large biological diversity. However some features that will be mentioned in the models, like the **columnar organization**, are more specific to the mammalian cerebral cortex. The cerebral cortex is also called gray matter, it is a tissue at the surface of the mammalian brain, its thickness being approximately of 4 mm in humans. The axons connecting various regions of the cerebral cortex form the best part of the white matter located below. In large mammals the gray matter is folded. The neocortex is, from the phylogenetic viewpoint, the most recent part of the cerebral cortex. The neocortex posses a laminar structure: it is organized in six different horizontal layers. Moreover anatomical data reveal that neurons in various layers connect vertically to form small microcircuits, called columns. These cortical columns may have specific functions.

One of the best example of this columnar functional organization is exemplified in the work of Hubel and Wiesel (see for example the article [Hubel and Wiesel, 1962]), for which they were granted the Nobel Prize in 1981, and where they showed that the coding of a particular orientation of an element in a visual scene is related to the activity of specific populations in the primary visual cortex. More precisely they showed that certain neurons, called simple cells, located in the area V1 of the visual cortex (of a cat) were sensitive to two characteristics: the retinian position and the orientation at this position. Moreover when an electrode was put perpendicularly to the surface of the cortex to record the activity of the column, they found that the preferred location and orientation remained more or less constant (with only the spatial phase varying). A cortical column, perpendicular to the surface of the cortex, gathers neurons that have nearly identical receptive fields. This is a functional definition. We may make a distinction between minicolumns encoding only one feature, whereas hypercolumns gather horizontally several

minicolumns. For instance in the original model of Hubel and Wiesel, a minicolumn encodes a position and an orientation whereas an hypercolumn is made of several minicolumns encoding the same position but with the whole range of orientations[2].

The order of magnitude of the number of neurons in an hypercolumn is approximately 10000. The mean field methods presented in this thesis, though they will not be applied to detailed biophysical models of columns, constitute the right framework to understand the dynamics resulting from the interplay of so many neurons at a mesoscopic scale.

1.1.4 The neural code

Once these basic groundings have been mentioned, a very significant question must be asked: what is the neural code? Since there is a consensus in the neuroscience community saying that information is carried by the spikes, we must understand how the information is represented and coded into spikes (if you look at an African mask, a precise spike pattern in the brain's neurons is assumed to represent it). There are many conflicting views on this topic.

One of the most common assumption is that the neural code is a **population rate code**. Indeed in most experiments where a stimulus is presented to an animal it is usually possible to find a group of neurons whose firing rate (defined as the number of spikes in a certain time window) will increase compared to the background activity. This view can be challenged in two ways.

First it may be possible that only a single neuron is sensitive to a particular complex object or concept. We speak in this case of a "grandmother cell" to mean that a single cell "represents" your grandmother. Highly specific neurons have been found in the inferior temporal cortex of the monkey for example.

Second, if the precise spike pattern must be taken into account, i.e if precise spike timing or high-frequency firing-rate fluctuations carry information, we speak of a temporal code (rather than rate code). In some experiments, the temporal resolution of the neural code (determined by the precision necessary in the measurement of spike times to extract the information) has been found to be high, so there must be some sort of temporal coding.

[2] actually, angles varying from 0 to π

Furthermore we must take into account the possibility of **correlations**. At the single neuron level, if all the information is coded in the time-dependent firing rate $r(t)$, the code is called an independent-spike code [Dayan and Abbott, 2001]. But it may be that correlations between spike times carry also information (though recent experiments show that this correlation-encoded information is only of the order of 10 percent). One of the simplest example of a correlation code is to have some information coded in the interspike interval. In the independent-spike hypothesis, all the temporal characteristics of the neural code are given by the evolution of $r(t)$, so that if it does not evolve too rapidly, the code is typically a rate code, and otherwise it is a temporal code.

Eventually correlations may also exist between different neurons within a population. Our contribution to this topic will be addressed in section 8.2.1.

1.2 Firing-Rate models

In order to allow an analytical treatment of the mean field equations that we will derive in part II, we will restrict ourselves to neurons described by firing-rate models and assume therefore implicitly a rate code.

In computational neuroscience, there are models describing the dynamics of individual neurons in terms of the action potentials generation. By contrast to firing-rate models they are called spiking neuron models. One of the most famous and elaborate spiking neuron models is given by the Hodgkin and Huxley equations (for which they were granted the Nobel Prize in 1963). It is a set of nonlinear coupled ordinary differential equations. The main variable of interest is the value of the membrane potential V, which is coupled to three other variables (n, m, and h) describing the activation of the different ionic currents involved in spike generation. These equations are precise but hard to study, so different reductions to models involving only two state variables (the membrane potential V and an adaptation variable w) have been proposed. The celebrated Fitzhugh-Nagumo model is an example of such a reduction. Other types of models are integrate-and-fire neurons where the membrane potential is described by a (stochastic) differential equation and spikes are emitted when this potential reaches a threshold (the potential is then reset).

Rate models are often considered valid at the macroscopic level as describing population activity, and as such might not be good models of single cells. However, defining the instantaneous firing rate as a trial aver-

age [Gerstner and Kistler, 2002, Dayan and Abbott, 2001] can be more relevant from this viewpoint. The approximation will be all the more accurate that the synapses are relatively slow and that the synaptic inputs are mostly uncorrelated so that we can effectively replace the input spike trains by instantaneous firing rates.

We can now give the very simple equation giving the *evolution of the membrane potential* V^i of a neuron i coupled to other neurons through the synaptic weights J_{ij}. Neurons interact through their firing rates, classically modeled as a **sigmoidal transform** of their membrane potential. These sigmoidal functions are assumed to be smooth (Lipchitz continuous), increasing functions that tend to 0 at $-\infty$ and to 1 at ∞. The firing rate of the presynaptic neuron j, modulated by the synaptic efficiency J_{ij}, is an input to the postsynaptic neuron i. The firing rate exponentially relaxes to zero with a time constant τ when it receives no input, and otherwise the neuron integrates both external input $I(t)$ and the current generated by its neighbors. Therefore the evolution of $V^i(t)$ is given by:

$$\frac{dV^i(t)}{dt} = -\frac{V^i(t)}{\tau} + \sum_{j=1}^{N} J_{ij} S(V^j(t)) + I(t) \tag{1.1}$$

1.3 What is noise?

We must now explain what are the possible sources of noise at the neuronal level in order to include it in our equations. Careful definitions must be given. The three main recent reviews that we will use are the ones by Yarom [Yarom and Hounsgaard, 2011], Ermentrout [Ermentrout et al., 2008] and Faisal [Faisal et al., 2008].

1.3.1 Definition

The question of the nature and meaning of randomness in the natural sciences pertains to epistemology. For example, Claude Bernard, considered as the founder of experimental medicine wrote in 1865 in his most famous book [Bernard, 1966]: "Il y a un déterminisme absolu dans tout phénomène vital; dès lors il y a une science biologique" [3]. In physics, the reluctance of Einstein to accept the probabilistic nature of quantum mechanics is also well-known. However noise, or randomness, is nowadays mentioned in numerous

[3] "There is an absolute determinism in every vital phenomenon, hence there is a biological science"

neuroscience papers. Quantum noise is even considered by researchers like Penrose [Penrose, 1989] as a possible explanation of consciousness [4].

Indeed fluctuations are present at all scales in neurobiology. Cortical neurons fire very irregularly in vivo, as measured by a coefficient of variation C_v very close to 1, nearly consistent with a completely random process [Softy and Koch, 1993]. Neurons *in vivo* in awake animals and anesthetized animals [Destexhe and Paré, 1999] are spontaneously active and emit spikes at rates of about 10 Hz in an approximately Poissonian way. Similarly a high trial-to-trial variability is observed in the spike trains of cortical neurons when they are submitted to identical stimuli. If some characteristics of spike trains are not reliable (e.g. the spike times) this poses constraints on the neural code. For example information may not be encoded in the exact spike times, but in the probability distribution of spike trains. Let us now define what we mean by noise.

The concept of noise is closely related to the one of a signal. Noise is **a random perturbation (fluctuation) to a meaningful signal**. However this definition raises some questions. First it is not easy to properly isolate the signal from the noise in neural processing. Second these random fluctuations are not necessarily detrimental and we will see in the following many examples where this noise term may be useful at the functional level. Eventually it must be noted that in a system as complex as the brain, high irregularity is not necessary the mark of a random process, though many studies have found that spike trains can be described quite accurately by random Poisson processes. This irregularity may be the sign of deterministic chaos ([Faure et al., 2000]), so that if every law was known up to the molecular level, we could describe the spike dynamics in purely deterministic terms [5]. This distinction depends also on the scale of the measurement: for exam-

[4] This trend of research is called quantum mind hypothesis. In his first book on consciousness [Penrose, 1989], published in 1989, Penrose asserted, thanks to a controversial interpretation of Godel's incompleteness theorem, that the brain can perform functions that no computers can perform and called these types of processing non-computable. He then argued that random quantum wave collapse may be the support of this non-computability, without exhibiting any plausible biological counterparts. Later, in collaboration with Stuart Hameroff, they proposed that microtubules be the seat of quantum processing. This theory is now outdated as it was shown that the coherent quantum condensates envisaged cannot exist at the usual temperature of biological tissue. Though most physicists think that quantum systems would decohere too quickly in the brain and therefore that quantum states cannot be invoked in cognitive science, new quantum mind theories have emerged.

[5] For the French mathematician Emile Borel: "Le hasard, ce sont les lois que nous ne connaissons pas."

ple macroscopic variables such as EEG or local field potentials display more coherent behavior and seem to be described accurately by low or high dimensional chaos (respectively in the case of epileptic and awake cortex), whereas the microscopic neuronal dynamics is better described by stochastic random processes [El-Boustani and Destexhe, 2009a]. We now turn to the list of the different possible sources of noise in the central nervous system.

1.3.2 Sources of noise

A classification of the different types of noise in the nervous system can be found for example in [Faisal et al., 2008]. First there is the **sensory noise**, taking into account the fact that external sensory stimuli are intrinsically noisy and also the fluctuations at the level of the transducers. There is also the **cellular noise** integrating, at both the biophysical and biochemical level, all the seemingly random processes inside the cellular machinery. Noise is all the more important that characteristic length scales are small, so that there is a high fluctuation in the number of molecules involved in these processes.

There is also **electrical noise** whose dominant form is **channel noise**, that we have already introduced in section 1.1.2. Channel noise (i.e. the electrical current produced by the random opening of voltage-gated ion channels) and its impact on the dynamics of the membrane potential has mathematically been studied in Gilles Wainrib's PhD thesis [Wainrib, 2010], in the framework of piecewise deterministic Markov processes. Other forms of electrical noise like Johnson noise and shot noise are two or three orders of magnitude smaller than channel noise.

A recent study [Goldwyn and Shea-Brown, 2011] deals with the best way to incorporate channel noise in the usual deterministic Hodgkin-Huxley (HH) equations. The authors consider various possibilities: an additive white noise in the input (current noise) , subunit noise (affecting the dynamics of the gating variables n, m, and h) and conductance noise (affecting the total conductances for Na+ and K+ currents) and conclude that the addition of fluctuations in conductance terms is the best solution. Conductance noise is multiplicative since the conductances are multiplied by the voltage in the HH equations. In this thesis we will incorporate noise in firing-rate models, hence we do not consider subunits, since we have only one state variable, the potential V. In chapter 4, we will use an **additive** white noise, but in chapter 6, we will also introduce a **multiplicative** noise, by considering fluctuating synapses.

Eventually one type of noise we will be very interested in this thesis (see in particular chapter 6) is **synaptic noise**: e.g. when a presynaptic cell in vitro is driven repeatedly with identical stimuli, there is variability across trials in the postsynaptic potentials. This synaptic variability has many causes: the spontaneous miniature postsynaptic currents [Fatt and Katz, 1952], the fact that the number of vesicles and neurotransmitters involved is finite and quite low, hence subject to fluctuations from trial to trial, the randomness of the diffusion in the synaptic cleft and the probabilistic nature of the molecules' release. Hence noise accumulates and all the biological phenomena described above seem to explain the trial-to-trial variability. In this context, approximating noise by some additive random processes, such as Poisson or Gaussian processes is the simplest mathematical approach and the best assumption when data is lacking.

Furthermore all the types of noise mentioned above were mainly dealing with one isolated neuron. We must also take into account the fact that a neuron embedded in a neural network receives inputs from approximately 10000 afferents neurons. Therefore each neuron is submitted to an intense *synaptic bombardment*. This background synaptic activity is often modeled in computational studies by a noise term as it seems the best assumption to capture the complexity originating from so many inputs. Nevertheless we must never forget that intricate dynamics can also be the signature of deterministic chaos and the fact of modeling our "ignorance" by noise is an hypothesis that must be made clear.

1.3.3 Role of noise in the brain

The question of the role of the noise in the brain is heavily debated. The first question that we may ask is indeed: "How a reliable behavior is possible if the brain is so noisy?". Yet, recently, several studies ([Ermentrout et al., 2008], [Faisal et al., 2008], [Yarom and Hounsgaard, 2011]) have given interesting insights into this topic. They all stress that the noise has not only purely disruptive effects and may on the contrary play a **positive functional role**. In a recent paper [Deco et al., 2009], Gustavo Deco even proposes "stochastic dynamics as a principle of brain function", highlighting the functional benefits of noise. We list below several of them.

Computational studies [Lindner et al., 2004] have underlined for example the concept of **stochastic resonance**. Stochastic resonance corresponds to the fact that there exists a particular level of noise maximizing the regularity

of an oscillatory output related to periodic forcing. This is a universal phenomenon with many applications and benefits [Wiesenfeld and Moss, 1995]. In neuroscience it contributes to a better signal detectability, when noise is added to a subthreshold signal.

Computational studies have also exhibited the phenomenon of **coherence resonance** [Pakdaman et al., 2001]. In this case adding noise increases the regularity of an output (in the absence of a periodic forcing). Theoretical models predict therefore that noise can lead to more patterned firing, but coherence resonance has not yet been observed in real neurons [Ermentrout et al., 2008].

As we have already seen, noise may have a lot of counterintuitive effects. Noise can increase the regularity of a signal. But it can also increase its reliability. This is shown in the Figure 1.3 published in a paper by Mainen and Sejnowski [Mainen and Sejnowski, 1995]. If a cortical neuron is submitted repeatedly to a constant input, the first spike will occur more or less at a fixed time, but there will be high variability in the timing of subsequent spikes. Quite surprisingly, if we add to the stimulus a Gaussian white noise, the response of the cell is way **more reliable**.

Many theoretical models have also studied, using the Phase Response Curve (PRC), how oscillators driven by noise may **synchronize**. Correlated noise can induce synchronization even when neurons are not directly connected [Galán et al., 2006]. Moreover two uncoupled nonlinear oscillators can synchronize if driven by identical weak noise [Rosenblum et al., 1996]. And it turns out that these synchronization phenomena are really significant from a biological viewpoint. Indeed macroscopic measurements like Local Field Potentials and EEG display high-amplitude oscillatory patterns, a sign of oscillatory synchronization of many neurons at the microscopic level. Oscillatory synchronization is also observed in pathological cases, like during epileptic seizures. Besides, though controversial, it has been proposed that oscillatory synchronization encodes information about stimuli and even plays a crucial role in awareness. This hypothesis, called temporal binding, suggests that "neural synchrony with a precision in the millisecond range is crucial for conscious processing, and may be involved in arousal, perceptual integration, attentional selection and working memory" [Engel et al., 1999].

On a more global scale, some of the arguments proposed in favor of a positive functional role of noise are the following. Yarom [Yarom and Hounsgaard, 2011] points that variation may reflect

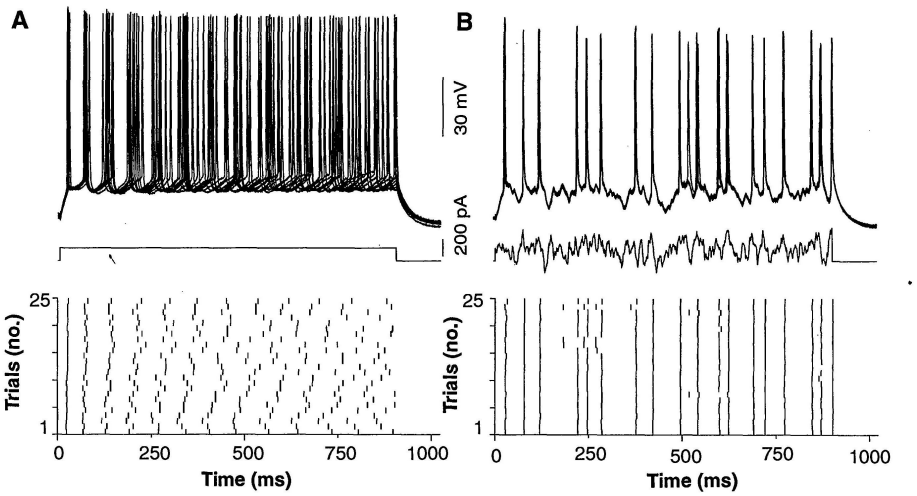

Fig. 1. Reliability of firing patterns of cortical neurons evoked by constant and fluctuating current. (**A**) this example, a superthreshold dc current pulse (150 pA, 900 ms; middle) evoked trains of actic potentials (approximately 14 Hz) in a regular-firing layer-5 neuron. Responses are shown superimpose (first 10 trials, top) and as a raster plot of spike times over spike times (25 consecutive trials, bottom). (**I** The same cell as in (A) was again stimulated repeatedly, but this time with a fluctuating stimulus [Gaussia white noise, μ_s = 150 pA, σ_s = 100 pA, τ_s = 3 ms; see (*14*)].

Figure 1.3: Reliability of spike trains when a Gaussian white noise is added to the constant stimulus. Reproduced from Mainen and Sejnowski [Mainen and Sejnowski, 1995]

"alternative versions of goal-directed responses in the execution of accurate performance albeit in different ways with each repetition." Hence noise may provide adaptability through a more comprehensive exploration of alternate behaviors. A probabilistic behavior has also advantages in decision-making [Deco et al., 2009] by preventing deadlocks. Besides, neuronal networks that have developed in the presence of noise will be more robust and explore more states, which is an advantage for learning in a perpetually changing environment [Krogh and Hertz, 1992].

The analysis of *the influence of the noise parameter in the mean-field equations* developed in the second part of this thesis will shed some light on the question of the functional role of noise.

Chapter 2

Goal and Organization of the thesis

Overview

In this chapter we explain why mean field equations are of central importance in neuroscience. First they correspond to the level of investigation of most **imaging techniques**. Second they are also suited to the **columnar organization** of the cortex, which plays a tremendous functional role. As they are limit equations describing the behavior of an arbitrarly large number of neurons, we recall also elementary **convergence theorems** (the law of large numbers and the central limit theorem) that allow us to grasp the meaning of some equations that will be introduced later in this thesis (chapters 4 and 5). However these theorems are based on independence hypotheses that are obviously not checked due the neurons' interactions. We present nevertheless the concept of **"propagation of chaos"**, a form of asymptotic independence. The main focus of this thesis will be to understand the qualitative influence of various sorts of noise in mesoscopic neural dynamics given by mean field equations. A link can therefore be made with the theory of **stochastic bifurcations** (see Appendix D).

Contents

2.1 Motivation and goal

The motivation of this thesis is the modeling of neural activity at scales integrating the effect of thousands of neurons, i.e **at a mesoscopic scale**. The mean field approach allows us to extract the *effective process* in play emerging from the interaction of a very large number of neurons. This is of central importance in neuroscience for several reasons.

First, we must note that most non-invasive imaging techniques (EEG, MEG, fMRI, optical imaging) provide different spatial and temporal resolutions (with a characteristic trade-off between these two resolutions for each type of measure) but are not able to measure individual neuron activity, i.e activity at a microscopic scale. Instead they are measuring **mesoscopic** effects resulting from the interplay of several hundreds to several hundreds of thousands of neurons.

Second, the **columnar organization** of the cortex is of tremendous importance to understand the functions it performs. We have already mentioned columns and hypercolumns in section 1.1.3. A drawing of columns, represented as cylindric units perpendicular to the surface of the cortex, is shown in Figure 2.1. These columns can be subdivided in layers. Within a column neurons can also be gathered according to neuroanatomy (e.g. pyramidal neurons, interneurons). Hence we view the column as a collection of homogeneous populations. Within each population, the neurons share the same statistical parameters and the same inputs. The mean field approach we propose can consequently be considered as a theoretical attempt to model a cortical column, keeping in mind two hypotheses: the column is made of interacting populations, and the total number of neurons in a column (and also in each population) is very large. Alternatively, our models can be seen as hypercolumn models, where the activity of a whole cortical column is modeled by the classical Wilson and Cowan equations (see section 3.1).

Another advantage of our mean field modeling is that, once we will have established the mean field equations, we will be able to **quantify the effect of the noise**. Indeed starting from microscopic descriptions that integrate the various types of noise listed above, we will obtain equations where the amount of microscopic noise, for example synaptic noise, appears as a *parameter*.

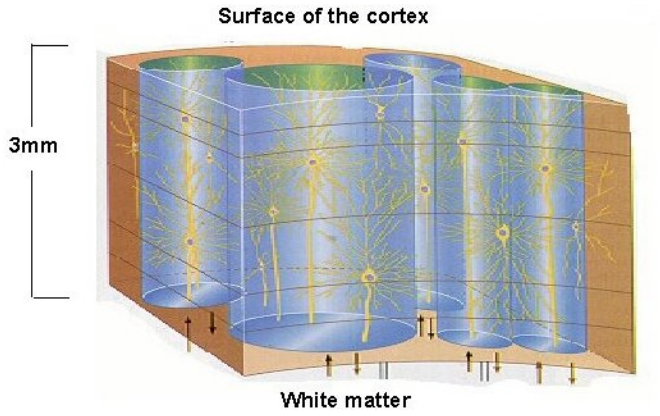

Figure 2.1: Representation of five cortical columns in the cortex. Note the subdivision in 6 layers.

2.2 Elementary mathematical overview

We give here a **very informal** glimpse into the mathematical facts underpinning our approach, in the case of one population of interacting neurons. Rigorous proofs and formalization will be given in part II.

If we add into the equation 1.1 an additive white noise of intensity $\lambda(t)$, the mean field approach boils down to finding the limit, when the number of neurons, N, tends to infinity, of a set of interacting diffusion processes described by the following equations, for $i = 1...N$

$$dV^i(t) = \left(-\frac{1}{\tau} V^i(t) + I(t) + \sum_{j=1}^{N} J_{ij} S(V^j(t)) \right) dt + \lambda(t) dB_t^i \tag{2.1}$$

Informally, the main question is therefore to find the limit of the sum $\sum_{j=1}^{N} J_{ij} S(V^j(t))$ when $N \to \infty$. We see first that in order to remain finite (but nonzero), the mean of each J_{ij} must scale as $\frac{1}{N}$.

2.2.1 The Law of Large Numbers

In the first case, treated in details in chapter 4, there is no variability in the synaptic weights and each one is set to a fixed value $\bar{J}$, characteristic of the population, scaled by N.

If we make the **assumption** that the V^j are independent (and identically distributed within the same single population), then, according to the Law of

Large Numbers (LLN):

$$\bar{J}\sum_{j=1}^{N}\frac{1}{N}S(V^j(t))$$

converges towards:

$$\bar{J}\mathbb{E}[S(\bar{V}(t))]$$

And we would get the mean field equation, giving the evolution of a characteristic neuron $\bar{V}$ by replacing the sum by the expectation in equation 2.1. However since all the neurons are interacting we **cannot** assume a priori the independence of the V^j.

2.2.2 The Central Limit Theorem

A way more complex case, treated in details in chapter 5, consists in modeling each J_{ij} by a random variable. Each J_{ij} is the realization of a Gaussian random variable of mean $\frac{\bar{J}}{N}$ and of standard deviation $\frac{\sigma}{\sqrt{N}}$[1]. This model accounts for the **inhomogeneity** of the weights and the equations are more difficult to establish since, contrary to the preceding case, we have lost the **exchangeability** property.

However the equation can be guessed if we make once more an **independence assumption**: if we suppose that the V^j are pairwise independent, identically distributed within the same population, and that the V_j are also independent of the weights J_{ij}, we can apply the Central Limit Theorem (CLT) to show that

$$\sum_{j=1}^{N}J_{ij}S(V_j(t))$$

converges towards a Gaussian Process of mean $\bar{J}\mathbb{E}[S(\bar{V}(t))]$ and covariance $\sigma^2\mathbb{E}[S(\bar{V}(t))S(\bar{V}(s))]$.

Proof. Indeed let's denote by X^j the random variable $X^j = J_{ij}S(V^j)$. For convenience we do not consider here the dependence on time. According to the central limit theorem and to our independence assumption:

$$\sqrt{N}\frac{1/N\sum_{j=1}^{N}X^j - \mathbb{E}[X^j]}{\sqrt{Var[X^j]}}$$

converges in law to the Gaussian $\mathcal{N}(0,1)$.

[1]Note in the following proof that this scaling of the variance is necessary to get a nonzero and finite limit when $N \to +\infty$.

It remains to evaluate $\mathbb{E}[X^j]$ and $Var[X^j]$, keeping in mind our independence assumption.

$$\mathbb{E}[X^j] = \mathbb{E}[J_{ij}]\mathbb{E}[S(V^j)] = \frac{\bar{J}}{N}\mathbb{E}[S(\bar{V})]$$

Similarly:

$$\begin{aligned} Var[X^j] = \mathbb{E}[J_{ij}^2 S(V^j)^2] - (\mathbb{E}[J_{ij}S(V^j)])^2 &= \mathbb{E}[J_{ij}^2]\mathbb{E}[S(\bar{V})^2] - \frac{\bar{J}^2}{N^2}(\mathbb{E}[S(\bar{V})])^2 \\ &= (Var[J_{ij}] + (\mathbb{E}[J_{ij}])^2)\mathbb{E}[S(\bar{V})^2] - \frac{\bar{J}^2}{N^2}(\mathbb{E}[S(\bar{V})])^2 \\ &= \frac{\sigma^2}{N}\mathbb{E}[S(\bar{V})^2] + \frac{\bar{J}^2}{N^2}Var[S(\bar{V})] \end{aligned}$$

Putting all things together we obtain that:

$$\frac{\sum_{j=1}^N X^j - \bar{J}\mathbb{E}[S(\bar{V})]}{\sqrt{\sigma^2\mathbb{E}[S(\bar{V})^2] + \frac{\bar{J}}{N}Var[S(\bar{V})]}}$$

converges in law to the Gaussian $\mathcal{N}(0,1)$. Hence:

$$\sum_{j=1}^N X^j = \sum_{j=1}^N J_{ij}S(V^j) \to \mathcal{N}(\bar{J}\mathbb{E}[S(\bar{V})], \sigma^2\mathbb{E}[S(\bar{V})^2])$$

when $N \to +\infty$. □

And we would get the mean field equation, giving the evolution of a characteristic neuron $\bar{V}$ by replacing the sum by the Gaussian Process (completely characterized by its mean and covariance) in equation 2.1. However, since all the neurons are interacting through their synaptic weights, we **cannot** assume a priori this independence.

2.2.3 Propagation of chaos

We have proposed above two **heuristic** derivations of mean field equations based on different assumptions on the synaptic weights. These derivations are simply based on the LLN and the CLT. However both make a crucial use of an a priori independence hypothesis. In reference to the work of Boltzmann in statistical physics these assumptions can be called "*molecular chaos*". The term *chaos* is here understood in the statistical physics sense: Boltzmann's molecular chaos ("Stoßzahlansatz") corresponds to the independence between the velocities of two different particles before they collide. This is very different from the notion of chaos in deterministic dynamical systems.

We will show in the remaining of the thesis that, for all the models considered, **the propagation of chaos property applies**. This property states that, provided the initial conditions are independent and identically distributed for all neurons[2], then in the limit $N \to \infty$, all neurons, chosen among a finite subset, will behave independently, and have the same law which is given by an implicit equation (mean field equation) on the law of the limiting process (the chaos of the initial condition is *propagated* for all time $t > 0$). In details, the law of $(V^{i_1}(t), \dots, V^{i_k}(t), t \leq T)$ for any fixed $k \geq 1$ and $(i_1, \dots, i_k)$, converges towards $\nu \otimes \dots \otimes \nu$ when $N \to \infty$, where ν denotes the law of the solution of the mean field equation.

However showing the propagation of chaos property is not enough to derive the equations. Indeed the propagation of chaos is only valid for a finite number of neurons[3], and is only true asymptotically. It is hence not rigorous to assume a priori the molecular chaos hypothesis, though it allows us to guess the right equations.

2.3 Organization of the thesis

In chapter 3, we will **review** various mean field approaches used in computational neuroscience. The point is that the term mean field is used in many different contexts and we need to clarify the assumptions between rival mean field models. One of the most important criterion is the exchangeability property of the sequence of the random variables $V^j, j = 1...N$. We will also describe models aiming at going "beyond mean field", i.e. computing the fluctuations associated with *finite-size corrections*.

In the three remaining chapters, that constitute the core of our contribution, we will mainly be interested in the influence of noise levels on neural mean field dynamics. The difference between these three chapters lies mainly **in the modeling of the noise**.

In chapter 4, the microscopic dynamics is described by equations similar to 2.1, except that we consider multiple populations interacting. The noise source is modeled by an **additive** white noise. In this case, we derive rigorously the mean field equations associated and show the propagation of chaos. We study extensively the impact of the noise on the dynamics, especially its role in generating oscillations.

[2]Such initial conditions are said to be "chaotic".

[3]or at best for $k = o(\sqrt{N})$ neurons

In chapter 5, we add an **uncertainty on the synaptic weights** that are modeled by random variables (frozen at the beginning of the evolution). The resulting equation is more complex since, contrary to the preceding case, it is not Markovian. An analytical treatment of the influence of the noise parameter (i.e. the variance of the synaptic weights) is therefore difficult, but we exhibit interesting simulations of these equations.

In chapter 6, we consider a different type of **synaptic noise** affecting the weights. This time the weights are modeled by stochastic processes. Here again we derive the resulting mean field equation, which is Markovian, and study the influence of the noise on the dynamics.

In the Conclusion III, we summarize the different results and dwell on the different dynamical behaviors generated by different types of noise. We propose ideas to extend these models so that they are more biologically plausible: this gives rise to more intricate mathematical equations, a priori preventing the kind of qualitative understanding of the influence of the noise parameter we have achieved in this thesis. Eventually we discuss the implications of our mathematical findings at the biological level, stressing the possible **functional role of noise**. In Appendix (IV), we give some technical results and present detailed bifurcation diagrams related to the text, before presenting also an elementary approach to **stochastic bifurcations** in D.

Chapter 3

Review of the literature on mean field equations in neuroscience

Overview

The brain is composed of a very large number of neurons interacting in a complex nonlinear fashion and subject to noise. Arising from this interaction, emergent coherent responses are provided to stimuli, presenting an important reliability. The problem of understanding the emergence of reliable and complex behaviors from such interacting neurons has been a longstanding problem in neuroscience. Generally, we will denote by **mean field equations** the ones obtained when the number of neurons in a network becomes **arbitrarly large**. We will distinguish between three different approaches that can be found in the computational neuroscience community, and that are mainly based on the statistical physics literature. First an approach describing **sparsely connected networks** of excitatory and inhibitory spiking neurons and relying on a *diffusion approximation*, which allows to describe the network by a *Fokker-Planck equation*. Second, an approach coming from the study of **spin-glasses** which gives a *non-Markovian* description of the network. Eventually we will present an approach based on a **master equation**, and designed to understand the corrections to mean field in a *finite size* network.

Contents

3.1 What is the mean field approach?

Mean field methods may be related to the century-old works of Boltzmann about the kinematic gas theory in statistical physics. We give here a definition of mean field covering most approaches in neuroscience: mean field analysis deals with the description of **the activity of large populations of neurons** (the number of neurons can be arbitrarily large).

Indeed, most models describing the emergent behavior arising from the interaction of neurons in large-scale networks have relied on continuum limits since the seminal works of Wilson and Cowan and Amari [Amari, 1972, Amari, 1977, Wilson and Cowan, 1972, Wilson and Cowan, 1973].

The Wilson-Cowan equations are coupled nonlinear differential equations describing the dynamics of populations of excitatory and inhibitory neurons. In their original form, these equations are [1]:

$$\tau_e \frac{dE}{dt} = -E + S_e(c_1 E - c_2 I + P)$$
$$\tau_i \frac{dI}{dt} = -I + S_i(c_3 E - c_4 I + Q)$$

In theses equations, the $c_j, j = 1, 2, 3, 4$ are (positive) connectivity coefficients, representing the average number of excitatory or inhibitory synapses per excitatory or inhibitory cell. The S_j, $j = i, e$ are non linear sigmoidal response functions. P and Q represent exterior inputs and τ_j, $j = i, e$ are time constants. Eventually, $E(t)$ and $I(t)$ are the proportion of excitatory (respectively inhibitory) cells firing per unit time at the instant t. Such models represent the activity of the network through a *global variable*, like the population-averaged firing rate, which is generally assumed to be **deterministic**. Many analytical properties and numerical results have been derived from this type of equations and related to cortical phenomena, for instance in the case of the problem of spatio-temporal pattern formation in spatially extended models (see e.g. [Coombes and Owen, 2005, Ermentrout, 1998, Ermentrout and Cowan, 1979, Bressloff et al., 2002]). This approach implicitly makes the assumption that the effect of noise *vanishes* in large populations.

[1] We give them here for spatially localized populations, with an absolute refractory period set to zero. Extensions to spatial interactions and inclusion of time delays are possible.

However, as mentioned in the section 1.3.3, increasingly many researchers now believe that the different intrinsic or extrinsic noise sources participate in the processing of information. Rather than having a pure disturbing effect there is the interesting possibility that noise conveys information and that this can be an important principle of brain function [Rolls and Deco, 2010]. In order to study the effect of the stochastic nature of the firing in large networks, many authors strived to introduce randomness in a tractable form. A number of computational studies that successfully addressed the case of sparsely connected networks of integrate-and-fire neurons are based on the analysis of large assemblies that fire in an **asynchronous regime** [Abbott and van Vreeswijk, 1993, Amit and Brunel, 1997, Brunel and Hakim, 1999]. Because of the assumption of sparse connectivity, correlations of the synaptic inputs can be *neglected* for large networks. The resulting asynchronous irregular state resembles the discharge activity recorded in the cerebral cortex of awake animals [Destexhe, 2008].

Other models have been introduced to account for the presence of noise in neuronal networks, such as the *population density method* and related approaches [Cai et al., 2004], allowing efficient simulation of large neuronal populations. In order to analyze the collective dynamics, most population density-based approaches involve expansions in terms of the moments of the resulting random variables, and the moment hierarchy needs to be truncated in order to get a closed set of equations, which can raise a number of technical issues (see e.g. [Ly and Tranchina, 2007]).

Yet other models of the activity of large networks are based on the definition of a **Markov chain** governing the firing dynamics of the neurons in the network, where the transition probability satisfies a differential equation called the *master equation*. Seminal works of the application of such modeling for neuroscience date back to the early 90s and have been recently developed by several authors [Ohira and Cowan, 1993, El-Boustani and Destexhe, 2009b]. Most of these approaches are proved correct in some parameter regions using statistical physics tools such as *path integrals* [Buice and Cowan, 2007] and *Van-Kampen expansions* [Bressfloff, 2009]. They motivated a number of interesting studies of quasicycles [Bressloff, 2010] and power-law distribution of avalanche phenomena [Benayoun et al., 2010]. In many cases the authors consider one-step Markov chains, implying that at each update of the chain, only one neuron in the whole network either fires or stops firing, which raises biological plausibility issues. Moreover, analytical approaches mainly address the dynamics of a finite number of moments of the firing activity, which can also raise such issues as the well-posedness [Ly and Tranchina, 2007]

and the adequacy of these systems of equations with the original Markovian model [Touboul and Ermentrout, 2011].

Eventually other approaches have been mainly interested in the **synchronization of oscillators**, characterized by their phase θ_i. The typical equations describing the network of oscillators are for example:

$$\frac{d\theta_i}{dt} = w_i - \sum_{j=1}^{N} K_{ij} \sin(\theta_i - \theta_j) \tag{3.1}$$

Here, w_i is the intrinsic frequency of each oscillator and the K_{ij} are coupling constants. The study of such equations has been initiated by Kuramoto, using statistical physics tools [Kuramoto and Nishikawa, 1987]. For example in the case where there is only one global coupling constant $K_{ij} = \frac{K}{N}$, we can introduce the order parameter $Z(t) = |Z(t)|e^{i\theta_m(t)} = \frac{1}{N}\sum_{j=1}^{N} e^{i\theta_j(t)}$, and show that for weak coupling the oscillators behave independently ($|Z| \to 0$), whereas a strong coupling creates a coherent state ($|Z| \to 1$). Understanding such "Kuramoto models" is still an active area of research as exemplified by the recent article [Giacomin et al., 2011]. We will compare our own approach of mean field with classical Kuramoto models in 7.2.4.

3.2 The asynchronous irregular state in sparsely connected networks

The dynamics of sparsely connected networks of binary excitatory and inhibitory neurons has been studied by van Vreeswijk and Sompolinsky. In particular, in a seminal paper [van Vreeswijk and Sompolinsky, 1996], it is proposed that an approximate balance between the excitatory and inhibitory inputs to a neuron results in the very irregular neuronal firing patterns observed *in vivo*. The assumptions are simple. The connection is random and sparse: on average each neuron is connected to K excitatory neurons, K inhibitory neurons and K external neurons, with K large but much smaller than the total number of neurons in the network N. The sparseness assumption implies that the number of inputs shared by two cells is very low, so that the firing patterns of these two cells will be only weakly correlated. Hence we can consider the inputs to a single cell as being independent and apply the central limit theorem for large K: the mean input will be of order K and the fluctuations of order $\sqrt{K}$. The second assumption is that the individual connections are strong and that only $\sqrt{K}$ excitatory inputs are necessary to cross the

firing threshold. Hence the total synaptic input would always massively hyperpolarize or depolarize the cell, unless we suppose that the mean excitatory input nearly equals the inhibitory one. In this regime the fluctuations will be dominant and of the same order of magnitude of the threshold: this will lead to the very irregular firing. The **balanced state** in this simple model has many advantages: the balance condition can naturally emerge without a fine tuning of parameters in simulations and it provides networks with a response time much faster than the integration time of single neurons.

It is noteworthy that the irregular firing in the balanced state emerges without the addition of any stochastic inputs. The dynamics is more akin to *deterministic chaos* even when the external input is constant. Contrary to the Wilson-Cowan equations, fluctuations are not averaged away, and there is no need of computing finite-size corrections to classical mean field results to understand why the brain seems so noisy.

Nicolas Brunel [Brunel, 2000] developed a similar analytical approach for sparse networks of integrate-and-fire neurons. This time a *diffusion approximation* applies when individual neurons receive a large number of inputs per integration time and when each input makes a small contribution relative to the firing threshold. The network is hence again assumed to be sparse but synapses are not assumed to be strong. In that case, the dynamics of the network can be described by a **Fokker-Planck equation**. Depending on the synaptic time distributions, the external input frequency and the balance between excitation and inhibition, *four regimes* are distinguished [Fourcaud and Brunel, 2002, Brunel, 2000]. These four regimes are the synchronous regular state, the asynchronous irregular, the asynchronous regular and the asynchronous irregular. The asynchronous state is defined by a stationary global activity (the global firing frequency is constant) and the synchronous state by an oscillatory global activity. In the irregular state the individual firing is strongly irregular. The **asynchronous irregular state** (when inhibition dominates excitation in an intermediate range of external frequencies) is the one that most closely matches spontaneous cortical activity [Destexhe and Paré, 1999].

3.3 The spin glass approach

We start by summing up, without going into the technical details and assumptions, the mathematical theory of spin glasses, which is very intricate. We then present the statistical physics viewpoint that

was applied to neural networks by Sompolinsky, Crisanti and Sommers [Crisanti and Sompolinsky, 1987, Sompolinsky et al., 1988].

3.3.1 The mathematical setting

In [Arous and Guionnet, 1995], Ben Arous and Guionnet study the asymptotic behavior of asymmetrical spin glass dynamics. The J_{ij} are standard centered i.i.d. random Gaussian variables. $U(x)$ is defined on a bounded interval $[-A, A]$ and tends to infinitely sufficiently fast to ensure that the spins remain in this bounded interval. The dynamics is given by the following equations, where a particular realization of the J_{ij} specifies the disorder of system:

$$\begin{cases} dx_t^i = -\nabla U(x_t^i)dt + dB_t^i + \frac{\beta}{\sqrt{N}} \sum_{j=1}^N J_{ij} x_t^j dt \\ Law\ of\ x(0) = \mu_o^{\otimes N} \end{cases} \tag{3.2}$$

We remark that in this model the variance scales as $\frac{1}{N}$. For any number N of particles, any temperature $T = 1/\beta$ and $J = (J_{ij})_{1 \leq i,j \leq N}$, the system defined by 3.2 has a unique weak solution. We designate this probability measure by $P_\beta^N(J)$ (until a fixed time T). The classical object one wishes to study is the empirical measure defined by: $\bar{\mu}^N = \frac{1}{N} \sum_{i=1}^N \delta_{x^i}$. It has the advantage of living in a fixed space whatever the value of N. However, contrary to the problem of McKean-Vlasov interacting diffusion processes (studied e.g. by Sznitman [Sznitman, 1984b]) and that we have developed in 4, the variables are **not exchangeable** for a fixed interaction. In that case there is not the same amount of information in the empirical measure as in $(x^1, ..., x^n)$. A strategy is hence to study the law of the empirical measure $\bar{\mu}^N = \frac{1}{N} \sum_{i=1}^N \delta_{x^i}$, *averaged on the interactions*, to get what is called *annealed* results. *Quenched* results, i.e. results for a given interaction (the J-almost sure properties) are harder to obtain.

Let $(\Omega, \bar{\mathcal{F}}, \gamma)$ be a probability space and J_{ij} i.i.d. random variables on Ω such that they are standard centered Gaussian variables under γ. One can define an averaged probability measure:

$$Q_\beta^N = \int P_\beta^N(J(\omega))d\gamma(\omega)$$

$\Pi_{\beta,T}^N$ is the law of the empirical measure under Q_β^N, i.e:

$$\Pi_{\beta,T}^N(B) = Q_\beta^N(\bar{\mu}^N \in B) = \int P_\beta^N(J(\omega))(\bar{\mu}^N \in B)d\gamma(\omega)$$

The main result of [Arous and Guionnet, 1995] is that $\Pi^N_{\beta,T}$ satisfies a **full Large Deviation Principle** (LLP) with a rate function H[2]. The convergence of $\Pi^N_{\beta,T}$ is then obtained by studying the minima of H. It turns out that H achieves its minimal value at a **unique non Markovian probability measure** Q, solution of an intricate implicit stochastic differential system. As a consequence, Ben Arous and Guionnet prove an averaged propagation of chaos result (in a high temperature and short time regime) in the sense that, if $\beta^2 A^2 T < 1$, for any $k \in \mathbb{N}$ and continuous bounded functions $(f^1, ..., f^k)$:

$$\lim_{N\to+\infty} \int \Big(\int f^1(x^1)...f^k(x^k) P^N_\beta(J(\omega))(dx) \Big) d\gamma(\omega) = \Pi^k_{i=1} \int f^i(x^i) dQ(x)$$

This means that, averaged on the interactions, the distribution of $(x^1, ...x^k)$ converges to $Q^{\otimes^k}$.

In [Guionnet, 1997], Alice Guionnet studies the laws of a particle for a spin glass dynamics, with no restriction on time or temperature. Furthermore with supplementary hypotheses on the function U and the law μ_0 (corresponding to the absence of an external magnetic field) she gets a **quenched propagation of chaos** result. Indeed, if U is even and μ_0 is symmetric, then for any bounded continuous functions $(f^1, ..., f^k)$:

$$\int f^1(x^1)...f^k(x^k) dP^N_\beta(J) \text{ converges in probability to } \Pi^k_{i=1} \int f^i(x) dQ(x)$$

3.3.2 Application to neural networks

The statistical study of neural networks interacting through i.i.d. random synaptic weights was pioneered by Amari [Amari et al., 1977]. Later Sompolinsky and collaborators [Crisanti and Sompolinsky, 1987] studied, with statistical physics tools, a network satisfying the following equations:

$$\frac{dh^i_t}{dt} = -h^i_t + \sum_{j=1}^{N} J_{ij} \phi(h^j_t) \tag{3.3}$$

where h^i is a local field associated to neuron i, ϕ is a nonlinear gain function (e.g. $\phi(x) = tanh(gx)$) and the J_{ij} are centered Gaussian random variables of variance $\frac{\beta^2}{N}$. Up to some modifications, this is a form of the equation 3.2 (take for instance $U(x) = x^2/2$ and add the nonlinearity ϕ). In [Sompolinsky et al., 1988], the long-time properties of the dynamical system 3.3 are studied in the limit $N \to +\infty$. The main finding is that there

[2] Rather informally it means that for large N, $\Pi^N_{\beta,T}(B)$ behaves as $e^{-N \inf_B H}$

is a critical value of disorder above which the dynamics is chaotic. More precisely, there is a transition between a stationary phase to a chaotic phase when the gain parameter gJ crosses a critical value. Note that here *chaos* is to be understood in the dynamical system sense (e.g. as measured by positive Lyapunov exponents).

In [Cessac et al., 1994], Cessac and collaborators studied the precise *route to chaos* for discrete neural networks. Moynot and Samuelides [Moynot and Samuelides, 2002], using the same techniques as Ben Arous and Guionnet, i.e. thanks to a Large Deviation Principle, have proven that if the connection weights satisfy a general condition of domination by gaussian tails, then the distribution of the activation potential of each neuron converges weakly towards an explicit gaussian law, the characteristics of which are contained in the mean-field equations stated in [Cessac et al., 1994]. The idea of using LLP for finding mean field equations is hence very fruitful.

3.4 The master equation approach: finite-size effects

The third approach we wish to comment on is inspired by statistical physics and is based on a phenomenological **master equation** describing the evolution of the network. It has mostly been developed by Michael Buice, Carson Chow, Paul Bressloff, Jack Cowan, Sami El Boustani and Alain Destexhe [Buice and Cowan, 2007, Buice and Cowan, 2009, Buice et al., 2010, Bressloff, 2009, El-Boustani and Destexhe, 2009b]. This approach is designed to take into account the finite size corrections to the standard mean field models that are obtained in the thermodynamic limit $N \to +\infty$. Whereas this large N limit is deterministic (we recover variants of the standard Wilson-Cowan equations), second-order statistics appear for finite N.

Typically (see [Bressloff, 2009]) the model can be summarized as follows. The configuration of a network composed of M populations is described by a vector $\mathbf{m}(t) = (m_1(t), m_2(t), ..., m_M(t))$ where $m_i(t)$ is the number of active neurons in population i in the interval $[t, t+dt[$. Neurons can indeed be either quiescent or active (i.e. emitting an action potential). The stochasticity of the variable $m_i(t)$ is introduced by describing it by a **one-step jump Markov process**. The rate of the transitions are precisely chosen such that in the thermodynamic limit usual equations of the Wilson-Cowan type are recovered. The master equation expresses the evolution of the probability for the network

to be in the state $\mathbf{m}(t) = \mathbf{n} = (n_1, n_2, ..., n_M)$:

$$\frac{dP(\mathbf{n},t)}{dt} = \frac{1}{\tau}\sum_i \Big[(n_i+1)P(\mathbf{n}_{i+},t) - n_i P(\mathbf{n},t) + Nf\Big((W_{ii}(n_i-1)/N + \sum_{j\neq i} W_{ij}n_j/N\Big)P(\mathbf{n}_{i-},t) - Nf\Big(\sum_j W_{ij}n_j/N\Big)P(\mathbf{n},t)\Big]$$

for $0 \leq n_i \leq N$. τ is the time constant, f the nonlinear gain function, W_{ij} the synaptic strength (independent of N) and eventually $\mathbf{n}_{i+}$ or $\mathbf{n}_{i-}$ denote the state of the network where n_i has been replaced by n_{i+1} or respectively n_{i-1}.

Starting from this type of equation various techniques exist to derive, for large but finite N, the lowest order corrections to the standard rate equations. There are the path integral method [Buice and Cowan, 2007, Buice and Cowan, 2009, Buice et al., 2010] coming from quantum field theory and the Van Kampen system-size expansion [Bressfloff, 2009] coming from the study of chemical reactions. These techniques are relatively intricate and care must be taken when truncating the successive moments in order to get at the end a closed system of equations. A comparison of the dynamics resulting from these two types of derivations has been done in [Touboul and Ermentrout, 2011]. To conclude, let's emphasize that one of the most important feature of this master equation approach is that, due to its founding microscopic assumptions, it results in a Markovian dynamics.

Part II

Derivation and study of some mean field equations

Chapter 4

A mean field equation with additive noise

Overview

Based on the analysis of a simple neuronal network, we are interested in the emergent properties in large networks of interconnected neurons. In order to study these phenomena in large-scale assemblies of neurons, we consider networks of firing-rate neurons receiving **noisy additive currents**. Asymptotic equations are derived based on propagation of chaos techniques developed for instance by McKean, Sznitman, Tanaka and coworkers. These equations are implicit on the probability distribution of the solutions which generally makes their direct analysis difficult. However, in our case, **the solutions are Gaussian**, and their moments satisfy a closed system of nonlinear ordinary differential equations (ODEs), which are much easier to study than the original stochastic network equations, and the statistics of the empirical process uniformly converge towards the solutions of these ODEs. Based on this description, **we analytically and numerically study the influence of noise on the collective behaviors**, and compare these asymptotic regimes to simulations of the network. We observe that the mean field equations provide an accurate description of the solutions of the network equations for network sizes as small as a few hundreds of neurons. In particular, we observe that the level of noise in the system qualitatively modifies its collective behavior, producing for instance synchronized oscillations of the whole network, desynchronization of oscillating regimes, and stabilization or destabilization of stationary solutions. These results shed a new light on the role of noise in shaping collective dynamics of neurons, and gives us clues for understanding similar phenomena observed in biological networks. The main results of this chapter are presented in a paper [Touboul et al., 2011] written in collaboration with Jonathan Touboul and Olivier Faugeras, which has been accepted for publication in the SIAM Journal on Applied Dynamical Systems.

Contents

4.1 Introduction

In the present chapter, we apply a probabilistic method to derive the limit behavior resulting from the interaction of an infinite number of firing-rate neurons nonlinearly interconnected. This approach differs from other works in the literature presented in chapter 3 on several points. First, unlike [Buice and Cowan, 2007] it relies on a description of the microscopic dynamics without taking as granted the description of the dynamics by a phenomenological equation. Second, unlike [Brunel and Hakim, 1999], it does not make the assumption of a sparse connectivity and considers a network globally coupled. Eventually, unlike [Sompolinsky et al., 1988], the synaptic weights are not drawn from a distribution, but considered constant and depending only on the populations they are coupling. Our model takes into account the fact that cortical columns feature **different populations**.

The approach consists in deriving the limit equations as the total number of neurons tends to infinity, based on results obtained in the field of **large-scale systems of interacting particles**. This problem has been chiefly studied for solving statistical physics questions, and has been a very active field of research in mathematics during the last decades [McKean, 1966, Dobrushin, 1970, Tanaka, 1978, Tanaka, 1984, Sznitman, 1989]. The problem of propagation of chaos for mean field interacting diffusions has been particularly studied by Alain-Sol Sznitman [Sznitman, 1984a, Sznitman, 1984b, Sznitman, 1986]. In general, the equations obtained by such rigorous approaches are extremely hard to analyze. They can be either seen as implicit equations in the set of stochastic processes, or as non-local partial differential equations on the probability distribution through the related Fokker-Planck equations. But in both cases, understanding the dynamics of these equations is very challenging, even for basic properties such as the existence and uniqueness of stationary solutions and a priori estimates [Herrmann and Tugaut, 2010]. It appears even more difficult to understand qualitatively the effects of noise on the solutions and to interpret them in terms of the underlying biological processes.

Yet, we aim at answering this question. In the case we address, the problem is rigorously reducible to the analysis of a set of ordinary differential equations. This is because the solution of the mean field equations is a **Gaussian process**. It is therefore completely determined by its first two moments which we prove to be the solutions of ordinary differential equations. This allows us to go much deeper into the analysis of the dynamical effects of the parameters, in particular those related to the noise, and to understand their influence on the solutions. The analysis of this Gaussian process also provides a rich

amount of information about the non-Gaussian solution of the network when its size is large enough.

This chapter is organized as follows. In the first section 4.2 we deal with the modeling, the derivation of the mean field equations and of the related system of ordinary differential equations. We then turn in section 4.3 to the analysis of the solutions of these equations and the influence of noise. We show in details how noise strongly determines the activity of the cortical assembly. We then return to the problem of understanding the behavior of finite-size (albeit large) networks in section 4.4 and compare their behavior with those of the solutions of the mean field equations (infinite-size network). The analysis of the network behaviors in the different regimes of the mean field equations provides an interpretation of the individual behaviors responsible for collective reliable responses.

4.2 Model and mean field equations

In all this chapter, as well as in the remaining of this thesis, we work in a complete probability space $(\Omega, \mathcal{F}, \mathbb{P})$ assumed to satisfy the usual conditions.

We are interested in the large scale behavior arising from the nonlinear coupling of a large number N of stochastic diffusion processes representing the membrane potential of neurons in the framework of rate models (see e.g. [Dayan and Abbott, 2001, Gerstner and Kistler, 2002]) introduced in section 1.2. Hence the variable characterizing the neuron state is its firing rate, that exponentially relaxes to zero when it receives no input, and the neuron integrates both an external input and the current generated by its neighbors. The network is composed of P neural *populations* that differ by their intrinsic dynamics, the input they receive and the way they interact with the other neurons[1]. Each population $\alpha \in \{1, \dots, P\}$ is composed of N_α neurons, and we assume that the ratio N_α/N converges to a constant δ_α in $]0, 1[$ when the total number of neurons N becomes arbitrarily large. We define the population function p that maps the index $i \in \{1, \dots N\}$ of any neuron to the index α of the population neuron i belongs to: $p(i) = \alpha$.

For any neuron i in population α, the membrane potential V_t^i has a linear intrinsic dynamics with a time constant τ_α. The membrane potential of

[1] Our model can be viewed as a column model but, alternatively, it can be seen as a hypercolumn model, each diffusion process characterizing the activity of a whole cortical column modeled by Wilson and Cowan equations.

each neuron returns to zero exponentially if it receives no input. The neuron i in population α receives an external current, which is the sum of a deterministic part $I_\alpha(t)$ and a stochastic additive noise modulated by $\lambda_\alpha(t)$ and driven by $B^i(t)$ where the B^i are N independent adapted Brownian motions. This **additive noise** term accounts for different biological phenomena [Faisal et al., 2008], such as sensory noise (the external inputs being intrinsically noisy), cellular noise (accounting for the inherent variability in the biochemical functioning of the neural cell), and most importantly channel noise [White et al., 2000] produced by the random opening and closing of ion channels. All these phenomena have been described in section 1.3.2 and we choose to model them by additive *independent* white noise [2].

Neurons interact through their firing rates, given by sigmoidal transforms of the potentials. The firing rate of the presynaptic neuron j, multiplied by the synaptic weight J_{ij}, is an input current to the postsynaptic neuron i. We classically assume that the synaptic weight J_{ij} is equal to $J_{p(i)p(j)}/N_{p(j)}$. In practice this synaptic weight randomly varies depending on the local properties of the environment. Models including this type of randomness will be introduced in chapter 6. The scaling assumption is necessary to ensure that the total input to a neuron does not depend on the network size.

The network behavior is therefore governed by the following set of stochastic differential equations:

$$dV^i(t) = \left(-\frac{1}{\tau_\alpha} V^i(t) + I_\alpha(t) + \sum_{\beta=1}^{P} \frac{J_{\alpha\beta}}{N_\beta} \sum_{j:\, p(j)=\beta} S_\beta(V^j(t)) \right) dt + \lambda_\alpha(t) dB_t^i \tag{4.1}$$

As already mentioned, we see that these equations represent a set of interacting diffusion processes. Such processes have been studied for instance by McKean, Tanaka and Sznitman among others [McKean, 1966, Tanaka, 1983, Tanaka, 1978, Sznitman, 1989]. It is essential to point out that in our case the sequence of the $V^i(t)$ belonging to the same population (i.e. for $p(i) = \alpha$) constitute an *exchangeable* sequence of random variables. This means that for a finite or infinite sequence $(V^i(t) : p(i) = \alpha)$, any finite permutation σ

[2] This will be a quite accurate description if cellular and channel noise are predominant. Indeed as they are intrinsic to the cell, we can in first approxiation model them as independent. On the contrary the noise originating from the input is shared by many neurons. Hence the independence hypothesis is a simplifying one, and extensions to colored noise should be considered in more subtle models.

of the indices $i : p(i) = \alpha$ (i.e. any permutation σ that leaves all but finitely many indices fixed for neurons in population α), the joint probability distribution of the permuted sequence $(V^{\sigma(i)}(t) : p(i) = \alpha)$ is the same as the joint probability distribution of the original sequence.

We now show that the resulting dynamics is encapsulated in a *Markovian* equation, of McKean-Vlasov type, and that the **propagation of chaos** property (see 2.2.3) applies.

The limit mean field equation and the propagation of chaos property are the subject of the following theorem:

Theorem 4.2.1. *Let $T > 0$ a fixed time. Under the previous assumptions, we have:*

(i). The process V^i for i in population α, solution of equation (4.1), converges in law towards the process $\bar{V}^\alpha$ solution of the mean field implicit equation:

$$d\bar{V}^\alpha(t) = \left[-\frac{1}{\tau_\alpha}\bar{V}^\alpha(t) + I_\alpha(t) + \sum_{\beta=1}^{P} J_{\alpha\beta}\mathbb{E}\left[S_\beta(\bar{V}^\beta(t))\right] \right] dt + \lambda_\alpha(t) dB^\alpha(t) \tag{4.2}$$

as a process for $t \in [0, T]$, in the sense that there exists $(\bar{V}_t^i)_{t\geq 0}$ distributed as $(\bar{V}_t^\alpha)_{t\geq 0}$ such that

$$\mathbb{E}\left[\sup_{0\leq t\leq T} |V_t^i - \bar{V}_t^i|\right] \leq \frac{\tilde{C}(T)}{\sqrt{N}}$$

where $\tilde{C}(\cdot)$ is a function of time depending on the parameters of the system. As a random variable, it converges uniformly in time in the sense that:

$$\sup_{0\leq t\leq T} \mathbb{E}\left[|V_t^i - \bar{V}_t^i|\right] \leq \frac{C}{\sqrt{N}}$$

where C does not depend on time. In equations (4.2), the processes $(B^\alpha(t))_{\alpha=1\ldots P}$ are independent Brownian motions.

(ii). Equation (4.2) has a unique (pathwise and in law) solution which is square integrable.

(iii). The propagation of chaos applies, i.e. provided that the initial conditions of all neurons are independent and population-wise identically distributed [3]*, the law of* $(V^{i_1}(t), \dots, V^{i_k}(t), t \leq T)$ *for any fixed* $k \geq 2$ *and* $(i_1, \dots, i_k)$*, converges towards* $\nu_{p(i_1)} \otimes \dots \otimes \nu_{p(i_k)}$ *when* $N \to \infty$*, where we denoted* ν_α *the law of the solution of equation (4.2) corresponding to population* α*. This means that* $(V^{i_1}(t), \dots, V^{i_k}(t))$ *become independent processes.*

We underline the fact that the expectation term in equation (4.2) is the classical expectation of a function of a stochastic process. In details, if p_t^β is the probability density of $\bar{V}^\beta(t)$, $\mathbb{E}\left[S_\beta(\bar{V}^\beta(t))\right]$ is equal to $\int_{\mathbb{R}} S_\beta(x) p_t^\beta(x)\, dx$.

The proof of this theorem essentially uses results from the works of Tanaka and Sznitman, summarized in [Sznitman, 1989] and also presented in [Villani, 2001]. A distinction with these classical results is that the network is not totally homogeneous but composed of distinct neural populations. Thanks to the assumption that the proportion of neurons in each population is non-trivial ($N_\alpha/N \to \delta_\alpha \in]0, 1[$), the propagation of chaos occurs simultaneously in each population yielding our equations.

The main deep theoretical distinction is that the theorem claims a uniform convergence in time: most of the results proved in the kinetic theory domain show propagation of chaos properties and convergence results only for a finite time, and convergence estimates diverge as time increases. Uniform propagation of chaos is an important property as commented in [Cattiaux et al., 2008], and particularly in our case as we will further comment. Methods to prove uniformity are generally involved (see e.g. [Mischler et al., 2011] where uniformity is obtained for certain models using a dual approach based on the analysis of generator operators). Due to the linearity of the intrinsic dynamics, we provide here an elementary proof of this property in our particular system.

Proof. The existence and uniqueness of solutions can be performed in a classical fashion using Picard iterations of an integral form of equation (4.2) and a contraction argument. The proof of the convergence towards this law, and of the propagation of chaos can be performed using Sznitman's powerful **coupling method** (see e.g. [Sznitman, 1989]) [4], that consists in exhibiting an almost sure limit of the sequence of processes V_t^i as N goes to infinity by coupling the mean field equation with the network equation as follows. We

[3] The initial conditions are said to be chaotic.

[4] This method had already been introduced by Dobrushin [Dobrushin, 1970])

define the different independent processes $\bar{V}^i$ solution of equation (4.2) driven by the same Brownian motion $(B_t^i)_t$ as involved in the network equation (4.1), and with the same initial condition $V^i(0)$ as neuron i in the network. It is clear that these processes are *independent* (since the (B_t^i) are pairwise independent) and have the *same law as the solution of the mean field equation* (4.2). The almost sure convergence of (V_t^i) towards $(\bar{V}_t^i)$ will therefore imply the convergence in law towards the mean field equation. For a neuron i belonging to population α:

$$V_t^i - \bar{V}_t^i = \sum_{\beta=1}^{P} J_{\alpha\beta} \int_0^t e^{-(t-s)/\tau_\alpha} \frac{1}{N_\beta} \sum_{j:\, p(j)=\beta} \Big\{ \Big(S_\beta(V_s^j) - S_\beta(\bar{V}_s^j) \Big) + \Big(S_\beta(\bar{V}_s^j) - \mathbb{E}\left[S_\beta(\bar{V}_s^j) \right] \Big) \Big\} ds$$

We have, denoting by τ the maximal value of $(\tau_\beta, \beta = 1 \dots P)$:

$$|V_t^i - \bar{V}_t^i| \le K_\alpha \int_0^t e^{-(t-s)/\tau} \max_{j=1\dots N} |V_s^j - \bar{V}_s^j| \, ds + K'_\alpha \left| \frac{1}{N} \int_0^t e^{-(t-s)/\tau_\alpha} \sum_{j=1}^{N} \left(S_{p(j)}(\bar{V}_s^j) - \mathbb{E}\left[S_{p(j)}(\bar{V}_s^j) \right] \right) ds \right|, \quad (4.3)$$

where $K_\alpha = \sum_\beta |J_{\alpha\beta}| L$. L is the largest Lipschitz constant of the sigmoids $(S_\beta, \beta = 1 \dots P)$, and $K'_\alpha = \max_\beta |J_{\alpha\beta}| N/N_\beta$, quantity upperbounded, for N sufficiently large, by $\max_\beta |J_{\alpha\beta}| 2/\delta_\beta$.

Since the righthand side of (4.3) does not depend on the index i, taking the maximum with respect to i and the expected value of both sides of (4.3), we obtain

$$\mathbb{E}\left[\max_{i=1\dots N} |V_t^i - \bar{V}_t^i| \right] \le K \int_0^t e^{-(t-s)/\tau} \mathbb{E}\left[\max_{j=1\dots N} |V_s^j - \bar{V}_s^j| \right] ds + K' \mathbb{E}\left[\max_{\alpha=1,\dots,P} \left| \frac{1}{N} \int_0^t e^{-(t-s)/\tau_\alpha} \sum_{j=1}^{N} \left(S_{p(j)}(\bar{V}_s^j) - \mathbb{E}\left[S_{p(j)}(\bar{V}_s^j) \right] \right) ds \right| \right] \quad (4.4)$$

Since the random variables $A_j(s) = S_{p(j)}(\bar{V}_s^j) - \mathbb{E}\left[S_{p(j)}(\bar{V}_s^j) \right]$ are independent and centered, using the fact that the sigmoids S_β take their values in the interval $[0, 1]$, using Cauchy-Schwartz and posing $\bar{\tau} = \max_\alpha \tau_\alpha + 1 = \tau + 1$,

we have:

$$\begin{aligned}
&\mathbb{E}\left[\max_\alpha \left(\frac{1}{N}\int_0^t e^{-(t-s)/\tau_\alpha}\sum_{j=1}^N \left(S_{p(j)}(\bar{V}_s^j) - \mathbb{E}\left[S_{p(j)}(\bar{V}_s^j)\right]\right) ds\right)^2\right] \\
&\quad = \frac{1}{N^2}\mathbb{E}\left[\max_\alpha \left(\int_0^t \left(e^{-(t-s)\frac{\bar{\tau}-\tau_\alpha}{\bar{\tau}\tau_\alpha}}\right)\left(\sum_{j=1}^N e^{-(t-s)/\bar{\tau}} A_j(s)\right)\right)^2 ds\right] \\
&\quad \leq \frac{1}{N^2}\mathbb{E}\left[\max_\alpha \left(\int_0^t e^{-2(t-s)\frac{\bar{\tau}-\tau_\alpha}{\bar{\tau}\tau_\alpha}} ds\right)\left(\int_0^t e^{-2(t-s)/\bar{\tau}}\Big(\sum_{j=1}^N A_j(s)\Big)^2 ds\right)\right] \\
&\quad \leq \frac{1}{N^2}\mathbb{E}\left[\left(\int_0^t e^{-2(t-s)/(\tau(\tau+1))} ds\right)\left(\int_0^t e^{-2(t-s)/(\tau+1)}\Big(\sum_{j=1}^N A_j(s)\Big)^2 ds\right)\right] \\
&\quad = \frac{1}{N^2}\frac{\tau(\tau+1)}{2}(1-e^{-2t/(\tau(\tau+1))})\int_0^t e^{-2(t-s)/(\tau+1)}\mathbb{E}\left[\sum_{j=1}^N A_j(s)^2\right] ds \\
&\quad \leq \frac{1}{N}\frac{\tau(\tau+1)}{2}\int_0^t e^{-2(t-s)/(\tau+1)} ds \\
&\quad \leq \frac{1}{N}\frac{\tau(\tau+1)^2}{4} = \frac{\tau'}{N}
\end{aligned}$$

By Cauchy-Schwartz inequality, we can upperbound the second term of the righthand side of inequality (4.4) by $\sqrt{\tau'/N}$. Therefore, defining $M_t = \mathbb{E}\left[\max_i |V_t^i - \bar{V}_t^i|\right]$, $K = \max_\alpha K_\alpha$ and $K' = \max_\alpha K'_\alpha$ we have:

$$M_t \leq K\int_0^t e^{-(t-s)/\tau} M_s\, ds + K'\sqrt{\frac{\tau'}{N}}$$

implying, using Gronwall's lemma,

$$M_t \leq \frac{K'\sqrt{\tau'}e^{K\tau}}{\sqrt{N}}.$$

This inequality readily yields the almost sure convergence of V_t^i towards $\bar{V}_t^i$ as N goes to infinity, uniformly in time, and hence convergence in law of V_t^i towards $\bar{V}_t^\alpha$.

The almost sure convergence of $(V_t^i)_{t\in[0,T]}$ (considered as a process) towards $(\bar{V}_t^i)_{t\in[0,T]}$ can be proved in a similar fashion. Indeed, upperbounding the exponential term in (4.3) by 1 and taking the supremum, it is easy to see that:

$$\mathbb{E}\left[\sup_{0\leq t\leq T}\max_{i=1\ldots N}|V_t^i - \bar{V}_t^i|\right] \leq K\int_0^T \mathbb{E}\left[\sup_{s\in[0,t]}\max_{j=1\ldots N}|V_s^j - \bar{V}_s^j|\right] dt + \frac{K'T}{\sqrt{N}},$$

using the fact that:

$$\begin{aligned}
\mathbb{E}\left[\max_{\alpha}\sup_{t\in[0,T]}\left(\frac{1}{N}\int_0^t e^{-(t-s)/\tau_\alpha}\sum_{j=1}^{N}\left(S_{p(j)}(\bar{V}_s^j)-\mathbb{E}\left[S_{p(j)}(\bar{V}_s^j)\right]\right)ds\right)^2\right] \\
\leq \frac{T}{N^2}\int_0^T \mathbb{E}\left[\left|\sum_{j=1}^{N}\left(S_{p(j)}(\bar{V}_s^j)-\mathbb{E}\left[S_{p(j)}(\bar{V}_s^j)\right]\right)\right|^2\right]ds \\
= \frac{T}{N^2}\sum_{j=1}^{N}\int_0^T \mathbb{E}\left[\left|S_{p(j)}(\bar{V}_s^j)-\mathbb{E}\left[S_{p(j)}(\bar{V}_s^j)\right]\right|^2\right]ds \\
\leq \frac{T^2}{N}
\end{aligned}$$

using the independence of the $\bar{V}^j$ and Cauchy-Schwartz inequality. This last estimate readily implies, using Gronwall's inequality:

$$\mathbb{E}\left[\sup_{0\leq t\leq T}\max_{i=1\dots N}|V_t^i-\bar{V}_t^i|\right]\leq\frac{K'Te^{KT}}{\sqrt{N}}.$$

The propagation of chaos property (iii) stems from the almost sure convergence of $(V^{i_1}(t),\dots,V^{i_k}(t),t\leq T)$ towards $(\bar{V}^{i_1}(t),\dots,\bar{V}^{i_k}(t),t\leq T)$, which are independent, as a process and uniformly for fixed time, and is proved in a similar fashion.[5]. □

The P equations (4.2), which are P implicit stochastic differential equations, describe the asymptotic behavior of the network. However, the characterization and simulation of their solutions is a challenge. Fortunately, due to their particular form in our setting, these equations can be substantially simplified. Indeed, under some assumptions, the solutions of the mean field equations are shown to be **Gaussian**, allowing to exactly reduce the dynamics of the mean field equations to the study of **coupled ordinary differential equations** as we now show.

Proposition 4.2.2. *Let us assume that $\bar{V}(0)=(\bar{V}^\alpha(0))_{\alpha=1\dots P}$ is a P-dimensional Gaussian random variable. We have:*

- *The solutions of the P mean field equations (4.2) with initial conditions $\bar{V}(0)$ are Gaussian processes for all time.*
- *Let $\mu(t)=(\mu_\alpha(t))_{\alpha=1\dots P}$ denote the mean vector of the process $(\bar{V}^\alpha(t))_{\alpha=1\dots P}$ and $v(t)=(v_\alpha(t))_{\alpha=1\dots P}$ its variance. Let also $f_\beta(x,y)$*

[5]In fact it is easily seen that the propagation of chaos would still hold not only for k neurons (in fixed number), but also for $k=o(\sqrt{N})$, for example $k=\log(N)$.

denote the expectation of $S_\beta(U)$ for U a Gaussian random variable of mean x and variance y. We have:

$$\begin{cases} \dot{\mu}_\alpha(t) = -\frac{1}{\tau_\alpha}\mu_\alpha(t) + \sum_{\beta=1}^{P} J_{\alpha\beta} f_\beta(\mu_\beta(t), v_\beta(t)) + I_\alpha(t) & \alpha = 1 \dots P \\ \dot{v}_\alpha(t) = -\frac{2}{\tau_\alpha}\, v_\alpha(t) + \lambda_\alpha^2(t) & \alpha = 1 \dots P \end{cases} \tag{4.5}$$

with initial condition $\mu_\alpha(0) = \mathbb{E}\left[\bar{V}^\alpha(0)\right]$ and $v_\alpha(0) = \mathbb{E}\left[(\bar{V}^\alpha(0) - \mu_\alpha(0))^2\right]$. In equation (4.5), the dot denotes the differential with respect to time.

Proof. The unique solution of the mean field equations (4.2) starting from a square integrable initial condition $\bar{V}(0)$ measurable with respect to $\mathcal{F}$ can be written in the form:

$$\bar{V}^\alpha(t) = e^{-\frac{t}{\tau_\alpha}}\bar{V}^\alpha(0) + e^{-\frac{t}{\tau_\alpha}}\Big(\int_0^t e^{\frac{s}{\tau_\alpha}} (I_\alpha(s) + \sum_{\beta=1}^{P} J_{\alpha\beta}\mathbb{E}\left[S_\beta(\bar{V}^\beta(s))\right])ds + \int_0^t e^{\frac{s}{\tau_\alpha}} \lambda_\alpha(s)\, dB_s^\alpha \Big). \tag{4.6}$$

We observe that if $\bar{V}^\alpha(0)$ is a Gaussian random variable, then the righthand side of (4.6) is necessarily Gaussian as the sum of a deterministic term and an Itô integral of a deterministic function, and hence so is the solution of the mean field equation. Its law is hence characterized by its mean and covariance functions. The formula (4.6) involves the expectation $\mathbb{E}\left[S_\beta(\bar{V}_\beta(s))\right]$, which, because of the Gaussian nature of $\bar{V}^\beta$, only depends on $\mu_\beta(s)$ and $v_\beta(s)$, and is denoted by $f_\beta(\mu_\beta(s), v_\beta(s))$. Taking the expectation of both sides of the equality (4.6), we obtain the equation satisfied by the mean of the process $\mu_\alpha(t) = \mathbb{E}\left[\bar{V}^\alpha(t)\right]$:

$$\mu_\alpha(t) = e^{-\frac{t}{\tau_\alpha}} \left(\mathbb{E}\left[\bar{V}^\alpha(0)\right] + \int_0^t e^{\frac{s}{\tau_\alpha}} \left(\sum_{\beta=1}^{P} J_{\alpha\beta}\mathbb{E}\left[S_\beta(\bar{V}^\beta(s)\right] + I_\alpha(s) \right) ds \right).$$

Taking the variance of both sides of the equality (4.6), we obtain the following equation:

$$v_\alpha(t) = e^{-\frac{2t}{\tau_\alpha}} \left(v_\alpha(0) + \int_0^t e^{\frac{2s}{\tau_\alpha}} \lambda_\alpha^2(s)\, ds \right),$$

and this concludes the proof. □

Remark 1.

- *In order to fully characterize the law of the process $\bar{V}$, we need to compute the covariance matrix function $Cov(\bar{V}^\alpha(t_1), \bar{V}^\beta(t_2))$ for t_1 and t_2 in*

$\mathbb{R}^{+*}$. *For* $\alpha \neq \beta$ *this covariance is clearly zero using equation* (4.6), *and we have:*

$$Cov(\bar{V}^\alpha(t_1), \bar{V}^\alpha(t_2)) = e^{-\frac{t_1+t_2}{\tau_\alpha}} Var(\bar{V}_0^\alpha) + \int_0^{t_1 \wedge t_2} e^{\frac{2s}{\tau_\alpha}} \lambda_\alpha^2(s)\, ds \qquad (4.7)$$

for $t_1, t_2 \in \mathbb{R}^{+*}$, *hence only depends on the parameters of the system and is in particular not coupled to the dynamics of the mean. The description of the solution given by equations* (4.5) *is hence sufficient to fully characterize the solution of the mean field equations* (4.2).

- *The uniformity in time of the propagation of chaos has deep implications in regard of equations* (4.5). *Indeed, we observe that the solution of the mean field equation is governed by the mean of the process, the expectation being a deterministic function depending on the parameters of the system. The uniformity in particular implies that, for* i *in population* α*:*

$$\sup_{t\geq 0} \left| \mathbb{E}\left[V_t^i\right] - \mu_\alpha(t) \right| \leq \sup_{t\geq 0} \mathbb{E}\left[|V_t^i - \bar{V}_t^i| \right] \leq \frac{C}{\sqrt{N}} \qquad (4.8)$$

  implying uniform convergence of the empirical mean, as a function of time, towards $\mu_\alpha(t)$.

- *If* $\bar{V}^0$ *is not Gaussian, the solution of equation* (4.2) *asymptotically converges exponentially towards a Gaussian solution. The important uniformity convergence property towards the mean field equations ensures that the Gaussian solution is indeed the asymptotic regime of the network, which strengthens the interest of the analysis of the differential system* (4.5).

The functions f_β depend on the choice of the sigmoidal transform. A particularly interesting choice is the erf sigmoidal function $S_\alpha(x) = \mathrm{erf}(g_\alpha x + \gamma_\alpha)$. In that case we are able to express the function f_β in closed form, because of the following lemma:

Lemma 4.2.3. *In the case where the sigmoidal transforms are of the form* $S_\alpha(x) = \mathrm{erf}(g_\alpha x + \gamma_\alpha)$, *the functions* $f_\alpha(\mu_\alpha, v_\alpha)$ *involved in the mean field equations* (4.5) *with a Gaussian initial condition take the simple form:*

$$f_\alpha(\mu, v) = \mathrm{erf}\left(\frac{g_\alpha\, \mu + \gamma_\alpha}{\sqrt{1 + g_\alpha^2 v}} \right). \qquad (4.9)$$

Proof. The proof is given in Appendix A.1. □

In summary, we have shown that, provided that the initial conditions of each neuron are independent and Gaussian, the large-scale behavior of our linear model is governed by a set of ordinary differential equations (theorem 4.2.1 and proposition 4.2.2). This is very interesting since it reduces the study of the solutions to the very complex implicit equation (4.2) bearing on the law of a process to a much simpler setting, ordinary differential equations. As shown below this allows us to understand the effects of the system parameters on the solutions. For this reason we assume from now on that the initial condition is Gaussian, and focus on the effect of the noise on the dynamics.

4.3 Noise-induced phenomena

We will see that the noise leads to an effective noise-dependent scaling of the gain of the nonlinear firing rate function and we will explore how this noise-dependent gain affects the bifurcation structure of one and two-population models.

In this section we mathematically and numerically study the influence of the noise levels λ_α on the dynamics of the neuronal populations. Thanks to the uniform convergence of the empirical mean towards the mean of the mean field system (equation (4.8)) and the propagation of chaos property for the network process, it is relevant to study such phenomena through the thorough analysis of the solutions of the mean field equations given by the ODEs (4.5). This is what we do in the present section.

As observed in equation (4.5), in the case of a Gaussian initial condition, the equation of the variance v is decoupled from the equation on the mean μ in. The variance satisfies a non-autonomous equation:

$$\dot{v}_\alpha = -\frac{2}{\tau_\alpha} v_\alpha + \lambda_\alpha^2(t).$$

which is easily integrated as:

$$v_\alpha(t) = e^{-\frac{2t}{\tau_\alpha}} \left(v_\alpha(0) + \int_0^t e^{\frac{2s}{\tau_\alpha}} \lambda_\alpha^2(s)\, ds \right).$$

$v_\alpha(t)$ is therefore independent of the mean μ. This implies that the equations on μ are a set of non-autonomous ordinary differential equations.

These ordinary differential equations are similar to those of a single neuron. They differ in that the terms in the sigmoidal functions depend on the external noise levels $\lambda_\alpha(t)$. They read:

$$\dot{\mu}_\alpha = -\frac{\mu_\alpha}{\tau_\alpha} + \sum_{\beta=1}^{P} J_{\alpha\beta}\mathrm{erf}\left(\frac{g_\beta\,\mu_\beta + \gamma_\beta}{\sqrt{1 + g_\beta^2 e^{-2t/\tau_\beta}\left(v_\beta(0) + \int_0^t e^{2s/\tau_\beta}\lambda_\beta^2(s)\,ds\right)}}\right) + I_\alpha$$

hence the slope g_β and the threshold γ_β are scaled by a time-varying coefficient which is always smaller than one.

We now focus on the stationary solutions when the noise parameter λ does not depend upon time. In that case, the variance is equal to:

$$v_\alpha(t) = \tau_\alpha\lambda_\alpha^2/2 + e^{-\frac{2t}{\tau_\alpha}}(v_\alpha(0) - \tau_\alpha\lambda_\alpha^2/2),$$

and converges exponentially fast towards the constant value $\tau_\alpha\lambda_\alpha^2/2$. Asymptotic regimes of the mean field equations are therefore Gaussian random variables with constant standard deviation. Their mean is solution of the equation:

$$\dot{\mu}_\alpha = -\frac{\mu_\alpha}{\tau_\alpha} + \sum_{\beta=1}^{P} J_{\alpha\beta}\mathrm{erf}\left(\frac{g_\beta\,\mu_\beta + \gamma_\beta}{\sqrt{1 + g_\beta^2\tau_\beta\lambda_\beta^2/2}}\right) + I_\alpha \quad \alpha = 1, \cdots, P$$

In other words, the presence of noise has the effect of modifying the slope g_α and the threshold γ_α of the sigmoidal erf function, but the type of the equations is the same as that of the equation of each individual neuron, it is a rate equation.

We observe that the larger the noise amplitude λ, the smaller the slope of the sigmoidal transform. **Noise has the effect of smoothing the sigmoidal transform**. This will have a strong influence on the bifurcations of the solutions to the mean field equations and hence on the behaviors of the system. We demonstrate these effects for two simple choices of parameters in one- and two-populations networks.

4.3.1 The external noise can destroy a pitchfork bifurcation

Let us start by considering the case of a one-population network. We drop the index α since no confusion is possible. We assume for simplicity that the threshold γ of the sigmoid is null and that the time constant τ is equal to

one. By doing so, we do not restrict the generality of the study, since τ can be eliminated by rescaling the time and γ can be absorbed into I by a simple change of origin for μ. The network equations read:

$$dV_t^i = \left(-V_t^i + \frac{J}{N} \sum_{j=1}^{N} \operatorname{erf}\left(g\, V_t^j\right) + I(t) \right) dt + \lambda dB_t^i \quad i = 1, \cdots, N,$$

and we are interested in the limit in law of their solutions as the number of neurons N tends to infinity.

In order to analytically study the effect of the parameter λ, we set $I \equiv -\frac{J}{2}$. In that case, and in the absence of noise, the solution $V = 0$ is a fixed point of the network equations. The following proposition characterizes their solutions in the deterministic and stochastic cases.

Proposition 4.3.1. *In a non-stochastic finite-size network, the null solution is:*

- *stable if* $J < 0$ *or if* $J > 0$ *and* $g < g_c := \sqrt{2\pi}/J$,
- *unstable for* $J > 0$ *and* $g > g_c$.
- *For* $J > 0$, *the system undergoes a pitchfork bifurcation at* $g = g_c$.

In the mean field limit of the same stochastic network, the pitchfork bifurcation occurs for a new value of $g = g^* = \frac{\sqrt{2\pi}}{\sqrt{J^2 - \pi\lambda^2}} > g_c$ *if* $J > 0$ *and* $\lambda < J/\sqrt{\pi}$. *Furthermore the null solution is:*

- *stable if:*
  - $J < 0$ *or*
  - $J > 0$ *and* $\lambda > J/\sqrt{\pi}$ *(large noise case) or*
  - $J > 0$, $\lambda < J/\sqrt{\pi}$ *and* $g < g^*$,
- *unstable for* $J > 0$, $\lambda < J/\sqrt{\pi}$ *and* $g > g^*$, *and*
- *the system undergoes a pitchfork bifurcation at* $g = g^*$ *when* $J > 0$ *and* $\lambda < J/\sqrt{\pi}$.

This proposition is a bit surprising at first sight. Indeed, it says that noise can stabilize a fixed point which is unstable in the same non-stochastic system. Even more interesting is the fact that if the system is driven by a sufficiently large noisy input, **the zero solution will always stabilize**. It is known, see, e.g., [Mao, 2008], that noise can stabilize the fixed points of a deterministic system of dimension greater than or equal to 2. The present observation extends these results to a one-dimensional case, in a more complicated setting because of the particular, non-standard, form of the mean field equations. Also note that this proposition provides a precise quantification of the value of the parameter that destabilizes the fixed point. This is a *stochastic bifurcation* of the mean field equation (a P-bifurcation –P for phenomenological– in the sense of [Arnold, 1998]). This estimation will be used as a yardstick for the evaluation of the behavior of the solutions to the network equations in section 4.4.

Proof. We start by studying the finite-size deterministic system. In the absence of noise, it is obvious because of our assumptions that the solution $V^i = 0$ for all $i \in \{1, \dots, N\}$ is a fixed point of the network equations. At this point, the Jacobian matrix reads $-Id_N + \frac{J}{N}\frac{g}{\sqrt{2\pi}}\mathbb{1}_N$, where Id_N is the $N \times N$ identity matrix and $\mathbb{1}_N$ is the $N \times N$ matrix with all elements equal to one. The matrix $\mathbb{1}_N$ is diagonalizable, all its eigenvalues are equal to zero except one which is equal to N. Hence, all eigenvalues of the Jacobian matrix are equal to -1, except one which is equal to $\frac{J\,g}{\sqrt{2\pi}} - 1$. The solution where all V^i are equal to zero in the deterministic system is therefore stable if and only if $g\,J < \sqrt{2\pi}$. The eigenvalue corresponding to the destabilization corresponds to the eigenvector $\overrightarrow{1}$ whose components are all equal to 1. Interestingly, this vector does not depend on the parameters, and therefore it is easy to check that at the point $g = g_c$ the system loses stability through a pitchfork bifurcation. Indeed, because of the symmetry of the erf function, the second derivative of the vector field projected on this vector vanishes, while the third derivative does not (it is equal to $-(1 + g^2)$).

Considering now the stochastic mean field limit, the stationary mean firing rate in that case is solution of the equation:

$$\dot{\mu} = -\mu + J\mathrm{erf}\left(\frac{g\,\mu}{\sqrt{1 + g^2\lambda^2/2}}\right) + I$$

Here again, the null firing rate point $\mu = 0$ is a fixed point of the mean field equations, and it is stable if and only if $-1 + J\,\frac{g}{\sqrt{2\pi(1+g^2\lambda^2/2)}} < 0$. The remaining of the proposition readily follows from the fact that the stability changes at $g = g^*$ where $J\,\frac{g^*}{\sqrt{2\pi(1+g^{*2}\lambda^2/2)}} = 1$. □

Note that the results in this proposition only depend on λ and its effect on the slope of the sigmoid. It is a general phenomenon that goes beyond the example in this section: increasing λ decreases the slope of the sigmoidal transform and the threshold. In section 4.4 we will see that this phenomenon can be observed at the network level, and a good agreement will be found between the finite-size network behavior and the predictions obtained from the mean field limit.

We now turn to an example in a two-dimensional network, where the presence of oscillations will be modulated by the noise levels.

4.3.2 The external noise can destroy oscillations

The same phenomenon of nonlinear interaction between the noise intensity and the sigmoid function can lead, in higher dimensions, to more complex phenomena such as the disappearance or appearance of oscillations. In order to study phenomena of this type, we instantiate a simple two-populations network model in which, similarly to the one-dimensional case, all the calculations can be performed analytically. The network we consider consists of an excitatory population, labeled 1, and an inhibitory population, labeled 2. Both populations are composed of the same number $N/2$ of neurons (N is assumed in all the subsection to be even), and have the same parameters $\tau_1 = \tau_2 = \tau$, $g_1 = g_2 = g$ and $\lambda_1 = \lambda_2 = \lambda$. We choose for simplicity the following connectivity matrix:

$$M = J \frac{2}{N} \begin{pmatrix} 1 & -1 \\ 1 & 1 \end{pmatrix},$$

and we assume that the inputs are set to $I_1 = 0$ and $I_2 = -J$. The zero solution where all neurons have a zero voltage is a fixed point of the equations whatever the number of neurons N in each population. We have the following result:

Proposition 4.3.2. *In the deterministic finite-size network, the null solution is:*

- *stable if $J < 0$ or if $J > 0$ and $g < g_c := \sqrt{2\pi}/J$,*
- *unstable for $J > 0$ and $g > g_c$ and the solutions are oscillating on a periodic orbit.*
- *For $J > 0$ the system undergoes a supercritical Hopf bifurcation at $g = g_c$.*

In the mean field limit of the same stochastic network, the Hopf bifurcation occurs for a new value of the slope parameter $g = g^* = \frac{\sqrt{2\pi}}{\sqrt{J^2-\pi\lambda^2}} > g_c$.

Furthermore the null solution is:

- *stable if:*
  - $J < 0$ *or*
  - $J > 0$ *and* $\lambda > J/\sqrt{\pi}$ *(large noise case) or*
  - $J > 0$, $\lambda < J/\sqrt{\pi}$ *and* $g < g^*$,
- *unstable for* $J > 0$, $\lambda < J/\sqrt{\pi}$ *and* $g > g^*$, *and the system features a stable periodic orbit.*
- *The system undergoes a supercritical Hopf bifurcation at* $g = g^*$ *when* $J > 0$ *and* $\lambda < J/\sqrt{\pi}$.

Note that proposition 4.3.2 is quite similar to proposition 4.3.1, the qualitative difference being that the system is oscillating. The proof is closely related and is presented in less details.

Proof. In the deterministic network model, the Jacobian matrix at the null equilibrium can be written as

$$A = -Id_N + \frac{g}{\sqrt{2\pi}} M \otimes \mathbb{1}_{N/2}$$

where $\otimes$ denotes the Kronecker product (see e.g. [Neudecker, 1969, Brewer, 1978]), i.e. the Jacobian matrix is built from $N/2$ blocs of size 2×2 and each of these blocks is a copy of $\frac{g}{\sqrt{2\pi}} M$. The eigenvalues of a Kronecker product of two matrices are all possible pairwise products of the eigenvalues of the matrices. Since the eigenvalues of M are equal to $\frac{2J}{N}(1 \pm \mathbf{i})$ where $\mathbf{i}^2 = -1$, and as noted previously, the eigenvalues of $\mathbb{1}_{N/2}$ are 0 with multiplicity $N/2-1$ and $N/2$ with multiplicity 1, we conclude that the Jacobian matrix A has $N-2$ eigenvalues equal to -1, and two eigenvalues equal to $-1 + g\,J/\sqrt{2\pi}(1 \pm \mathbf{i})$. The null equilibrium in this deterministic system is therefore stable if and only if the real parts of all eigenvalues are smaller than 0, i.e. $gJ < \sqrt{2\pi}$. Therefore, for a fixed J, the system has a bifurcation at $g_c = \sqrt{2\pi}/J$. The analysis of the eigenvectors allows to check the genericity and transversality conditions of the Hopf bifurcation (see e.g. [Guckenheimer and Holmes, 1990]) in a very similar fashion to the proof of proposition 4.3.1.

In the mean field model, the same analysis applies and, as in the one-dimensional case, the bifurcation point is shifted to g^* when this value is well-defined, which concludes the proof of the proposition 4.3.2. □

We have therefore shown that noise can destroy the oscillations of the network. The results of propositions 4.3.1 and 4.3.2 are summarized in figure 4.1.

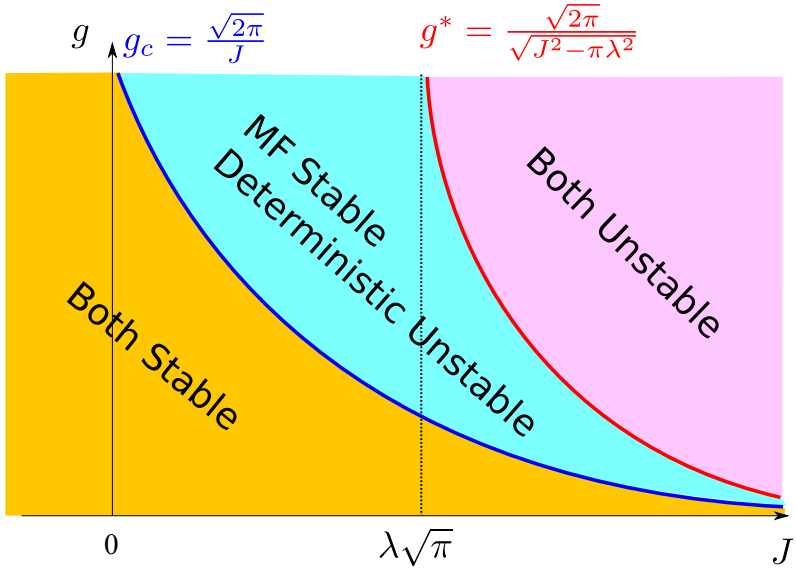

Figure 4.1: Summary of the results of propositions 4.3.1 and 4.3.2, see text. The additive noise parameter λ smoothly modifies the pitchfork or the Hopf bifurcation curve in the (g, J) plane. For λ large enough, the null solution of the mean field equation is always stabilized whatever g. MF: mean field limit, Deterministic: finite-size deterministic network. The blue (respectively red) curve is one branch of the hyperbola of equation $gJ = \sqrt{2\pi}$ (respectively $g\sqrt{J^2 - \pi\lambda^2} = \sqrt{2\pi}$).

An even more interesting phenomenon is that noise can also produce regular cycles in the mean part of the solution of the mean field equations, for parameters such that the deterministic system presents a stable equilibrium. This is the subject of the following section.

4.3.3 The external noise can induce oscillations

In order to uncover further effects of the noise on the dynamics, we now turn to the numerical study of a two-populations network including excitation and inhibition. The time constant τ, sigmoidal transforms S, noise intensity λ and the initial condition on the variance are chosen identical for both population. Under these hypotheses, the variances of the two populations are identical and denoted by $v(t)$. We further assume that $S(x) = \mathrm{erf}(g\,x)$, (we

set $g = 1$) and hence the mean-field nonlinear function $f(\mu, v)$ is given by lemma 4.2.3. The connectivity matrix is set to $J = \frac{1}{N}\begin{pmatrix} 15 & -12 \\ 16 & -5 \end{pmatrix}$. The inhibitory population inhibits itself in this case. The input currents I_1 and I_2 are considered constant. The mean field equations in that case read:

$$\begin{cases} \dot{\mu}_1 = -\frac{\mu_1}{\tau} + J_{11} f(\mu_1, v) + J_{12} f(\mu_2, v) + I_1 \\ \dot{\mu}_2 = -\frac{\mu_2}{\tau} + J_{21} f(\mu_1, v) + J_{22} f(\mu_2, v) + I_2 \\ \dot{v} = -2\frac{v}{\tau} + \lambda^2 \end{cases}$$

The **codimension two bifurcation diagram** of the system, obtained when the noise parameter and the input on the first population are varied (setting I_2 to a fixed value: $I_2 = -3$), is displayed in Figure 4.2 (qualitative results turn out to change smoothly when I_2 is also allowed to vary). It features two cusps (CP) and one Bogdanov-Takens bifurcations (BT). In addition to these local bifurcations, we observe that the Hopf bifurcation manifold (shown in pink in Figure 4.2) and the saddle-homoclinic bifurcation curve (green line) present a turning point, i.e. change monotony as a function of λ.

The diagram can be **decomposed into** 4 **different regions depending on the dynamical features** (number and stability of fixed points or cycles): the "trivial" zone where the system features a unique stable fixed point (not colored), a zone with 2 unstable and 1 stable fixed point (green zone (a)) separated by the saddle-homoclinic bifurcation curve from region (b) (yellow) where an additional stable cycle exists. Zone (c) (orange) features a stable cycle and an unstable fixed point, and zone (d) (green, again) features 2 stable and 1 unstable fixed points.

Let us for instance fix $I_1 = 0$. As λ is increased, several noise-induced transition occur leading the system successively in zone (a), (b), (c) and the trivial zone (see codimension one bifurcation diagram in Figure 4.2 (i)). In details, for small noise levels the system features a unique stable fixed point (zone (a)). A family of large amplitude and small frequency periodic orbits appears from the saddle-homoclinic bifurcation yielding a bistable regime (zone (b)) before the stable fixed point disappears through a saddle-node bifurcation (zone (c)). The amplitude of these cycles progressively decreases and their frequency progressively increases as the noise intensity is increased, and they eventually disappear through a supercritical Hopf bifurcation leading to the trivial behavior with a single fixed point. We emphasize here the fact that the **sudden appearance of large amplitude slow oscillations** can be compared to epileptic spikes, which are characterized by the presence of collective

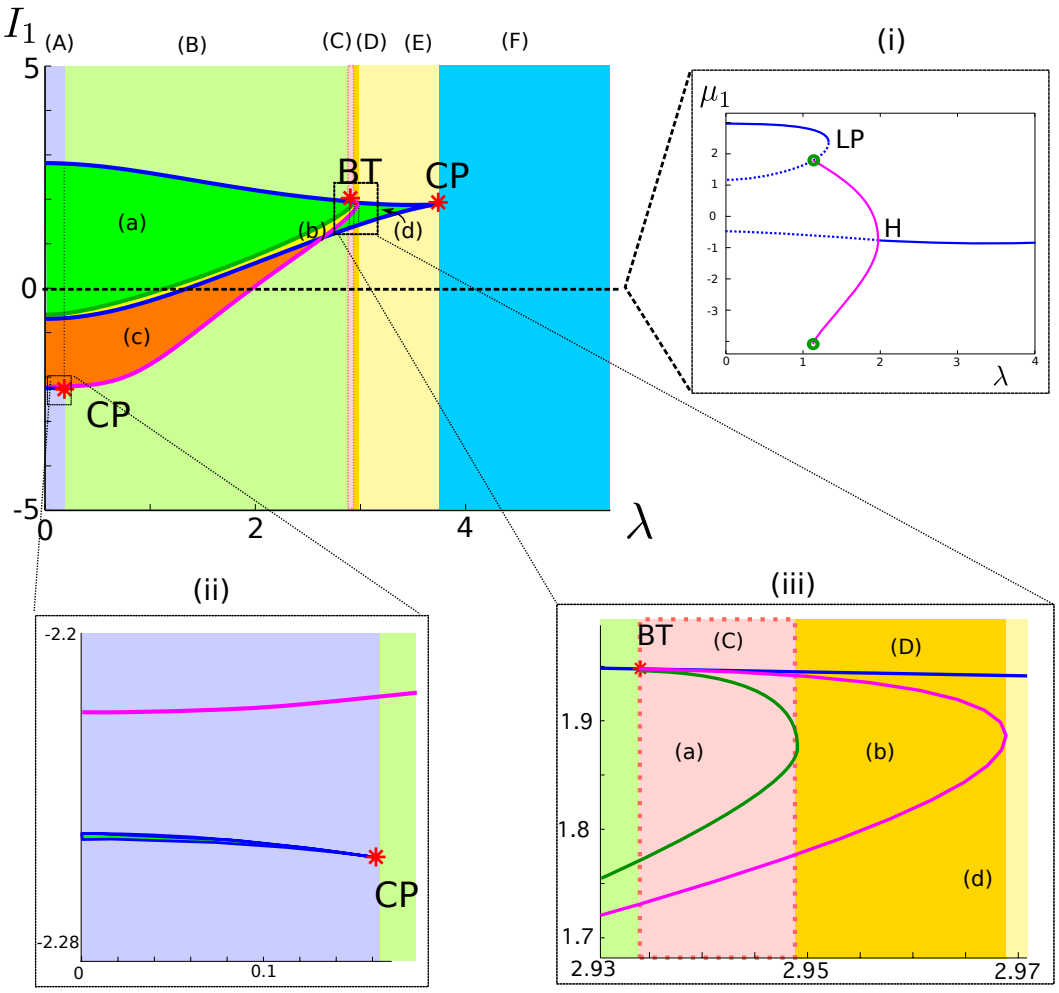

Figure 4.2: Codimension two bifurcation diagram (upper left) and zooms (subfigures (ii) and (iii)) for the mean field equations as I_1 and λ are varied. We distinguish, apart from the trivial regime with a single fixed point, three dynamical regimes labeled (a), (b) and (c) (see text) and 6 ranges of λ, labeled (A) through (F). Blue: saddle-node bifurcations, pink: Hopf bifurcations, green: saddle homoclinic bifurcations, BT: Bogdanov Takens bifurcation, CP: cusp. Individual behaviors in each zone are summarized in appendix A.2. (i): Codimension 1 bifurcation diagram for $I_1 = 0$ as a function of λ: we observe a saddle-node (LP), a Hopf (H) and a saddle homoclinic bifurcation (green circles). There are three main different noise regimes: a high-state equilibrium regime, a periodic regime and a low-state equilibrium regime. A small interval of values of λ corresponds to the co-existence of cycles and a fixed point close to the saddle-homoclinic orbit. Diagrams obtained with XPPAut [Ermentrout, 2002] and MatCont package [Dhooge et al., 2003b, Dhooge et al., 2003a].

oscillations of large amplitude and small frequency suddenly appearing in a population of neurons (see [Touboul et al., 2010]). This comparison will turn out to be relevant from the microscopic viewpoint: network simulations of section 4.4 will indeed show a sudden synchronization of all neurons at this transition.

The diagram can also be **decomposed into six different noise levels intervals** (labels (A) through (F) in Figure 4.2) corresponding to qualitatively different codimension 1 bifurcation diagrams as I_1 is varied (the six corresponding bifurcation diagrams are presented in appendix A.2). The presence of these different zones illustrate how noise influences the response of the neural assembly to external inputs. For instance, for λ large enough, no cycles exist whatever I_1 (zones (E-F)), whereas for λ small enough (zones A-D), cycles always exist for some values of the input. Such partitions may provide an experimental design for evaluating a noise level range as a function of the observed dynamics when varying the input to the excitatory population for instance.

We therefore conclude from the analysis of these simulations that noise does not only destroy structures and regularity, **it can also generate oscillations**. These noise-induced oscillations are very interesting from the biological viewpoint. Indeed, oscillations are essential for the brain function. The link between oscillations and noise level is therefore a very relevant piece of information, that strengthens interpretations of the functional role of the noise. We will comment further on this topic in the Conclusion III.

4.4 Back to the network dynamics

Thus far, we studied the dynamics of the mean field equations representing regimes of the network dynamics in the limit where the number of neurons is infinite. We now compare the regimes identified in this analysis with simulations of the finite-size stochastic network. We are particularly looking for potential finite-size effects, namely qualitative differences between the solutions to the network and the mean field equations. This will provide us with information about the accuracy of an approximation of the network dynamics by the mean field model, as function of the size of the network.

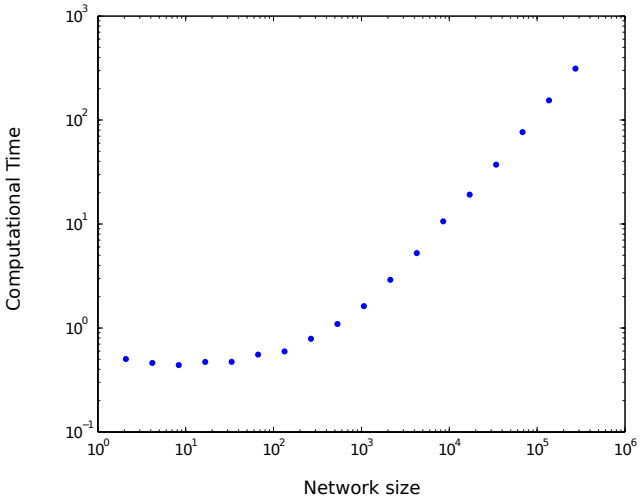

Figure 4.3: Computation time for the simulation of the stochastic network in logarithmic scale as a function of the network size.

4.4.1 Numerical simulations

Numerical simulations of the network stochastic differential equations (4.1) are performed using the usual Euler-Maruyama algorithm (see e.g. [Maruyama, 1955, Mao, 2008]) with fixed time step (less than 0.01) over an interval $[0, T]$. In order to observe oscillations, we choose T between 50 and 70. The simulations are performed with Matlab®, using a vectorized implementation that has the advantage to be very efficient even for large networks. The computation time stays below 1s for networks up to 2 000 neurons, and appears to grow linearly with the size of the network once the cache memory saturates (see Figure 4.3). For instance, for $T = 20$, $dt = 0.01$, the simulation of a 2 000 neurons network takes 0.89s, and for 525 000 neurons, 600s on a HP Z800 with 8 Intel Xeon CPU E5520 @ 2.27 GHz 17.4 Go RAM. The main limitation preventing the simulation of very large networks is the amount of memory required for the storage of the trajectories of all neurons.

An important property arising from theorem 4.2.1 is that asymptotically, neurons behave independently and have the same probability distribution. In our numerical simulations, we will make use of this asymptotic independence and, in order to evaluate an empirical mean of the process related to a given neuron in population α, will compute both the empirical mean over all neurons in that population and a mean over different independent realization of the process. This method allows to reduce sensitively the number of independent simulations in order to obtain a given precision in the empirical mean evaluation.

4.4.2 A one population case

We start by addressing the case discussed in section 4.3.1 where we showed analytically that the loss of stability of the null fixed point as the slope of the sigmoid was varied depended on the noise parameter λ. We now investigate numerically the stability of the 0 fixed point of the network equations. In order to check for the presence of a pitchfork bifurcation, we compute, for each value of the noise and for each value of the slope of the sigmoid, an estimated value of the mean of the membrane potential. This estimate is calculated by averaging out over 500 independent realizations the empirical mean of the membrane potentials of all neurons in the network at the final time. We display the average value and then compare these simulations with those of the mean field equations stopped at the same time as the network. We observe that both are very similar and show some differences with the bifurcation diagram that corresponds to the asymptotic regimes.

The results of the simulations, where we have also varied N, are shown in Figure 4.4 and reveal two interesting features. First, because we simulate over a finite time, we tend to smooth the pitchfork bifurcation: this is perceptible for both the network and the mean field equations. Second, we observe that the loss of stability of the zero fixed point arises at the value of λ predicted by the analysis of the mean field equations for networks as small as 50 neurons. The value reached by the simulations of the network is very close to that related to the mean field equation as soon as N becomes greater than 250.

4.4.3 Two populations case and oscillations

We now investigate the case shown in Figure 4.2(i) where cycles are created (through homoclinic bifurcation) or destroyed (through Hopf bifurcation) as the additive noise intensity parameter λ is increased.

Looking at Figure 4.2(i), we observe that for $\lambda \in [1.12, 1.33]$, stable periodic orbits coexist with stable fixed points in the mean field system. For smaller values of λ, the mean field system features a unique stable fixed point, while for $\lambda \in [1.33, 1.97]$, it features a unique stable limit cycle, and for $\lambda > 1.97$, the dynamics is reduced to a unique attractive fixed point. Numerical simulations confirm this analysis. Let us for instance illustrate the fact that the network features the bistable regime, the most complex phenomenon. Figure 4.5 shows simulations of a network composed of 5 000 neurons in each population (time step $dt = 5 \cdot 10^{-3}$, total time $T = 50$). Depending on the mean and on the standard deviation of the initial condition, we observe that the network either

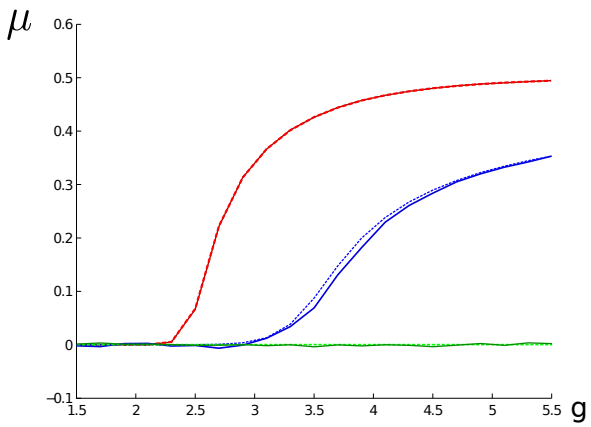

(a) Network Simulations vs mean field simulations, different λ, $N = 50\,000$

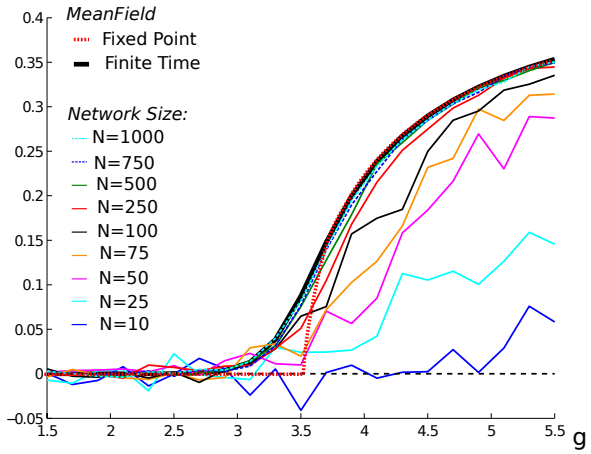

(b) Network simulations vs mean field simulations, different N, $\lambda = 0.4$

Figure 4.4: Comparison of the pitchfork bifurcations with respect to the slope parameter g for the network and the mean field equations, $T = 40$, $dt = 0.001$, number of sample paths: 100, initial condition $V^0 = 0.5$ (hence we only see the positive part of the pitchfork, symmetrical solutions are found for negative initial conditions, and are not plotted for legibility). (a): 50 000 neurons. Continuous curves correspond to network simulations, dashed curves to mean field simulations. When λ increases, as predicted by proposition 4.3.1, we observe that the value of the parameter g related to the pitchfork bifurcation increases as well, until the pitchfork disappears: red: $\lambda = 0$, blue: $\lambda = 0.4$, green: $\lambda = 0.8 > \sqrt{2\pi}/J \sim 0.56$. (b): $\lambda = 0.4$. The solution to the mean field equation undergoes a pitchfork bifurcation at $g = 3.55$. Large dotted red: theoretical pitchfork bifurcation. Large black: endpoint of mean field simulation at time $T = 40$. The other colored curves show the results of the network simulation for different values of the size of the network N. The 0 solution, which loses stability, is displayed in thin dashed black. We see that as N increases, the mean field equation describes accurately the network activity. For $N \geq 50$ (red, green, dotted blue and dotted cyan curves) the bifurcation diagram is quite close to the one predicted by the mean field analysis.

converges to the mean field fixed point or the periodic orbit. Both mean field equations show very close behaviors.

In the fixed point regime corresponding to small values of λ we observe that the membrane potential of every neuron randomly varies around the value corresponding to the fixed points of the mean field equation (see Figure 4.6, cases (a) and (b))), with a standard deviation that converges toward the constant value $\lambda^2/2$ as predicted by the mean field equations. The empirical mean and standard deviation of the voltages in the network show a very good agreement with the related mean field variables. For larger values of λ corresponding to the oscillatory regime (Figure 4.6, cases (c) and (d)), all neurons oscillate in phase. **These synchronized oscillations yield a coherent global oscillation of the network activity**. The statistics of the network are again in good agreement with the mean field solution. The standard deviation converges towards the constant solution of the mean field equation. This is visible at the level of individual trajectories, that shape a "tube" of solutions around the periodic mean field solution, whose size increases with λ. The empirical means accurately match the regular oscillations of the solution of the mean field equation. A progressive phase shift is observed, likely to be related with the time step dt involved in the simulation. Note that the phase does not depend on the realization. Indeed, according to theorem 4.2.1, the solution of the mean field equations only depends on the mean and the standard deviation of the Gaussian initial condition, which therefore governs the phase of the oscillations on the limit cycle (see Figure 4.7).

In the fixed point regime related to large values of λ, very noisy trajectories are obtained because of the levels of noise involved (see Figure 4.6, cases (e) and (f)). Though the individual neurons show very fluctuating trajectories, the empirical mean averaged out over all neurons in the network fits closely the mean field fixed point solution.

Eventually, we study the switching between a fixed-point regime and an oscillatory regime by extensively simulating the 10 000 neurons network for different values of λ and computing the Fourier transform of the empirical mean (see Figure 4.8). The three-dimensional plots show that the appearance and disappearance of oscillations occur for the same values of the parameter λ as in the mean field limit, and **the route to oscillations is similar**: at the homoclinic bifurcation in the mean field system, arbitrarily small frequencies are present, this is also the case for the finite-size network. At the value of λ related to the Hopf bifurcation, the system suddenly switches from a non-zero

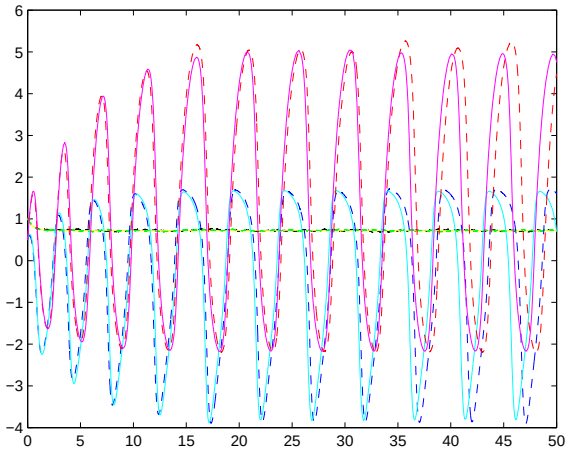

(a) $\lambda = 1.2$. **Oscillatory regime**. Statistics of the network compared to the mean field.

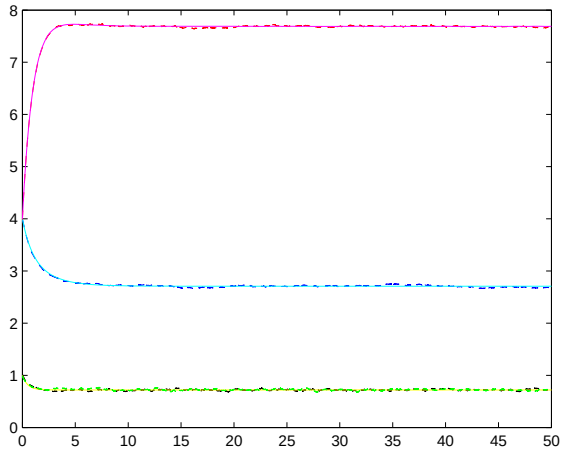

(b) $\lambda = 1.2$. **Fixed-point regime** Statistics of the network compared to the mean field.

Figure 4.5: **Featuring bistability**. In both cases $\lambda = 1.2$. The initial conditions for the mean field equation are chosen in agreement with the initial conditions of the network. The initial value of the membrane potential of each individual neuron in the network is drawn independently from a Gaussian distribution of variance 1 whose mean varies: (a) mean = 0.5. (b) mean = 4. Cyan (resp. magenta) curves: value of the mean variable of the mean field solution for population 1 (resp. 2). Dashed blue (resp. red) curves: empirical mean of population 1 (resp. 2). Yellow: value of the variance of the mean field solution. Dashed black (resp. green): empirical variance of population 1 (resp. 2).

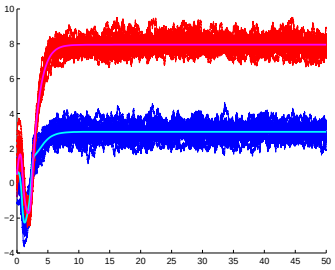

(a) $\lambda = 0.6$. **Fixed-point regime**. Individual trajectories vs mean field.

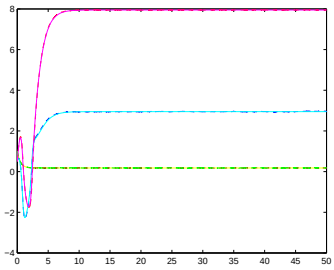

(b) $\lambda = 0.6$. **Fixed-point regime** Empirical network statistics vs mean field.

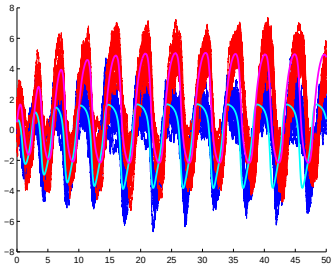

(c) $\lambda = 1.2$. **Oscillatory regime**. Individual trajectories vs mean field.

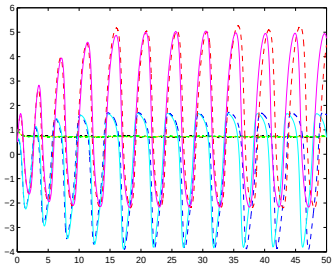

(d) $\lambda = 1.2$. **Oscillatory regime** Empirical network statistics vs mean field.

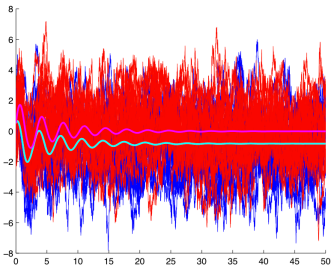

(e) $\lambda = 2.5$. **Noisy fixed point regime**. Individual trajectories vs mean field.

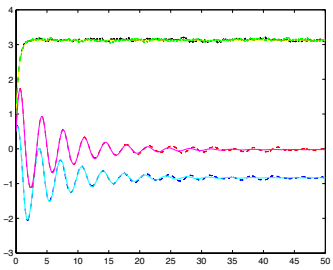

(f) $\lambda = 2.5$. **Noisy fixed point regime** Empirical network statistics vs mean field.

Figure 4.6: Solution of the network dynamics for different values of the noise parameter λ compared to the mean field solution. Simulations are run for 10 000 neurons, 5 000 in each population. (a), (c), (e): 40 individual trajectories of the membrane potentials of 40 neurons arbitrarily chosen in the network (20 in each population) compared to the solution of the mean field equations. Blue: population 1 (excitatory). Red: population 2 (inhibitory). Cyan (resp. magenta): mean of the mean field solution for population 1 (resp. 2). (b), (d), (f): Empirical statistics of the network compared to the mean field. Cyan (resp. magenta): mean of the mean field solution for population 1 (resp. 2). Yellow: variance of the mean field solution. Dashed blue (resp. red): empirical mean of population 1 (resp. 2). Dashed black (resp. green): empirical variance of population 1 (resp. 2). For $\lambda = 2.5$, due to the amplitude of noise, the statistics were computed over 10 realizations of the process.

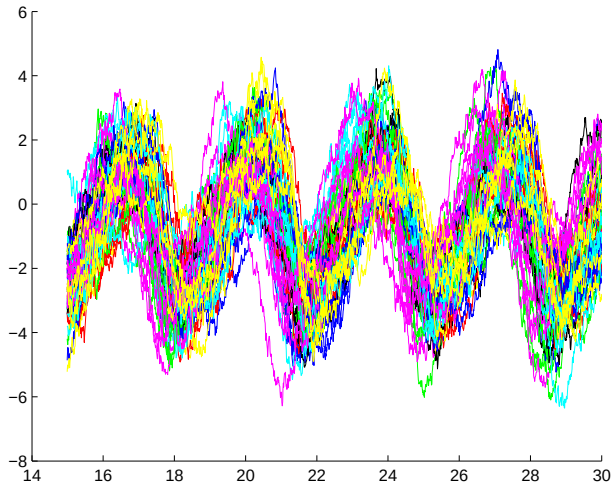

Figure 4.7: Different realizations of the stochastic network dynamics: the membrane potentials of 5 neurons among 5 000 of population 1 are plotted for 12 different realizations represented in different colors. All neurons oscillate in phase, and this phase does not depend on the realization.

frequency to a zero frequency in a form that is very similar to the network case. Therefore we conclude that the mean field equations accurately reproduce the network dynamics for networks as small as 10 000 neurons, and hence provide a good model, simple to study, for networks of the scale of typical cortical columns. As a side remark, we note that at a homoclinic bifurcation of the mean field system, very small frequencies appear and a precise description of the spectrum of the network activity would require very large simulation times to uncover precisely the spectrum at this point, even more so since the large standard deviation of the process disturbs the synchronization.

We conclude this section by discussing **heuristic arguments explaining the observed regular oscillations**. Let us start by stating that this phenomenon is a pure **collective effect**: indeed, two-neurons networks (one per population) do not present such regular oscillations as noise is varied. We observe that individual trajectories of the membrane potential of a 2-neurons networks for small noise levels stay close to the deterministic fixed point. However, when noise is increased, the system starts making large excursions with a typical shape resembling the cycle observed in the mean field limit, and these excursions occur randomly. Such excursions are typical of the presence of a homoclinic deterministic trajectory: when perturbed, the system catches the homoclinic orbit responsible for such large excursions. The codimension one

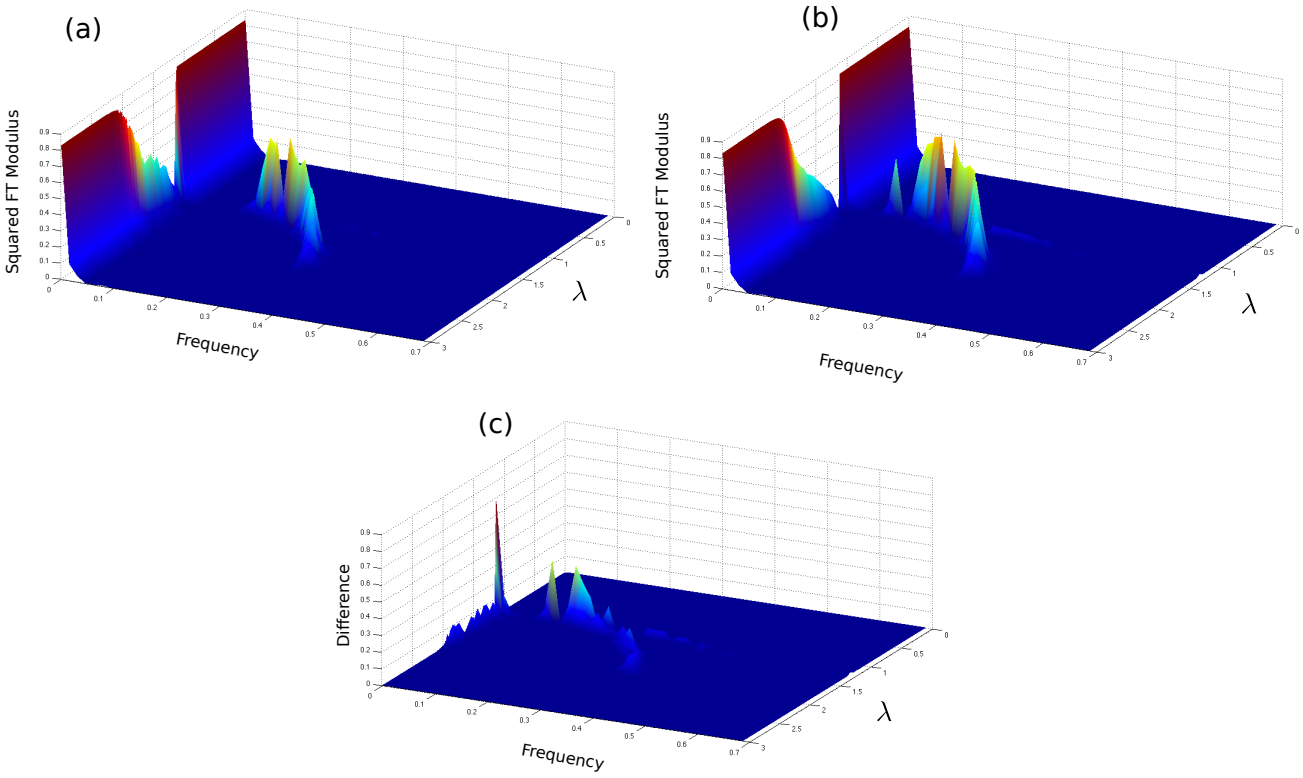

Figure 4.8: Squared moduli of the Fourier transforms (a) of the empirical mean for simulations of the network and (b) of the mean variable of the solution to the mean field equations as functions of the frequency (Hz) and the noise parameter λ. We observe that oscillations appear in the network for the same value of λ as in the mean field equations (Figure 4.2), first through what appears to be a homoclinic bifurcation (arbitrary small frequencies) and also disappear for the same value of λ through what seems to be a Hopf bifurcation (discontinuity in the power spectrum). (c) Magnitude of the difference between the two diagrams: we note that the frequency distribution reaches its maxima for these same values of λ, and the main differences are observed, as expected, around the putative homoclinic bifurcation point.

bifurcation diagram of the 2-neurons system indeed illustrates the presence of a homoclinic orbit as a function of I_1 (see diagram 4.2, and Figure A.2 (A))[6]. Noise can be heuristically seen as perturbing the deterministic value of I_1. For sufficiently small values of the noise parameter, the probability of I_1 to visit regions corresponding to the presence of a cycle is small. But as the noise amplitude is increased, this probability becomes non-negligible and individual trajectories will randomly follow the stable cycle. Such excursions produce large input to the other neurons which will either be inhibited or excited synchronously at this time, a phenomenon that may trigger synchronized oscillations if the coupling is strong enough and the proportion of neurons involved in a possible excursion large enough. If the noise parameter is too large, the limit cycle structure will be destroyed.

Another way to understand this phenomenon consists in considering the **phase plane dynamics** of the two-neurons network with no noise (see Figure 4.9). The system presents three fixed points, one attractive, one repulsive, and a saddle. The unstable manifold of the saddle fixed point connects with the stable fixed point in an heteroclinic orbit. The stable manifold of the saddle fixed point is a separatrix between trajectories that make small excursions around the stable fixed point, and those related to large excursions close to the heteroclinic orbit. As noise is increased, the probability distribution of each individual neuron, centered around the stable fixed point, will grow larger until it crosses the separatrix with a non-negligible probability, resulting in the system randomly displaying large excursions around the heteroclinic cycle. The fact that a homoclinic path to oscillations is found in the mean field limit can be accounted for by these observations, considering the fact that crossing the separatrix, when noise is of small amplitude, can take an arbitrary long time. The rhythmicity of the oscillations we found and the synchronization are related to the coupling in a complex interplay with the probability of large excursions.

4.5 Summary

We have been interested in the large-scale behavior of networks of firing rate neuron models with **additive noise**. Using a probabilistic approach, we addressed the question of the behavior of neurons in the network as its size tends to infinity. In that limit, we showed that the propagation of chaos property was checked and that the behavior of all neurons boiled down to a mean

[6]Indeed, the mean field equations with $\lambda = 0$ are precisely the equations of a two-neurons network since in that case $f(\mu, \lambda^2/2) = S(\mu)$.

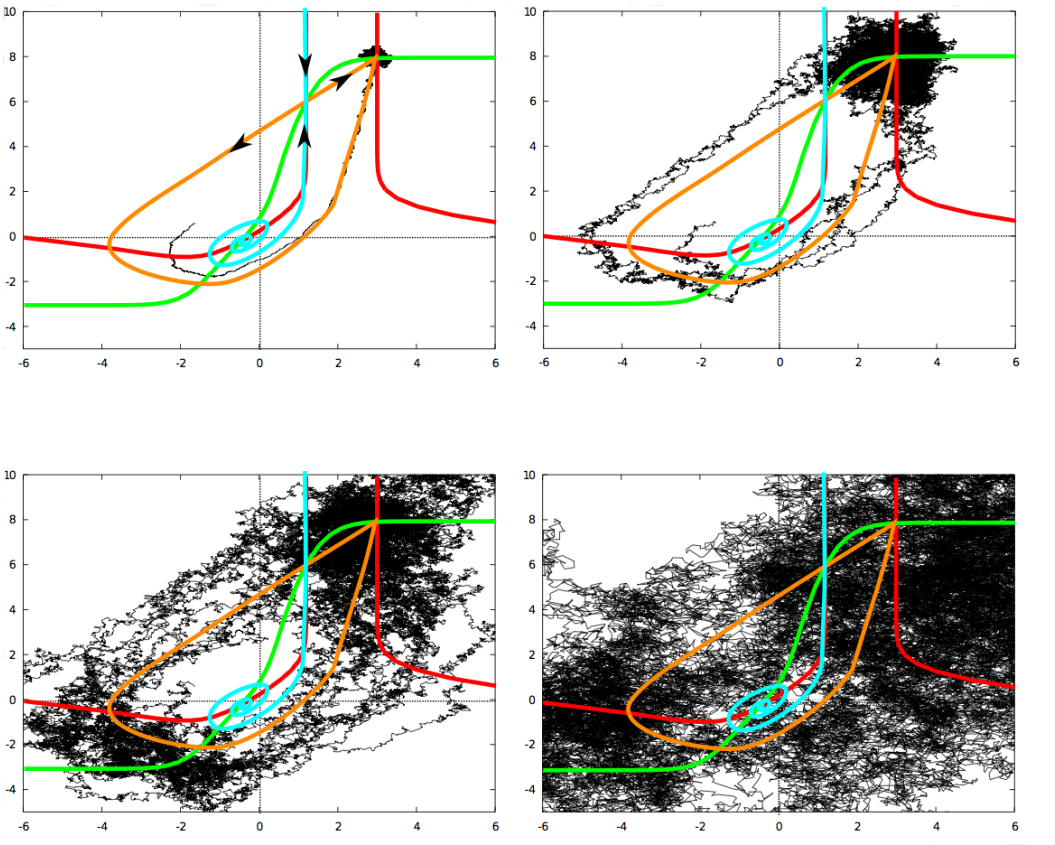

Figure 4.9: Trajectories in the phase plane for different values of λ superimposed on the phase diagram. Red curve: μ_1-nullcline, Green curve: μ_2-nullcline, Orange cycle: unstable manifold of the saddle fixed point (heteroclinic orbit) and Cyan curve: stable manifold of the saddle fixed point (note that it is almost superposed with part of the μ_1-nullcline), constituting the separatrix between those orbits that directly return to the stable fixed point and those following the heteroclinic cycle. Black: noisy trajectories. Upper left: $\lambda = 0.2$: no excursion, corresponds to the fixed point regime. Upper right: $\lambda = 1$: rare excursions do occur, corresponding to the bistable regime. Bottom left: $\lambda = 1.6$: excursions are frequent but occur irregularly (corresponding to the oscillatory regime). Bottom right: $\lambda = 5$: the heteroclinic cycle structure is lost, corresponding to the fixed point regime.

field equation whose solutions are Gaussian processes such that their mean and variance satisfy a closed set of nonlinear ordinary differential equations. Uniform convergence properties were obtained. We started by studying the solutions of the mean field equations, in particular their dependence with respect to the noise parameter using tools from dynamical systems theory. We showed that the noise had non-trivial effects on the dynamics of the network, such as stabilizing fixed points, inducing or canceling oscillations. A codimension two bifurcation diagram was obtained when simultaneously varying an input parameter and the noise intensity. The analysis of this diagram yielded several qualitatively distinct codimension one bifurcation diagrams for different ranges of noise intensity. Noise therefore clearly induces transitions in the global behavior of the network, structuring its Gaussian activity by inducing smooth oscillations of its mean. These findings have several implications that will be discussed in the conclusion of this thesis (8.2.2).

These classes of behaviors were then compared to simulations of the original finite-size networks. We obtained a very good agreement between the simulations of the finite-size system and the solution of the mean field equations, for networks as small as a few hundreds to few thousands of neurons. Transitions between different qualitative behaviors of the network matched precisely the related bifurcations of the mean field equations, and no qualitative systematic finite-size effects were encountered. Moreover, it appears that the convergence of the solution to a Gaussian process as well as the propagation of chaos property happen for quite small values of N, as illustrated in Figure 4.10. This figure represents the distribution of the voltage potential at a fixed time $T = 40$ for $N = 500$, simulated for 20 sample trajectories. The Kolmogorov-Smirnov test validates the Gaussian nature of the solution with a p-value equal to $7 \cdot 10^{-4}$. In order to test for the independence, we used the Pearson, Kendall and Spearman tests of dependence. We obtain the correlation values 0.0439 (p-value 0.33) for the first population, 0.0212 (p-value 0.4785) for the second, and 0.0338 (p-value 0.45) for the cross-correlation between populations, all of them clearly rejecting the dependence null hypothesis. This independence has deep implications in the efficiency of neural coding, an idea that we will further develop in the conclusion (8.2.1) of this thesis.

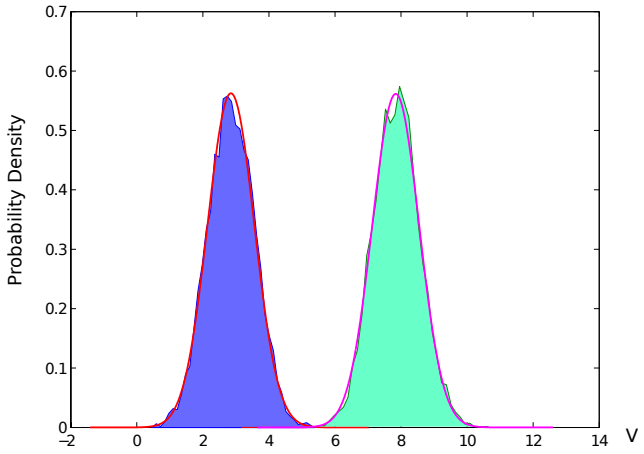

Figure 4.10: Empirical distribution of the values of $(V^i(T))_{i=1...N}$ for $N = 1000$ (500 neurons per population) in each population (blue and green filled distribution) versus theoretical mean field distribution. The Kolmogorov-Smirnov validates the fit of the distributions (see text).

Chapter 5

A mean field equation with inhomogeneity at the synaptic level

Overview

In this chapter, we are interested in characterizing the solutions of the mean-field equations obtained by Faugeras, Touboul and Cessac [Faugeras et al., 2009]. This model features random synaptic connections: the synaptic couplings between a neuron of population α and a neuron of population β are independent and distributed according to a Gaussian law of standard deviation $\sigma_{\alpha\beta}$. In the first section 5.1, we discuss the meaning of this synaptic inhomogeneity and present an **heuristic derivation** of the corresponding mean field equations. We then present in section 5.2 simulations of the mean field equations and of the related finite size network, in order to unravel the influence of σ on the dynamics. We observe that σ **also has a structuring effect on the dynamics** and can induce synchronized oscillations at the network level. However, due to the non-Markov nature of the equations, analytical results are difficult to obtain.

Contents

5.1 Model and mean field equations

5.1.1 Synaptic inhomogeneity

In this chapter we still consider networks of firing-rate neurons with a linear intrinsic dynamics. However we now model the synaptic weights by independent and population-wise identically distributed Gaussian random variables. The standard deviation of these random variables introduces a *disorder* term at the synaptic level. The **statistics** of these random variables depend only on the pre- and postsynaptic populations but two synaptic weights coupling together the same populations may take different values. We have:

$$J_{ij} \sim \mathcal{N}\left(\frac{J_{\alpha\beta}}{N_\beta}, \frac{\sigma_{\alpha\beta}}{\sqrt{N_\beta}}\right) \tag{5.1}$$

Keeping the same notations as before, the equations describing the network are hence:

$$dV^i(t) = \Big(-\frac{1}{\tau_\alpha} V^i(t) + \sum_{\beta=1}^{P} U_{i\beta}^{N_\beta}(t) + I_\alpha(t) \Big) dt + \lambda_\alpha dB^i(t) \tag{5.2}$$

where:

$$U_{i\beta}^{N_\beta}(t) = \sum_{j=1}^{N_\beta} J_{ij} S(V^j(t))$$

is the *interaction process*. We recall that τ_α is the time constant characteristic of population $p(i) = \alpha$, and λ_α is the (stationary) intensity of the additive noise. The network is made of P distinct populations and N_β is the number of neurons in population β.

The standard deviation $\sigma_{\alpha\beta}$ is a parameter that accounts for the level of disorder of the network, i.e. the dispersion of individual synaptic weights. If this parameter is very small, the network is almost homogeneous. We stress that the type of randomness considered here is totally different from the additive dynamic noise introduced in the preceding chapter 4. Here, the weights are drawn in a Gaussian law at initial time and then *frozen* during the whole evolution. The parameter $\sigma_{\alpha\beta}$, whose influence on the dynamics of the network will be our main focus in this chapter, can be called **synaptic inhomogeneity**.

5.1.2 Heuristic derivation of the mean field equations

The mean field equations corresponding to the network 5.2 with synaptic inhomogeneity have been presented by Faugeras, Touboul and Cessac [Faugeras et al., 2009]. The foundation of their result uses large deviation techniques, as discussed in section 3.3.1. We recall that Ben Arous and Guionnet [Arous and Guionnet, 1995, Arous and Guionnet, 1997, Guionnet, 1997] proved the annealed (averaged on all possible interactions) and quenched (J-almost surely) propagation of chaos in a similar setting applied to spin glasses.

In [Faugeras et al., 2009] the resulting mean field equation obtained is shown to have one and only one solution under some non-degeneracy conditions on the initial condition and the noise. Combined with a quenched propagation of chaos result, this means that provided that the initial conditions of all neurons are Gaussian, independent and population-wise identically distributed, the law of $(V^{i_1}(t), \dots, V^{i_k}(t), t \leq T)$ for any fixed $k \geq 2$ and $(i_1, \dots, i_k)$, converges towards $\nu_{p(i_1)} \otimes \dots \otimes \nu_{p(i_k)}$ when $N \to \infty$, where we denoted ν_α the law of the solution of the corresponding mean field equation for population α. We will now present an heuristic derivation of the resulting mean field equation.

An overview of this heuristic derivation was given in the introduction 2.2.2. Basically, it consists in applying a central limit theorem, *provided a certain independence hypothesis*. This hypothesis is called Amari's local chaos hypothesis and states that:

For N sufficiently large, all the V^i are pairwise stochastically independent, are independent of the connectivity parameters J_{ij}, and have a common distribution population per population.

Due to the form of the network equations, we obviously cannot assume a priori that this is true. Nevertheless it will allow us to derive the right mean field equations.

Indeed, under the local chaos hypothesis, the interaction process $U_{i\beta}^{N_\beta}(t) := \sum_{j=1}^{N_\beta} J_{ij} S_\beta(V^j(t))$ is the sum of independent identically distributed random variables. The *functional central limit theorem* applies, provided the convergence of the two first moments of the sum. The problem reduces to the computation of the limits of the mean and standard deviation of the interaction process when the number of neurons tends to infinity and was treated in section 2.2.2. From the convergence of the two first moments of the interaction process and the central limit theorem, we conclude to the convergence

of the sequence of processes $U_{i\beta}^{N_\beta}(t)$ to the **effective Gaussian interaction process** $U_{\alpha\beta}^{\bar{V}_\beta}(t)$, a Gaussian process of parameters:

$$\begin{cases} \mathbb{E}\left[U_{\alpha\beta}^{\bar{V}_\beta}(t)\right] = J_{\alpha\beta}\mathbb{E}[S_\beta(\bar{V}_\beta(t))]; \\ Cov(U_{\alpha\beta}^{\bar{V}_\beta}(t), U_{\alpha\beta}^{\bar{V}_\beta}(s)) = \sigma_{\alpha\beta}^2\mathbb{E}\Big[S_\beta(\bar{V}_\beta(t))S_\beta(\bar{V}_\beta(s))\Big]; \\ Cov(U_{\alpha\beta}^{\bar{V}_\beta}(t), U_{\gamma\delta}^{\bar{V}_\delta}(s)) = 0 \text{ if } \alpha \neq \gamma \text{ or } \beta \neq \delta. \end{cases}$$

where $\bar{V}_\beta(t)$ is the stochastic process giving the membrane potential of a neuron in population β.

We can now conclude our heuristic derivation. This is the subject of the following theorem.

Theorem 5.1.1. *Under the local chaos hypothesis, the process $V^i(t)$ for i in population α, solution of equation 5.2, converges in law towards the process $\bar{V}^\alpha$ solution of the mean field implicit equation:*

$$d\bar{V}^\alpha(t) = \Big[-\frac{1}{\tau_\alpha}\bar{V}^\alpha(t) + \sum_{\beta=1}^{P} U_{\alpha\beta}^{\bar{V}_\beta}(t) + I_\alpha(t)\Big]dt + \lambda_\alpha dB^\alpha(t) \tag{5.3}$$

Proof. : The solution of the network equations can be written:

$$V^i(t) = V^i(0)e^{-t/\tau_\alpha} + \sum_{\beta=1}^{P}\int_0^t e^{(s-t)/\tau_\alpha}U_{i\beta}^{N_\beta}(s)ds + \int_0^t e^{(s-t)/\tau_\alpha}I_\alpha(s)ds + \lambda_\alpha\int_0^t e^{(s-t)/\tau_\alpha}dB^\alpha(s)$$

Because of the convergence in law of the interaction process, we have the convergence in law of the integral term $\int_0^t e^{(s-t)/\tau_\alpha}U_{i\beta}^{N_\beta}(s)ds$ towards the effective term $\int_0^t e^{(s-t)/\tau_\alpha}U_{\alpha\beta}^{\bar{V}_\beta}(s)ds$ provided that Lebesgue's theorem applies.

Therefore, for any neuron i in population α, the potential converges in law towards the solution $\bar{V}^\alpha$ of the stochastic fixed-point equation:

$$\bar{V}^\alpha(t) = \bar{V}^\alpha(0)e^{-t/\tau_\alpha} + \sum_{\beta=1}^{P}\int_0^t e^{(s-t)/\tau_\alpha}U_{\alpha\beta}^{\bar{V}_\beta}(s)ds + \int_0^t e^{(s-t)/\tau_\alpha}I_\alpha(s)ds + \lambda_\alpha\int_0^t e^{(s-t)/\tau_\alpha}dB^\alpha(s) \tag{5.4}$$

□

By definition, under local chaos hypothesis, in the limit where the number of neurons tends to infinity, all the neurons of the same population have the same distribution and behave independently and we have proved that for any neuron in population α, its membrane potential is solution of the mean field equation 5.3.

The P equations 5.3, which are P implicit stochastic differential equations, describe the asymptotic behavior of the network. The characterization and simulation of their solutions is a real challenge. The effective interaction process is indeed an intricate functional of the solution of the equation. However, similarly as in the preceding chapter, we can show that the solutions of these new mean field equations are **Gaussian processes**, provided that the initial conditions are Gaussian. To characterize the solutions we need therefore only to compute their means and covariances. But this time, contrary to the case of a purely additive noise, we cannot reduce the mean field dynamics to a system of coupled ordinary differential equations. In fact the interplay between the mean and the covariance is way more complex since the covariance of the process depends on the whole history of the solutions. The detailed equations satisfied by the mean and covariance of a solution are the subject of the following proposition:

Proposition 5.1.2. *Let us assume that $\bar{V}(0) = (\bar{V}^\alpha(0))_{\alpha=1\dots P}$ is a P-dimensional Gaussian random variable. We have:*

- *The solutions of the P mean field equations 5.3 with initial conditions $\bar{V}(0)$ are Gaussian processes for all time.*
- *Let $\mu(t) = (\mu_\alpha(t))_{\alpha=1\dots P}$ denote the mean vector of the process $(\bar{V}^\alpha(t))_{\alpha=1\dots P}$ and $C(t,s) = (C_{\alpha\beta}(t,s))_{\alpha=1\dots P,\beta=1\dots P}$ its covariance. $\bar{V}(t)$ is a diagonal process so $C_{\alpha\beta}(t,s) = \delta_{\alpha\beta}C_{\alpha,\alpha}(t,s)$ and we write $C_\alpha(t,s)$ to alleviate notations. We have:*

$$\begin{cases} \dot{\mu}_\alpha(t) = -\frac{1}{\tau_\alpha}\mu_\alpha(t) + \sum_{\beta=1}^P J_{\alpha\beta}\int_{\mathbb{R}} S_\beta\left(x\sqrt{C_\beta(t,t)} + \mu_\beta(t)\right) Dx + I_\alpha(t) \\ C_\alpha(t,s) = e^{-(t+s)/\tau_\alpha}\Big[C_\alpha(0,0) + \frac{\tau_\alpha\lambda_\alpha^2}{2}\left(e^{2(t\wedge s)/\tau_\alpha} - 1\right) \\ + \sum_{\beta=1}^P \sigma_{\alpha\beta}^2 \int_0^t\int_0^s e^{(u+v)/\tau_\alpha}\Delta_\beta(u,v)dudv\Big], \\ \Delta_\beta(u,v) = \int_{\mathbb{R}}\int_{\mathbb{R}} S_\beta\left(\frac{\sqrt{C_\beta(u,u)C_\beta(v,v)-C_\beta(u,v)^2}}{\sqrt{C_\beta(u,u)}}x + \frac{C_\beta(u,v)}{\sqrt{C_\beta(u,u)}}y + \mu_\beta(v)\right) \\ S_\beta\left(y\sqrt{C_\beta(u,u)} + \mu_\beta(u)\right) Dx\, Dy. \end{cases} \tag{5.5}$$

with initial condition $\mu_\alpha(0) = \mathbb{E}\left[\bar{V}^\alpha(0)\right]$ and $v_\alpha(0) = C_\alpha(0,0) = \mathbb{E}\left[(\bar{V}^\alpha(0) - \mu_\alpha(0))^2\right]$. In equation 5.5, the dot denotes the differential

with respect to time and Dx is the probability density of a centered Gaussian variable of variance unity: $Dx = \frac{e^{-x^2/2}}{\sqrt{2\pi}}dx$

Proof. When written under the integral form 5.4, it is clear that the solution is a Gaussian process provided the initial condition is a Gaussian random variable, due to the Gaussian nature of the effective interaction process and the property of the stochastic Itô integral.

Taking the expectation of both sides of the equality 5.4, we obtain the equation satisfied by the mean of the process $\mu_\alpha(t) = \mathbb{E}\left[\bar{V}^\alpha(t)\right]$:

$$\begin{aligned}\dot{\mu}_\alpha(t) = -\frac{\mu_\alpha(t)}{\tau_\alpha} + \sum_{\beta=1}^{P} \mathbb{E}\left[U_{\alpha\beta}^{\bar{V}_\beta}(t)\right] + I_\alpha(t) = \\ -\frac{\mu_\alpha(t)}{\tau_\alpha} + \sum_{\beta=1}^{P} J_{\alpha\beta}\mathbb{E}[S_\beta(\bar{V}_\beta(t))] + I_\alpha(t) = \\ -\frac{\mu_\alpha(t)}{\tau_\alpha} + \sum_{\beta=1}^{P} J_{\alpha\beta}\int_R S_\beta(x)N(\mu_\beta(t), C_\beta(t,t), x)dx + I_\alpha(t)\end{aligned}$$

where $N(\mu_\beta(t), C_\beta(t,t), x)$ denotes the one-dimensional Gaussian law in variable x of mean $\mu_\beta(t)$ and variance $C_\beta(t,t)$.

A similar computation for the covariance shows that:

$$\begin{aligned}C_\alpha(t,s) = e^{-(t+s)/\tau_\alpha}\Big[C_\alpha(0,0) + \frac{\tau_\alpha\lambda_\alpha^2}{2}\left(e^{2(t\wedge s)/\tau_\alpha} - 1\right) \\ + \sum_{\beta=1}^{P}\int_0^t\int_0^s e^{(u+v)/\tau_\alpha}Cov(U_{\alpha\beta}^{\bar{V}_\beta}(u), U_{\alpha\beta}^{\bar{V}_\beta}(v))dudv\Big] = \\ e^{-(t+s)/\tau_\alpha}\Big[C_\alpha(0,0) + \frac{\tau_\alpha\lambda_\alpha^2}{2}\left(e^{2(t\wedge s)/\tau_\alpha} - 1\right) \\ + \sum_{\beta=1}^{P}\int_0^t\int_0^s e^{(u+v)/\tau_\alpha}\sigma_{\alpha\beta}^2\mathbb{E}\Big[S_\beta(\bar{V}_\beta(u))S_\beta(\bar{V}_\beta(v))\Big]dudv\Big] = \\ e^{-(t+s)/\tau_\alpha}\Big[C_\alpha(0,0) + \frac{\tau_\alpha\lambda_\alpha^2}{2}\left(e^{2(t\wedge s)/\tau_\alpha} - 1\right) \\ + \sum_{\beta=1}^{P}\sigma_{\alpha\beta}^2\int_0^t\int_0^s e^{(u+v)/\tau_\alpha}\Delta_\beta(u,v)dudv\Big]\end{aligned}$$

where:

$$\Delta_\beta(u,v) = \int_{\mathbb{R}}\int_{\mathbb{R}} S_\beta(x)S_\beta(y)N(\mu_\beta(u), \mu_\beta(v), \Sigma_\beta(u,v), x, y)dx\,dy$$

This time $N(\mu_\beta(u), \mu_\beta(v), \Sigma_\beta(u,v), x, y)$ denotes the two-dimensional Gaussian law in variable x and y of mean $\mu_\beta = \begin{pmatrix} \mu_\beta(u) \\ \mu_\beta(v) \end{pmatrix}$ and of covariance matrix $\Sigma_\beta(u,v) = \begin{pmatrix} C_\beta(u,u) & C_\beta(u,v) \\ C_\beta(u,v) & C_\beta(v,v) \end{pmatrix}$. We conclude the proof by a simple change of variable. □

We obtain therefore **coupled** equations on the mean and the covariance of the process. The mean is given by a differential equation, whereas the covariance is given by an intricate integral equation (a **non-linear Volterra equation**, see [Burton, 2005]). The mean satisfies obviously the same equation as in the chapter 4, corresponding to the case $\sigma_{\alpha\beta} = 0$. Indeed the mean field equation 4.2 can be rewritten, using the definition of the effective interaction process:

$$d\bar{V}^\alpha(t) = \Big[-\frac{1}{\tau_\alpha}\bar{V}^\alpha(t) + \sum_{\beta=1}^{P} \mathbb{E}[U_{\alpha\beta}^{\bar{V}_\beta}(t)] + I_\alpha(t) \Big] dt + \lambda_\alpha dB^\alpha(t)$$

However, the system defined by 5.1.2 is way more difficult to analyze than the one defined in 4.2.2. This is due to the fact that the covariance function $C_\alpha(t,s)$ depends this time on the **whole history of the system** from the initial time up to t and s as can be seen in the integral form of the equation giving the covariance. This is a signature of the non-Markovian nature of the system. Furthermore, though the equation of the mean involves only the *variance* $v_\alpha(t) = C_\alpha(t,t)$, it is necessary in order to compute it to know the whole *covariance* functions $C_\beta(u,v)$ and mean functions $\mu_\beta(u), \mu_\beta(v)$ for $(u,v) \in [0,t]^2$.

5.2 Simulations of the equations and comparison with a finite-size network

In order to understand the influence of the synaptic inhomogeneity $\sigma_{\alpha\beta}$ on the behavior of the solution of 5.3, we have simulated the system given in 5.1.2 for different values of the parameter. However, compared to the case presented in chapter 4, even the simulation of these equations is quite challenging due mainly to their non-Markovian nature. We nevertheless simulated these equations using a Picard iteration method, inspired by the constructive proof which gives existence and uniqueness of the solution. We spent much time in this thesis trying to optimize this simulation code in Matlab®, but were never totally satisfied by the results, as the simulation was very time-consuming and

sometimes failed to reach the level of precision desired, especially for large time. This may be due to the accumulation of numerical instabilities involved in the computation of the integrals (a *quadruple* integral at each time step). For relatively small time (e.g. $T = 20$), we yet succeeded in computing the whole covariance function and we now present these results.

5.2.1 The synaptic inhomogeneity can destroy oscillations

5.2.1.1 Simulations of the mean field equations

Here, we present the simulations for a network of 2 populations where the parameters (the synaptic weights $\bar{J}_{\alpha\beta}$ and the external inputs I_α) are chosen such that the noiseless system (neither additive noise nor synaptic inhomogeneity) presents a **limit cycle**. We set λ_α to zero[1], as we have already studied separately the influence of the additive noise and are here only interested in the influence of the parameters $\sigma_{\alpha\beta}$. To simplify, we assume that all the elements of the $2 * 2$ synaptic variance matrix are equal to σ and we are interested in the behavior of the system when this parameter σ is varied. The main result is that the periodic structure of the solution is lost when σ is increased. This is shown in Figure 5.1, concerning the covariance. We have of course checked that the periodicity of the mean was lost for the same value of σ.

5.2.1.2 Simulations of a finite network

We have also simulated the corresponding 2-populations finite-size network. All the parameters are the same as in the preceding section and the network is composed of 200 neurons, one hundred in each population. If the mean field is an accurate description of the network we expect to find that the periodic structure of the solutions will be destroyed for the same value of σ. We observe that for large values of σ the cycle is always lost but for intermediate values it is not possible to conclude unequivocally. Indeed, the network can either converge towards a fixed point or present oscillations, for the same value of σ, and the same initial conditions. This is linked to the particular realization of the Gaussian synaptic weights (which obviously changes at each new simulation of a finite network). This ambivalence, where the finite network may present different behaviors, whereas the limiting mean field equation presents only one possible behavior (for a given initial condition), is a **finite-size effect**. In the next Figure 5.2, we present the 4 covariance functions $C_{\alpha\beta}(t, s)$ for $\alpha, \beta = 1, 2$ for the same value of σ set to 2 for which the mean field solution still presents

[1]Rigorously the mean field equations are well posed only for a non-vanishing λ but we can take it arbitrary small in the simulations.

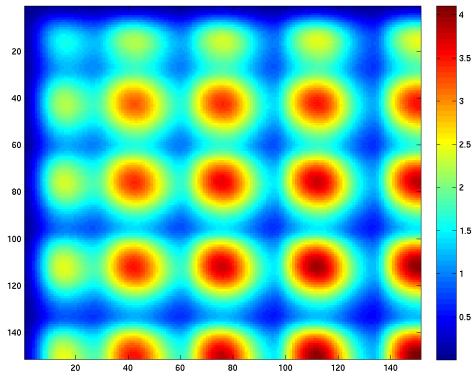

(a) Covariance $C_1(t,s)$ for $\sigma = 2$. The periodic structure is *preserved*. The variance is the diagonal of this matrix and we have checked that it has the same period as the mean.

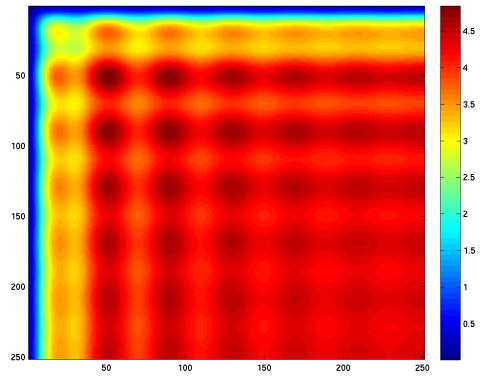

(b) Covariance $C_1(t,s)$ for $\sigma = 2.5$. The periodic structure of the covariance tends to disappear with time. A simulation on a longer time scale would be necessary to see how evolve the damped oscillations.

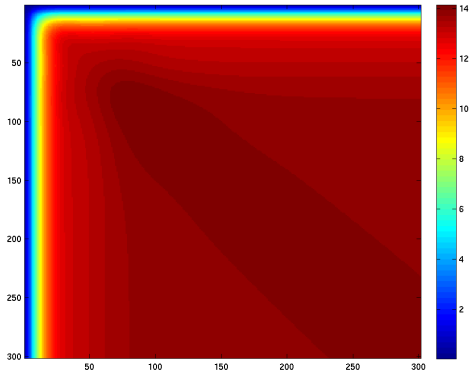

(c) Covariance C_1(t,s) for $\sigma = 4$. The covariance reaches a plateau and is stationary, for large enough time. Meanwhile the means have converged to fixed point values.

Figure 5.1: Simulation of the covariance function solution of the mean field equation, for increasing values of σ. When this parameter is too high, the oscillations (that were present in the deterministic system) are destroyed.

oscillations. We have also checked that the covariance between two distinct populations is null.

5.2.2 The synaptic inhomogeneity can induce oscillations

Eventually in order to check if the synaptic inhomogeneity could also create cycles, as it was observed in the additive noise case, we extensively simulated a large network (10 000 neurons with 5000 neurons in each population) for different values of σ and computed the Fourier transform of the empirical mean (see Figure 5.3). We also averaged the results over several Monte-Carlo simulations to reduce possible finite-size effects. We chose exactly the same parameters as those of Figure 4.8. The only difference is hence that in spite of varying λ, it is σ that is gradually increased. It turned out that we found very similar results in both cases which seems quite surprising at first when we think at the very different microscopic dynamics. Indeed not only did we find appearance and disappearance of oscillations, but **the route to oscillations is the same in both cases** with in 5.3 the onset of oscillations through a seemingly homoclinic bifurcation (arbitrary small frequencies are present) and their disappearance through a seemingly Hopf bifurcation (with a sudden switch in frequency). When oscillations are present at the network level, individual trajectories tend to synchronize (although less sharply than in the additive noise). Simulations of the trajectories of a finite network of 500 neurons with the same choice of parameters, as a function of σ, are presented in Figure 5.4.

5.2.3 Simulations of a one-population network

In this section we want to illustrate the proposition of Sompolinsky and colleagues [Sompolinsky et al., 1988] that for a one-population network with weights described by centered Gaussian variables of standard deviation σ and whose sigmoidal transform is centered ($S(0) = 0$), there is a transition between a stationary regime and a *chaotic regime*[2] for σ large enough at $\sigma^* \times S'(0) = 1/\tau$. The simulations of Figure 5.5 will allow us to better visualize the type of dynamics corresponding to these two regimes.

[2] in the dynamical system sense

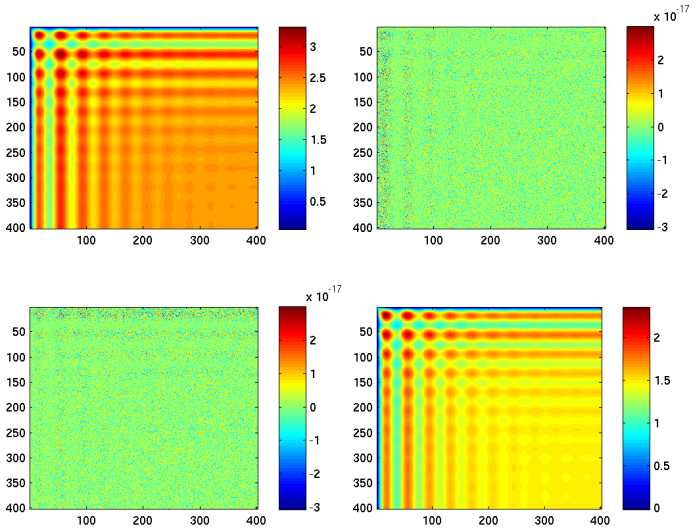

(a) Stationary case. We have plotted the 4 covariances $C_{\alpha\beta}(t,s)$ for $\sigma = 2$. Top left: $C_{11}(t,s)$. Top right: $C_{12}(t,s)$. Bottom left: $C_{21}(t,s)$. Bottom right: $C_{22}(t,s)$.

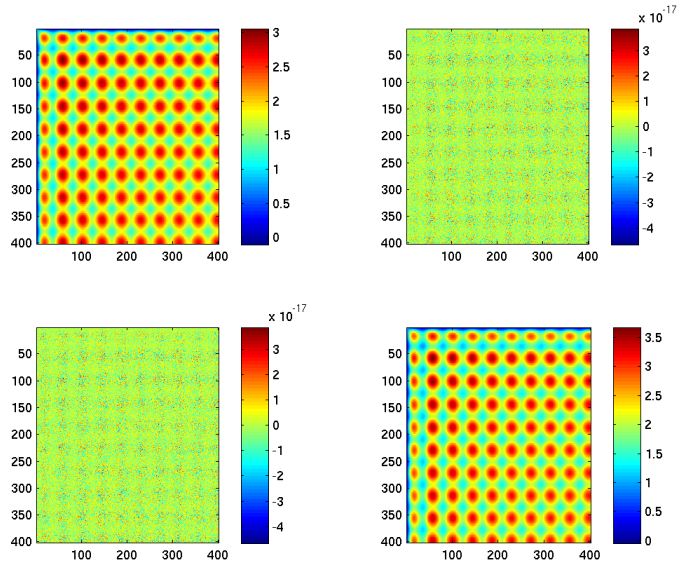

(b) Oscillatory case. We have plotted the 4 covariances $C_{\alpha\beta}(t,s)$ for $\sigma = 2$. Same legend as above.

Figure 5.2: Simulation of a 2-populations finite network with 100 neurons in each population. Two distinct behaviors are observed for the *same* value of σ and the same initial conditions. This is linked to various realizations of the spectrum of the random connectivity matrix. We remark that the covariance matrix between distinct populations is null, as expected.

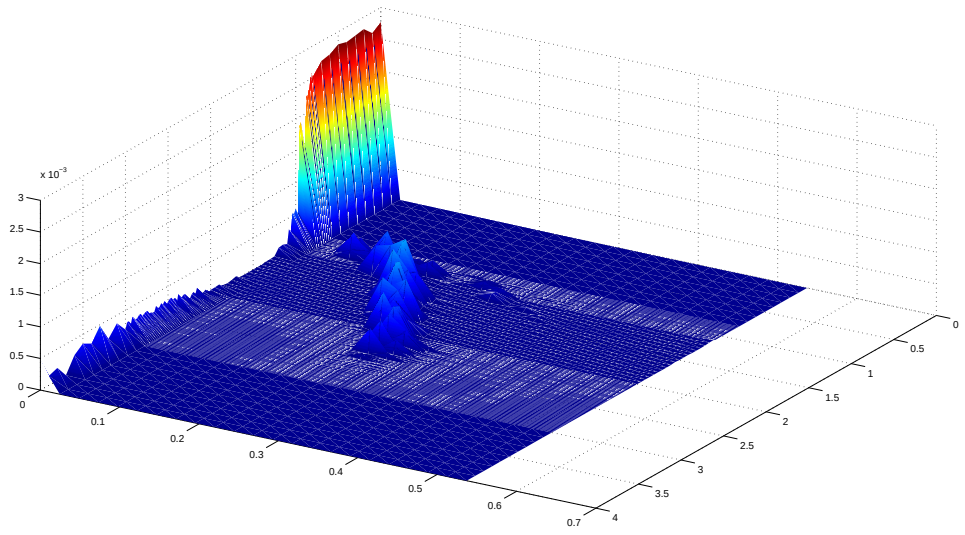

Figure 5.3: Squared modulus of the Fourier transforms of the empirical mean for simulations of the network as function of the frequency (Hz) and the noise parameter σ. We observe that oscillations appear in the network first through what appears to be a homoclinic bifurcation (arbitrary small frequencies) and also disappear through what seems to be a Hopf bifurcation (discontinuity in the power spectrum).

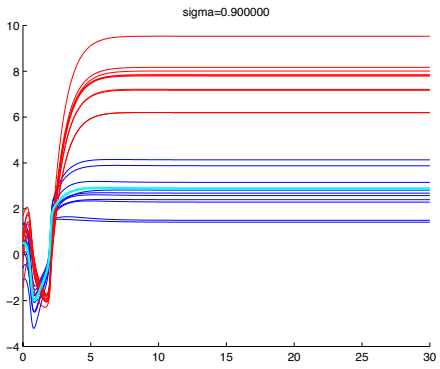

(a) $\sigma = 0.9$

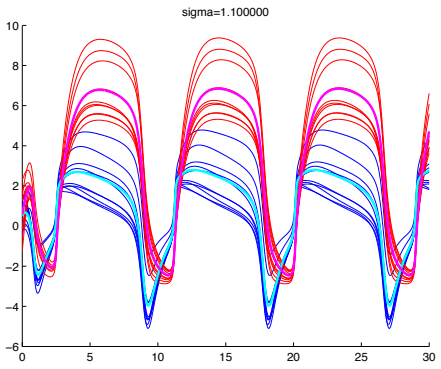

(b) $\sigma = 1.1$

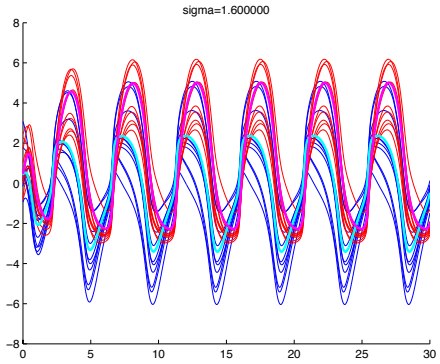

(c) $\sigma = 1.6$

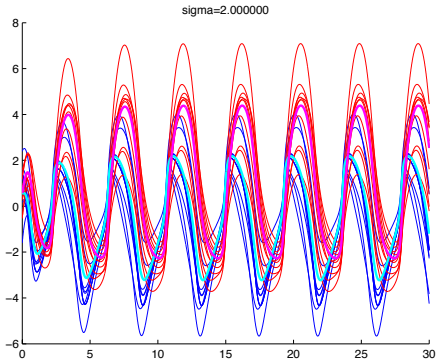

(d) $\sigma = 2$

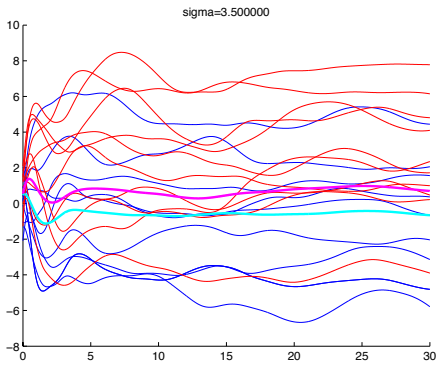

(e) $\sigma = 3.5$

Figure 5.4: Red and blue curves: **trajectories** of 10 neurons in each population (respectively population 1 and 2). The corresponding empirical mean of the network are the thicker curves in cyan and magenta.

In fact it is possible to find the critical value of σ by applying Girko's circular Law [3]. The Jacobian matrix of the finite-size network at 0 can be written:

$$Jac(0) = diag(-1/\tau) + S'(0) \times (J_{ij})_{i,j=1...N}$$

and in the limit $N \to +\infty$ the eigenvalues of J_{ij} will be uniformly distributed in the complex plane on the disk centered at the origin and of radius σ, so that the null solution will be destabilized for a σ such that at least one eigenvalue has a positive real part, and this happens for $-1/\tau + \sigma^* \times S'(0) = 0$.

Thanks to numerical studies we conjectured that this criterion was in fact still true for non-centered weights, i.e. $J \neq 0$. Our conjectured proposition is:

Proposition 5.2.1.

- *The mean* $\mu_0 = 0$ *is stable if and only if* $\alpha = -\frac{1}{\tau} + JS'(0) < 0$
- *The variance* $C_0(t,t) = 0$ *is stable if and only if* $\alpha < 0$ *and* $\sigma S'(0) < 1/\tau$

The statement on the mean is obvious by a linear stability analysis. However Girko's Law on *centered* random matrices does not apply here. Our goal was to linearize the system 5.1.2 about the null solution. We managed to obtain an equation (of Volterra type) giving us the evolution of the perturbation on the variance. This equation can even be explicitely solved using Bessel functions. However we were not able to find the right results and this is likely linked to the fact that for $C(t,s) = 0$ the equation becomes singular (a Gaussian random variable of null variance is a Dirac).

We also tried to linearize the system 5.1.2 about the solution $(\mu_0(t), C_0(t,s) = e^{-2(t+s)/\tau_\alpha})$ corresponding to $\lambda = 0$ and $\sigma = 0$, to obtain an equation depending on σ for the perturbation $\delta\mu(t)$ and to study its stability. Though we managed to do all the (involved) calculations and obtained a linear Volterra integro-differential equation for $\delta\mu$, usual stability theorems for Volterra equations (e.g. [Burton, 2005]) did not apply.

[3] Let λ be (possibly complex) eigenvalues of a set of random $N \times N$ real matrices with entries independent and taken from a standard normal distribution. Then as $N \to +\infty$, $\lambda/\sqrt{N}$ is uniformly distributed on the unit disk in the complex plane.

As we have already mentioned the analytical study of the system 5.1.2 is way more difficult than in the case of additive noise where the dynamics was summed up in a system of ordinary differential equations. It was then possible to apply the usual bifurcation theory to unravel the influence of the parameters, especially the noise λ. But this time, due to the non-Markovian nature of the equations, the variance at time t is an intricate functional of the mean $\mu(u)$ for $u \in [0, t]$. It would then be necessary to develop a bifurcation analysis in an infinite-dimensional setting. We have presented therefore in this section only numerical results. However we present in Appendix B.1 a way to reduce the non-linear Volterra equation giving the covariance to a simpler *linear Volterra equation* when σ is small.

We hence study numerically a one-population finite network. The centered sigmoidal transform has a slope at the origin of $g = S'(0) = 1/\sqrt{2\pi} \approx 0.4$. We set $\lambda = 0$ and $\tau = 1$. With these values of the parameters we expect, if $\alpha = -\frac{1}{\tau} + JS'(0) \approx -1 + 0.4J < 0$, the null mean and null variance to be stable. Both will be destabilized for $\alpha > 0$, i.e. $J > 2.5$. However, if $\alpha < 0$, i.e. $J < 2.5$, we expect the null mean to remain stable while the null variance to be destabilized for $\sigma S'(0) > 1/\tau$, i.e for a synaptic inhomogeneity large enough: $\sigma > \sqrt{2\pi}$. This is illustrated in the following Figure 5.5 where we have run the simulations for a network of 300 neurons (the total time of simulation is $T = 60$ and the time step is $dt = 0.01$). We averaged the empirical mean and variance over 3 successive Monte-Carlo simulations to get rid off the finite-size effects.

It is interesting to note the differences in the individual trajectories for a large synaptic inhomogeneity compared to the trajectories of a network submitted only to additive noise. In this last case the variance converges in the stationary regime to $\lambda^2 \frac{\tau}{2}$ and hence increases smoothly with the noise parameter λ whereas in the simulations presented in Figure 5.5, the variance abruptly switches from a null value to a strictly positive value when we increase σ. The high-σ regime corresponds to the chaotic regime described by Sompolinsky in [Sompolinsky et al., 1988].

5.3 Summary

In this chapter we have explained heuristically how to derive the mean field equations when the synaptic weights coupling the neurons are drawn at the beginning of the evolution in a Gaussian law with a non-zero standard deviation σ. Basically if we assume Amari's local chaos hypothesis we just have to

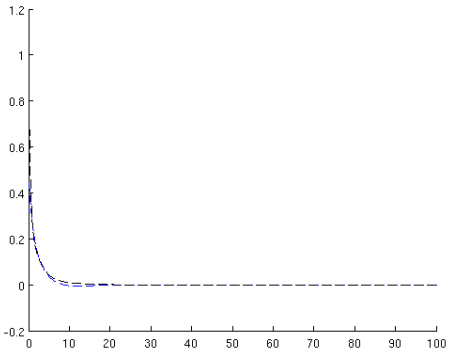

(a) Empirical mean (in blue) and variance (in black) for $J = 1$ and $\sigma = 0.9\sqrt{2\pi}$. **Both** the zero mean and zero variance are **stable**.

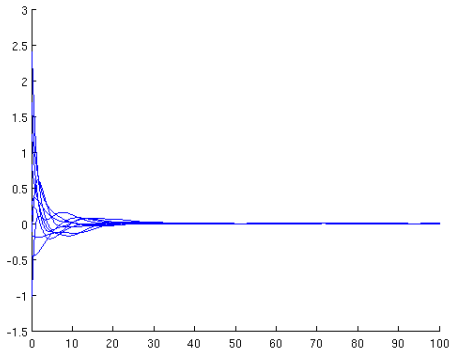

(b) Corresponding trajectories of 10 individual neurons in the network. Despite initial fluctuations they converge to a **stationary null value**.

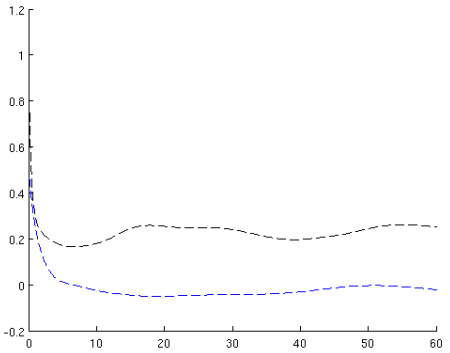

(c) Empirical mean (in blue) and variance (in black) for $J = 1$ and $\sigma = 1.1\sqrt{2\pi}$. The zero mean is still stable (though we observe fluctuations due to finite-size) but the zero variance is **destabilized**.

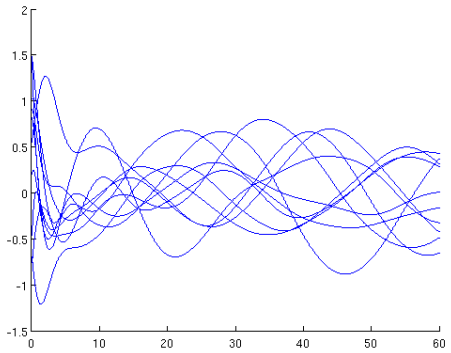

(d) Corresponding trajectories of 10 individual neurons in the network. Due to a non-zero variance, the trajectories **fluctuate** about the mean value.

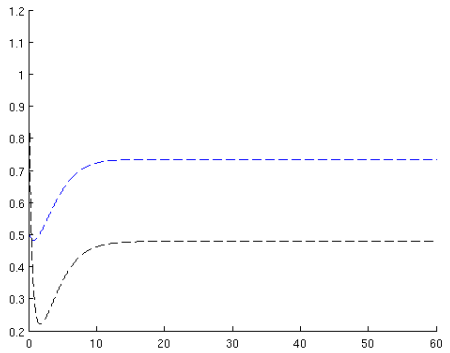

(e) Empirical mean (in blue) and variance (in black) for $J = 3$ and $\sigma = 0.9\sqrt{2\pi}$. **Both** the zero mean and zero variance have been **destabilized**.

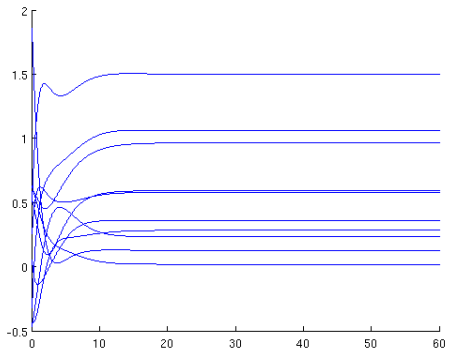

(f) Corresponding trajectories of 10 individual neurons in the network.

Figure 5.5: Illustration of proposition 5.2.1 for a **finite network** of 300 neurons.

apply a functional central limit theorem. The real proof uses large deviation techniques which are rather intricate. Moreover the resulting equations are non-Markovian which makes them difficult to simulate and analyze.

We have nevertheless simulated these equations (this time it is necessary to compute the whole covariance of the process) and when extensive simulations were out of reach we looked at a large but finite network. We found that the parameter σ had a structuring effect on the dynamics, in particular that it was able to generate oscillations of the mean solution of the mean field equations, which corresponds to the onset of *regular synchronous oscillations at the network level*. The synaptic inhomogeneity induces transitions in the global behavior of the network, structuring its Gaussian activity by inducing smooth oscillations of its mean *and its variance*. These findings have several implications that will be discussed in the conclusion of this thesis (8.2.2), where they will also be compared with findings of chapter 4. But, unlike the case of additive noise, it seems difficult to provide, even at a phenomenological level, an explanation for the structuring effect of σ.

Chapter 6

A mean field equation with synaptic noise

Overview

In this chapter we shall consider the effect of the stochastic variation of the synaptic efficiency on the mean field behavior. We first model **synaptic noise** in section 6.1. In order to study the effect of this noise in large-scale networks, we consider, as in the previous chapters, firing-rate neurons. Asymptotic equations as the number of neurons tends to infinity are derived in section 6.2. In the case of synaptic weights whose fluctuations are modeled by white noise, the dynamics again reduces to two coupled ordinary differential equations on the moments of the Gaussian solution, allowing to deal with the dynamics in a tractable form. We study the influence of synaptic noise on the collective behaviors, and compare these asymptotic regimes to simulations of the network in section 6.3. We study in particular the complex **codimension two bifurcation diagram** of the system as the external input and the level of synaptic noise are varied. We conclude by observing that, similarly to the previous cases, synaptic noise can trigger collective synchronized oscillations at the network level. However in that case, neurons will show a **high level of synchrony**, related to the fact that the standard deviation periodically vanishes.

Contents

6.1 Models of synaptic noise

Synaptic noise refers to the random fluctuations of the synaptic efficiency. The sources of this type of noise have been mentioned in the introduction part 1.3.2. For example, in a seminal paper [Fatt and Katz, 1952], the authors evidence the presence of spontaneous subthreshold activity at a normal synapse: miniature postsynaptic potentials are recorded in the absence of presynaptic input and they attribute it to the spontaneous release of neurotransmitters vesicles. Synaptic noise arises mainly from two factors: first the biochemical and biophysical process of synaptic transmission are inherently probabilistic, second the number of elements at stake in such processes (such as the number of neurotransmitters released) is finite and small and hence subject to important fluctuations from trial to trial[1].

6.1.1 White noise

In order to account for the stochasticity of the synaptic weights, the simplest model we can think of consists in considering that the synaptic weights fluctuate around the deterministic value $J_{p(i)p(j)}/N_{p(j)}$, and, due to the stochastic, and presumably uncorrelated nature of the random phenomena involved, use a white noise model to account for the fluctuations. This white noise will be assumed, for technical reasons, to only depend on the postsynaptic neuron and on the presynaptic population, considering that most of the variability is due to random local properties of the environment at the level of the postsynaptic cell. Rigorously, it also depends on the presynaptic neuron, but taking into account this dependency would considerably increase the complexity of the mathematical analysis.

We therefore model the network's synaptic weights J_{ij}, for $p(i) = \alpha$ and $p(j) = \beta$, as the sum of a deterministic value and a white noise:

$$J_{ij} = \frac{J_{\alpha\beta}}{N_\beta} + \frac{\sigma_{\alpha\beta}}{N_\beta}\frac{dW^{i\beta}(t)}{dt}$$

where the $W^{i\beta}$ are a family of independent standard Brownian motions and $\sigma_{\alpha\beta}$ models the amplitude of the noise (the notation $\frac{dW^{i\beta}(t)}{dt}$ is an abuse of notation, it will be made rigorous in equation 6.2). Note also that, contrary to

[1] Of course we cannot rule out the presence of deterministic chaos. But since it would result from the conjunction of very intricate deterministic processes extremely dependent on initial conditions, we think that modeling synaptic fluctuations by stochastic processes can be a suitable approximation.

the preceding chapter 5, where the synaptic weights were drawn at the beginning of the evolution in a Gaussian law, the standard deviation of the weights scales here as $1/N_\beta$ and not $1/\sqrt{N_\beta}$. This is important for the asymptotic limit to exist.

6.1.2 Ornstein-Uhlenbeck process

Alternatively we can also choose to model the synaptic weights by solutions of stochastic differential equations. Here again one of the simplest model would be to use an Ornstein-Uhlenbeck process because it is a stationary Gaussian process. We would therefore introduce the variable $X_{ij}(t)$ obeying:

$$dX_{ij}(t) = \theta(J_{\alpha\beta} - X_{ij}(t))dt + \sigma_{\alpha\beta}dW^{i\beta}(t)$$

and model the synaptic weights by $J_{ij} = X_{ij}/N_\beta$ to get the proper scaling. Here again $W^{i\beta}(t)$ are a family of independent standard Brownian motions and $\sigma_{\alpha\beta}$ accounts for the level of synaptic noise. Note that here again, for technical reasons, the Brownian motion depends on the postsynaptic neuron indexed by i and on the presynaptic *population* (β).

The main drawback of the two precedents models for the weights is that weights may change sign, which does not fit with the fact that the (overall majority of) synapses are either excitatory or inhibitory. However their means remain of constant sign and a parameter like θ allows us to control the average time during which the weights keep a constant sign.

6.1.3 CIR process

There is therefore the need of introducing stochastic processes that remain of constant sign. We can for example take a CIR process, named after John C. Cox, Jonathan E. Ingersoll and Stephen A. Ross, and defined by the following stochastic differential equation:

$$dX_{ij}(t) = \theta(J_{\alpha\beta} - X_{ij}(t))dt + \sigma_{\alpha\beta}\sqrt{X_{ij}(t)}\, dW^{i\beta}(t)$$

and define $J_{ij} = X_{ij}/N_\beta$ for the scaling. In this case the synaptic weights are no longer Gaussian.

6.1.4 Bounded stochastic processes

However the drawback of modeling synaptic weights by Ornstein-Uhlenbeck or CIR stochastic processes is that the processes $X_{ij}(t)$ are not bounded,

though their expectation remains bounded for all time. As we will see the boundedness of the synaptic weights is required from a biological viewpoint, but it is also a crucial assumption in the propagation of chaos proof that we will present. Hence we will consider synaptic weights defined by *bounded stochastic processes*. There are many possible choices. We may cite, for instance, any bounded function of a stochastic process or almost surely bounded diffusions. For concreteness, we may take $J_{ij} = X_{ij}/N_\beta$ with:

$$X_{ij}(t) = J_{\alpha\beta} + \sigma_{\alpha\beta} F(W^{i\beta}(t)) \tag{6.1}$$

where F is a bounded function, e.g. a centered sigmoidal function. In the following we will assume:

$$|X_{ij}(t)| \leq M \qquad a.s.$$

6.2 The Mean-field equations

6.2.1 Network model with "white noise" synaptic weights

The microscopic network model is the same as in chapter 4, except that the fluctuations of the weights about a constant value are modeled by white noise.

The network behavior is therefore governed by the following set of stochastic differential equations:

$$dV^i(t) = \left(-\frac{1}{\tau_\alpha} V^i(t) + I_\alpha(t) + \sum_{\beta=1}^{P} J_{\alpha\beta} \frac{1}{N_\beta} \sum_{j,\, p(j)=\beta} S_\beta(V^j(t)) \right) dt + \lambda_\alpha(t) dB_t^i + \sum_{\beta=1}^{P} \sigma_{\alpha\beta} \left(\frac{1}{N_\beta} \sum_{j,\, p(j)=\beta} S_\beta(V^j(t)) \right) dW_t^{i\beta} \tag{6.2}$$

where the Brownian motions $W^{i\beta}$ are independent of the B^i.

These equations represent a set of interacting diffusion processes. As for the precedent chapters we can prove a propagation of chaos result and derive the limit mean field equation. This is the subject of the following theorem:

Theorem 6.2.1. *Under the above assumptions:*

(i). The equations (6.2) converge towards the mean-field implicit equations:

$$d\bar{V}_\alpha(t) = \left[-\frac{1}{\tau_\alpha}\bar{V}_\alpha(t) + I_\alpha(t) + \sum_{\beta=1}^{P} J_{\alpha\beta}\mathbb{E}\left[S_\beta(\bar{V}_\beta(t))\right] \right] dt + \sum_{\beta=1}^{P} \sigma_{\alpha\beta}\mathbb{E}\left[S_\beta(\bar{V}_\beta(t))\right] dW^{\alpha\beta}(t) + \lambda_\alpha(t) dB^\alpha(t) \quad (6.3)$$

where $W^{\alpha\beta}(t), B^\alpha(t)$ are independent Brownian motions for $\alpha, \beta = 1 \dots P$.

(ii). Equation (6.3) has a unique (pathwise and in law) solution which is square integrable.

(iii). The propagation of chaos applies, i.e. provided that the initial conditions of all neurons are independent and population-wise identically distributed (the initial conditions are said to be chaotic), then the law of $(V^{i_1}(t), \dots, V^{i_k}(t), t \geq 0)$ for any fixed $k \geq 2$ and $(i_1, \dots, i_k)$ converges in the limit $N \to \infty$ to $\nu_{p(i_1)} \otimes \dots \otimes \nu_{p(i_k)}$ where ν_α is the law of the solution of equation (4.2) corresponding to population α, meaning that $(V^{i_1}(t), \dots, V^{i_k}(t))$ are independent processes.

The proof of this theorem is very similar to the one presented in chapter 4 and uses a coupling argument. The only difference lies in the fact that interactions occur in a stochastic term, which can be treated using Burkholder-David-Gundy theorem.

We now turn our attention to the case where synaptic weights are modeled by bounded stochastic processes and each neuron's intrinsic dynamics is *nonlinear*.

6.2.2 Network model with synaptic weights defined by bounded stochastic processes

The weights $J_{i\beta}$ are scaled by N_β, the number of neurons in the population β, so that the mean-field limit remains finite. The intrinsic dynamics is given by the function f_α which is not assumed linear any more. Similarly the additive noise is governed by the function g_α. The microscopic equations describing

the network are:

$$dV^i(t) = \left(f_\alpha(V^i(t)) + I_\alpha(t) + \sum_{\beta=1}^{P} \sum_{j:p(j)=\beta} J_{i\beta}(t) S_\beta(V^j(t)) \right) dt + g_\alpha(V^i(t)) dB^i(t)$$
$$= \left(f_\alpha(V^i(t)) + I_\alpha(t) + \sum_{\beta=1}^{P} X_{i\beta}(t) \sum_{j:p(j)=\beta} \frac{1}{N_\beta} S_\beta(V^j(t)) \right) dt + g_\alpha(V^i(t)) dB^i(t) \tag{6.4}$$

with $X_{i\beta}(t)$ a stochastic process dependent on $W^{i\beta}(t)$, such that:

$$|X_{i\beta}(t)| \leq M \quad \forall t \quad a.s.$$

We assume that the functions f_α and g_α are *Lipschitz continuous*. We note also that, in contrast with chapter 5, we have here an *exchangeability* property, if we consider the state vector of size $P+1$ constituted by V^i and $(J_{i\beta})_{\beta=1,..P}$. The propagation of chaos result and the resulting mean field equation are the subject of the following theorem:

Theorem 6.2.2. *Under the above assumptions:*

(i). The process $V^i(t)$ for i in population α, solution of equation (6.4), converges in law towards the process $\bar{V}^\alpha$ solution of the mean-field implicit equation:

$$d\bar{V}^\alpha(t) = \left(f_\alpha(\bar{V}^\alpha(t)) + I_\alpha(t) + \sum_{\beta=1}^{P} X_{\alpha\beta}(t) \mathbb{E}[S_\beta(\bar{V}^\beta(t))] \right) dt + g_\alpha(\bar{V}^\alpha(t)) dB^\alpha(t) \tag{6.5}$$

as a process for $t \in [0,T]$, in the sense that there exists $(\bar{V}^i_t)_{t\geq 0}$ distributed as $(\bar{V}^\alpha_t)_{t\geq 0}$ such that

$$\mathbb{E}\left[\sup_{0\leq t\leq T} |V^i_t - \bar{V}^i_t|^2 \right] \leq \frac{\tilde{C}(T)}{N}$$

where $\tilde{C}(\cdot)$ is a function of time depending on the parameters of the system. And the variable $X_{\alpha\beta}$ is a stochastic process defined in the same way as $X_{i\beta}(t)$ but dependent only on $W^{\alpha\beta}(t)$. $B^\alpha(t)$ and $W^{\alpha\beta}(t)$ are independent Brownian motions for $\alpha, \beta = 1 \dots P$.

(ii). Equation (6.5) has a unique (pathwise and in law) solution which is square integrable.

(iii). The propagation of chaos applies, i.e. provided that the initial conditions of all neurons are independent and population-wise identically distributed (the initial conditions are said to be chaotic), then the law of $(V^{i_1}(t), \dots, V^{i_k}(t), t \geq 0)$ *for any fixed* $k \geq 2$ *and* $(i_1, \dots, i_k)$ *converges in the limit* $N \to \infty$ *to* $\nu_{p(i_1)} \otimes \dots \otimes \nu_{p(i_k)}$ *where* ν_α *is the law of the solution of equation (6.5) corresponding to population* α*, meaning that* $(V^{i_1}(t), \dots, V^{i_k}(t))$ *are independent processes.*

Proof. The existence and uniqueness of solutions can be performed in a classical fashion using Picard iterations of an integral form of equation 6.5 and a contraction argument. The proof of the convergence towards this law, and of the propagation of chaos uses a coupling argument that consists in defining independent processes $\bar{V}^i(t)$ solution of equation (6.5) driven by the same Brownian motions $W^{i\beta}(t)$ defining the stochastic weights, the same Brownian motion $B^i(t)$ as involved in the network's equation (6.4) and with the same initial condition $V^i(0)$ as neuron i in the network.
We want to estimate $N_t = \max_{i=1\dots N} M_t^i$ where:

$$M_t^i = \mathbb{E}[\sup_{0\leq s\leq t} |V^i(s) - \bar{V}^i(s)|^2]$$

By writing the equation in the integral form, we have:

$$\begin{aligned}
|V^i(t) - \bar{V}^i(t)|^2 \leq\ & 4\Bigg(|\int_0^t (f_\alpha(V^i(s)) - f_\alpha(\bar{V}^i(s)))ds|^2 + \\
& |\int_0^t \sum_{\beta=1}^P X_{i\beta}(s) \sum_{p(j)=\beta} \frac{S_\beta(V^j(s)) - S_\beta(\bar{V}^j(s))}{N_\beta} ds|^2 + \\
& |\int_0^t \sum_{\beta=1}^P X_{i\beta}(s) \sum_{p(j)=\beta} \frac{S_\beta(\bar{V}^j(s)) - \mathbb{E}[S_\beta(\bar{V}^j(s))]}{N_\beta} ds|^2 + \\
& |\int_0^t (g_\alpha(V^i(s)) - g_\alpha(\bar{V}^i(s)))dB^i(s)|^2 \Bigg) = \\
& 4(A_t^2 + B_t^2 + C_t^2 + D_t^2).
\end{aligned}$$

By using Cauchy-Schwartz and the Lipschitz property of f_α (whose Lipschitz constant is denoted by $K_f(\alpha)$), we have:

$$A_s^2 \leq s \int_0^s |f_\alpha(V^i(u)) - f_\alpha(\bar{V}^i(u)))|^2 du \leq s K_f(\alpha)^2 \int_0^s |V^i(u) - \bar{V}^i(u)|^2 du$$

Hence we get taking the expectation and the supremum:

$$\mathbb{E}[\sup_{s\leq t} A_s^2] \leq tK_f(\alpha)^2 \int_0^t \mathbb{E}|V^i(u) - \bar{V}^i(u)|^2 du$$
$$\leq tK_f(\alpha)^2 \int_0^t \mathbb{E}[\sup_{0\leq v\leq u} |V^i(v) - \bar{V}^i(v)|^2] du = tK_f(\alpha)^2 \int_0^t M_u^i du$$

The upperbounding of B_s uses critically the fact that $X_{i\beta}(t)$ is bounded. Otherwise, we use Cauchy-Schwartz (C.S.) and the Lipschitz property of S_β whose Lipschitz constant is denoted by L_β to get:

$$\mathbb{E}[\sup_{s\leq t} B_s^2] = \mathbb{E}[\sup_{s\leq t} \left(\int_0^s \sum_{\beta=1}^P X_{i\beta}(u) \sum_{j:p(j)=\beta} \frac{S_\beta(V^j(u)) - S_\beta(\bar{V}^j(u))}{N_\beta} du \right)^2]$$
$$(C.S.) \leq \mathbb{E}[\sup_{s\leq t} s \int_0^s \left(\sum_{\beta=1}^P X_{i\beta}(u) \sum_{p(j)=\beta} \frac{S_\beta(V^j(u)) - S_\beta(\bar{V}^j(u))}{N_\beta} \right)^2 du]$$
$$(C.S. + |X| < M) \leq t\, P \int_0^t \sum_{\beta=1}^P M^2 \mathbb{E}[\left(\sum_{j:p(j)=\beta} \frac{S_\beta(V^j(u)) - S_\beta(\bar{V}^j(u))}{N_\beta} \right)^2] du$$
$$(C.S.) \leq t\, P\, M^2 \int_0^t \sum_{\beta=1}^P \mathbb{E}[N_\beta \sum_{j:p(j)=\beta} \left(\frac{S_\beta(V^j(u)) - S_\beta(\bar{V}^j(u))}{N_\beta} \right)^2] du$$
$$(S_\beta Lip.) \leq t\, P\, M^2 \int_0^t \sum_{\beta=1}^P \frac{1}{N_\beta} \sum_{j:p(j)=\beta}^P \mathbb{E}[L_\beta^2 |V^j(u) - \bar{V}^j(u)|^2] du$$
$$\leq t\, P\, M^2 \int_0^t \sum_{\beta=1}^P \frac{L_\beta^2}{N_\beta} \sum_{j:p(j)=\beta}^P \mathbb{E}[\sup_{0\leq v\leq u} |V^j(v) - \bar{V}^j(v)|^2] du$$
$$\leq t\, P\, M^2 \int_0^t \sum_{\beta=1}^P L_\beta^2 \max_{j:p(j)=\beta} M_u^j du$$
$$\leq t\, P\, M^2 \int_0^t \sum_{\beta=1}^P L_\beta^2 \max_{i=1\ldots N} M_u^i du$$

The upperbounding of C_s uses Cauchy-Schwartz, and the fact that the random

variables $c^j_\beta(s) = S_\beta(\bar{V}^j(s)) - \mathbb{E}[S_\beta(\bar{V}^j(s))]$ are independent and centered.

$$\mathbb{E}[\sup_{s\le t} C_s^2] = \mathbb{E}[\sup_{s\le t}\left(\int_0^s \sum_{\beta=1}^P X_{i\beta}(u) \sum_{p(j)=\beta} \frac{c^j_\beta(u)}{N_\beta} du\right)^2]$$

$$(C.S.) \le \mathbb{E}[\sup_{s\le t} s\int_0^s \left(\sum_{\beta=1}^P \frac{1}{N_\beta} \sum_{j:p(j)=\beta} J_{i\beta}(u) c^j_\beta(u)\right)^2 du]$$

$$(C.S.) \le t\,P \sum_{\beta=1}^P \int_0^t \mathbb{E}[\left(\frac{1}{N_\beta} X_{i\beta}(u) \sum_{j:p(j)=\beta} c^j_\beta(u)\right)^2] du$$

$$(|X| < M) \le t\,P\,M^2 \sum_{\beta=1}^P \int_0^t \frac{1}{N_\beta^2} \mathbb{E}\Big[\sum_{j:p(j)=\beta,k:p(k)=\beta} c^j_\beta(u) c^k_\beta(u)\Big] du$$

Thanks to the fact that the $c^j_\beta(u)$ are independent for $j \neq k$ and bounded by 1 and that $\frac{N}{N_\beta}$ is bounded for large N by $\frac{2}{\delta_\beta}$ (since we assumed that $\frac{N_\beta}{N}$ converges to a constant δ_β in $]0,1[$), we get:

$$\mathbb{E}[\sup_{s\le t} C_s^2] \le t\,P\,M^2 \sum_{\beta=1}^P \int_0^t \frac{1}{N_\beta^2} \mathbb{E}\Big[\sum_{j:p(j)=\beta,} (c^j_\beta(u))^2\Big] du$$

$$\le t^2\,P\,M^2 \sum_{\beta=1}^P \frac{1}{N_\beta}$$

$$\le 2\frac{t^2\,P^2\,M^2}{N} \max_\beta \frac{1}{\delta_\beta}$$

Concerning D_s, we use Burkholder-Davis-Gundy and the Lipschitz property of g_α (whose Lipschitz constant is denoted by $K_g(\alpha)$) to get:

$$\mathbb{E}[\sup_{s\le t} D_s^2] = \mathbb{E}[\sup_{s\le t}\left(\int_0^s (g_\alpha(V^i(u)) - g_\alpha(\bar{V}^i(u)))dB^i(u)\right)^2]$$

$$\le 4\mathbb{E}\int_0^t |g_\alpha(V^i(u)) - g_\alpha(\bar{V}^i(u))|^2 du$$

$$\le 4K_g(\alpha)^2 \int_0^t \mathbb{E}[\sup_{0\le v\le u} |V^i(v) - \bar{V}^i(v)|^2] du$$

$$\le 4K_g(\alpha)^2 \int_0^t M_u^i du$$

To sum up, we have, recalling that $t \le T$, and obviously that $M_u^i \le N_u$:

$$\mathbb{E}[\sup_{s\le t} A_s^2] \le T\,K_f(\alpha)^2 \int_0^t N_u du,$$

$$\mathbb{E}[\sup_{s\leq t} B_s^2] \leq T\,P^2\,M^2 \max_\beta L_\beta^2 \int_0^t N_u du,$$

$$\mathbb{E}[\sup_{s\leq t} C_s^2] \leq 2\frac{T^2\,P^2\,M^2}{N} \max_\beta \frac{1}{\delta_\beta},$$

$$\mathbb{E}[\sup_{s\leq t} D_s^2] \leq 4K_g(\alpha)^2 \int_0^t N_u du$$

Putting everything together, we get:

$$N_t \leq K_1 \int_0^t N_u du + \frac{K_2}{N}$$

where:

$$K_1 = 4\Big(T \max_\alpha K_f(\alpha)^2 + 4 \max_\alpha K_g(\alpha)^2 + T\,P^2\,M^2 \max_\beta L_\beta^2\Big)$$

and:

$$K_2 = 8\,T^2\,P^2\,M^2 \max_\beta \frac{1}{\delta_\beta}$$

We conclude using Gronwall's lemma that $\forall t \in [0,T]$:

$$N_t \leq \frac{K_2}{N}\exp(K_1 t)$$

The propagation of chaos property (iii) stems from the almost sure convergence of $(V^{i_1}(t),\ldots,V^{i_k}(t), t\leq T)$ towards $(\bar{V}^{i_1}(t),\ldots,\bar{V}^{i_k}(t), t\leq T)$, which are independent, as a process and uniformly for fixed time, and is proved in a similar fashion. □

We note that the assumption that the stochastic processes describing the weights are bounded is crucial. Indeed in the general case we could have introduced the stopping time $\tau_N(n)$ defined as follows for a natural number n:

$$\tau_N(n) = \inf\{t\in[0,T]; \max_{i=1\ldots N,\beta=1\ldots P} |J_{i\beta}(t)| \geq n\}$$

with the convention $\inf\{\emptyset\} = T$. Obviously, this sequence of stopping times is non-decreasing. And we would have got an upperbound of the form:

$$\mathbb{E}[\sup_{s\leq t\wedge\tau_N(n)} B_s^2] \leq (t\wedge\tau_N(n))\,P\,n^2 \int_0^{t\wedge\tau_N(n)} \sum_{\beta=1}^P L_\beta^2 \max_{j:p(j)=\beta} M_s^j ds$$

We assume here that the synaptic weights have a first moment. Then for a given N, for almost all ω in Ω, there exists $n_0(\omega)$ such that $\tau_N(n)(\omega) = T$ for

every $n \geq n_0(\omega)$. Since $t \in [0,T]$, $t \wedge \tau_N(n_0)(\omega) = t$ and we have the following upperbound for every $n \geq n_0(\omega)$:

$$\mathbb{E}[\sup_{s\leq t} B_s^2] = \mathbb{E}[\sup_{s\leq t\wedge\tau_N(n_0)} B_s^2] \leq Ptn_0^2 \int_0^t \sum_{\beta=1}^{P} L_\beta^2 \max_{j:p(j)=\beta} M_s^j ds$$

However, when we take the limit $N \to +\infty$, we cannot find a finite n_0, such that $\tau_N(n_0)(\omega) = T$ for every $n \geq n_0(\omega)$. We can even expect that for a finite n_0,

$$\lim_{N\to+\infty} \tau_N(n_0) = 0$$

as soon as $\tau_1(n_0)$ charges arbitrarily small times, which is the case of the Ornstein-Uhlenbeck process for instance.

We have checked that the upperbounding of $\mathbb{E}[\sup_{s\leq t} C_s^2]$ would work (with a slightly different argument) provided that the synaptic weights have a second moment. But assuming that all the weights have a first and second moment is not enough, in our framework, to prove a propagation of chaos result valid on $t \in [0,T]$. In fact the classical proof of Sznitman concerning interacting particle systems uses the fact that the interaction kernel between two particles is globally Lipschitz. In our case this interaction kernel is given by:

$$b_{\alpha\beta}(V^i(t), V^j(t), t) = X_{\alpha\beta}(t)S(V^j(t))$$

and is only locally Lipschitz continuous with respect to the second variable, since the variation in the second variable is unbounded if $X_{\alpha\beta}(t)$ is allowed to take arbitrarily large values. We have insisted on this subtlety, because, at first sight, we could have thought that assuming that the synaptic weights possess a second moment is enough. But in fact we have to make the stronger assumption that they are bounded. In the simulations we will see that the equation 6.5 provides nevertheless a good approximation of the network behavior in finite time when the weights have a second moment (e.g. are modeled by Ornstein-Uhlenbeck processes). In that case, for fixed N, $\tau_N(n_0)$ will tend to T when n_0 becomes arbitrarily large.

6.2.3 Reduction to a system of ODEs in the white noise model case

If the stochasticity of the synaptic weights is modeled by a white noise, the weights are Gaussian. In this case, we easily see that since the intrinsic dynamics is linear $f_\alpha(V) = -\frac{V}{\tau_\alpha}$, the mean-field solution of 6.3 is itself Gaussian, provided the initial condition is Gaussian. This can be seen by writing the

solution of the mean field equation in the integral form. The Gaussian solutions are then entirely characterized by their mean and standard deviation. We also make the simplifying assumption that $g_\alpha(V) = \lambda_\alpha$, i.e. the parameter modulating the additive noise is a constant. The system of coupled differential equations giving the mean and the variance of the Gaussian solution is the subject of the following proposition:

Proposition 6.2.3. *Let us assume that the initial condition is a Gaussian random variable and that the weights are modeled by white noise (see section 6.1.1). We have:*

- *The solutions of the mean-field equations 6.3 are Gaussian processes for all time.*
- *Let $\mu(t) = (\mu_\alpha(t))_{\alpha=1\dots P}$ denote the mean vector of the process $(V_\alpha, \alpha = 1\dots P)$ and $v(t) = (v_\alpha(t))_{\alpha=1\dots P}$ its standard deviation. Let also $f_\beta(x, y)$ denote the expectation of $S_\beta(U)$ for U a Gaussian random variable of mean x and standard deviation y. We have:*

$$\begin{cases} \dot{\mu}_\alpha(t) = -\frac{1}{\tau_\alpha}\mu_\alpha(t) + \sum_{\beta=1}^{P} J_{\alpha\beta} f_\beta(\mu_\beta, v_\beta) + I_\alpha(t) & \alpha = 1\dots P \\ \dot{v_\alpha} = -\frac{2}{\tau_\alpha} v_\alpha + \sum_{\beta=1}^{P} \sigma_{\alpha\beta}^2 f_\beta(\mu_\beta, v_\beta)^2 + \lambda_\alpha^2 & \alpha = 1\dots P \end{cases} \tag{6.6}$$

with initial condition $\mu_\alpha(0) = \mathbb{E}[X_\alpha^0]$ and $v_\alpha(0) = \mathbb{E}[(X_\alpha^0 - \mu_\alpha(0))^2]$. In equation (6.6), the dot denotes the differential with respect to time.

The proof is exactly similar to the one provided in chapter 4, and consists in writing the solution in the integral form. We recall that the functions f_β depend on the choice of the sigmoidal transform. A particularly suitable case is the erf sigmoidal function $S_\alpha(x) = \mathrm{erf}(g_\alpha x + \gamma_\alpha)$. In that case we are able to express the function f_β in closed form (see lemma 4.2.3).

The solutions of 6.5 would also be Gaussian if the weights were Gaussian processes. But this is *not possible* since these equations are only valid for bounded weights, and Gaussian processes are not bounded: they can take arbitrarily large values (though with small probability).

In the case of weights described by Gaussian stochastic processes, *if the equations 6.5 were valid*, we could also reduce the dynamics to a system of *non-autonomous* ordinary differential equations given by:

$$\begin{cases} \dot{\mu}_\alpha(t) = -\frac{1}{\tau_\alpha}\mu_\alpha(t) + \sum_{\beta=1}^{P} \mathbb{E}[X_{\alpha\beta}(t)] f_\beta(\mu_\beta, v_\beta) + I_\alpha(t) & \alpha = 1\dots P \\ \dot{v_\alpha} = -\frac{2}{\tau_\alpha} v_\alpha + \sum_{\beta=1}^{P} Var[X_{\alpha\beta}(t)] f_\beta(\mu_\beta, v_\beta)^2 + \lambda_\alpha^2 & \alpha = 1\dots P \end{cases} \tag{6.7}$$

These two systems (6.6 and 6.7) of coupled ordinary differential equations are very similar, except that the second one is non-autonomous. If we choose weights modeled by Ornstein-Uhlenbeck processes, with $\theta = 1$ (see section 6.1.2) we see that the non-autonomous coefficients $\mathbb{E}[X_{\alpha\beta}(t)]$ and $Var[J_{\alpha\beta}(t)]$ converge exponentially fast towards the coefficients of the first system: $J_{\alpha\beta}$ and $\sigma^2_{\alpha\beta}$ respectively. Furthermore if we set $X_{\alpha\beta}(0) = J_{\alpha\beta}$ and $Var[X_{\alpha\beta}(0)] = \sigma^2_{\alpha\beta}$ the mean and variance of the Ornstein-Uhlenbeck process are equal to their stationary values. In the next section we will study the bifurcation diagram of 6.6, which describes weights whose fluctuations are modeled by white noise.

6.3 Noise-induced phenomena and network dynamics

In this section we numerically study the influence of the synaptic noise level σ on the dynamics of the neuronal populations in the case of the white noise model. The results obtained are then compared to the numerical simulations of a finite network.

In the chapter 4, devoted to the case of a purely additive noise (no variation in the synaptic weights was considered), we observed that a global behavior appeared resulting from the interactions. This behavior was described by a Gaussian process whose variance (dependent on the variance of the initial value and of the additive noise parameter) was uncoupled with the mean variable which satisfied a deterministic ordinary differential equation. But, even in that case, the presence of noise was shown to have a non-trivial effect on the dynamics. We now turn to study the more complex case where noise in the synaptic transmission is taken into account. In that case, **the dynamics of the variance is no more uncoupled with the mean variable** (see the equation on the variance in 6.6), and we expect the nonlinear coupling between the mean and the standard deviation to produce non-trivial new behaviors. We explore in this section the behavior of the system as a function of the synaptic noise parameter σ. Note that in the present case, the nonlinear coupling and the complexity of the equations prevents from performing analytical studies. In particular, it is very difficult to identify fixed points, which precludes any stability analysis. This section is therefore mostly concerned with numerical bifurcation analysis.

6.3.1 How the synaptic noise does influence the dynamics of the population?

We take a two-populations network with the same parameters' values as in section 4.3.3. We consider a synaptic noise intensity $\sigma_{\alpha\beta}$ independent on the population (and denoted by σ). The value of the additive noise is set to zero for each population. We study the codimension two bifurcation diagram as I_1 and σ are varied.

The corresponding bifurcation diagram is displayed in Figure 6.1. We divide the diagram into 11 zones labeled A through K. Each of these zones is defined by a range of values of the noise parameter σ in which the codimension one bifurcation diagrams as a function of I_1 are qualitatively similar. **The 11 corresponding codimension 1 diagrams are given in the Annex C.1.** In other words, for any of the 11 zones, the variation of σ does not modify the qualitative codimension 1 bifurcation diagram of the system as a function of I_1.

The diagram features seven codimension two bifurcation of equilibria: 3 Bogdanov-Takens (BT) points, 3 cusps (CP) and one generalized Hopf (GH), which are labeled by red stars. The BT bifurcations give rise to saddle-homoclinic bifurcation curves (the green curves in the diagram) that either undergo bifurcations or present turning points as a function of σ.

For small values of σ, the system is characterized by a supercritical Hopf bifurcation and four saddle-node bifurcations. Note that two saddle-node bifurcations and a Hopf bifurcation appear in a very small range of parameter value ($I_1 \approx -2.2$), as displayed in the zoomed diagram at the bottom center of Figure 6.1. The Hopf bifurcation is supercritical, and hence is related with the presence of stable periodic orbits of the system that disappear through a saddle-homoclinic bifurcation (zone A). One of the branches of saddle-node bifurcations undergoes a supercritical Bogdanov-Takens bifurcation, yielding the appearance of a second family of stable limit cycles that disappear through a saddle-homoclinic bifurcation. This curve of saddle-homoclinic bifurcations presents a turning point (see the zoom on the bottom left of Figure 6.1), separating zone B and zone C where the two families of limit cycles are superimposed.

As σ is further increases, two saddle-node bifurcations merge into a cusp bifurcation and disappear, yielding zone D. In that zone, two Hopf and two

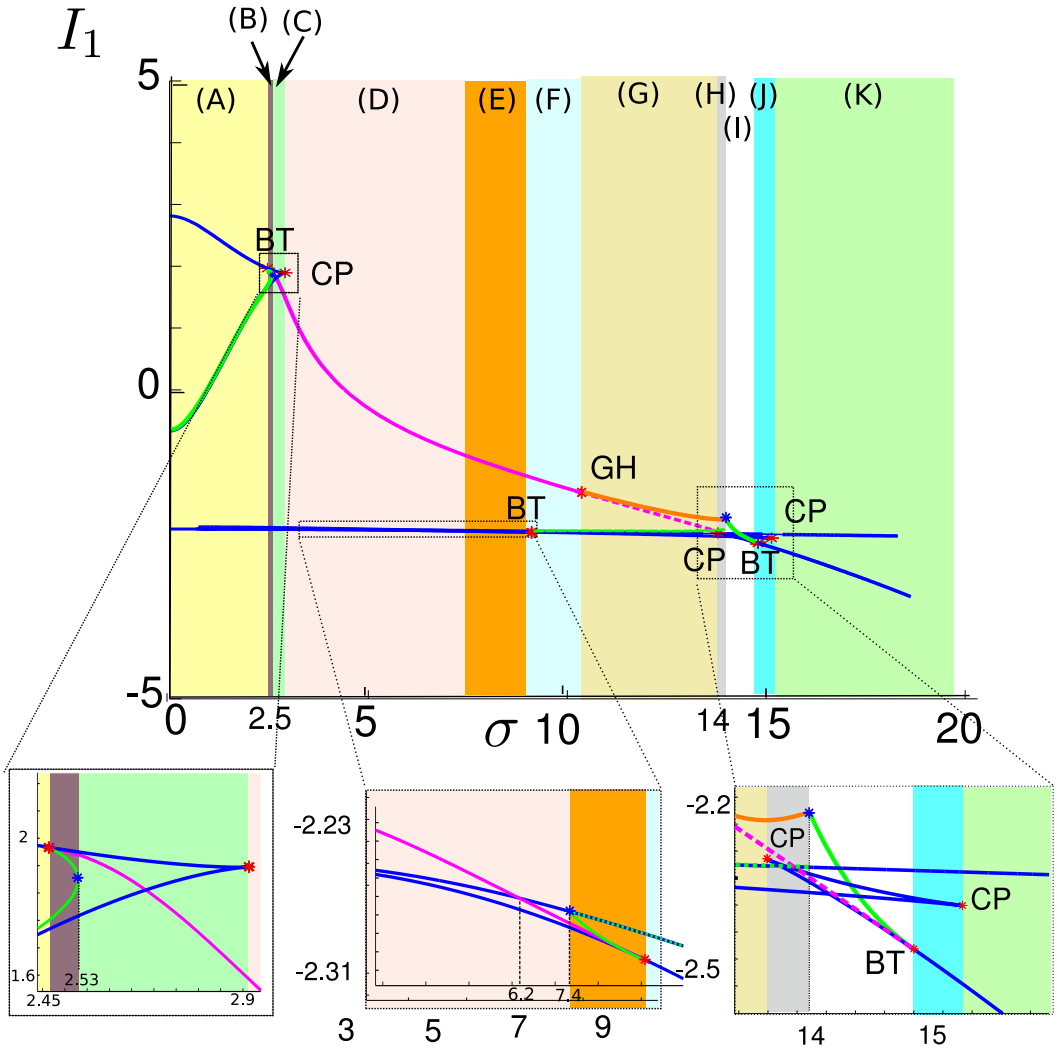

Figure 6.1: Codimension two bifurcation diagram as σ and I_1 are varied. Eleven different ranges of the parameter σ are identified, in which the bifurcation diagrams with respect to I_1 are qualitatively the same. Each zone differs in the number or stability of fixed points and limit cycles. Blue curves: saddle-node bifurcation manifolds. Pink curves: Hopf bifurcation manifolds. Green curves: saddle-homoclinic bifurcations. Dashed green curve: saddle-node homoclinic bifurcations. Orange curve: folds of limit cycles. BT: Bogdanov Takens bifurcation. CP: Cusp bifurcation. GH: Bautin (Generalized Hopf) bifurcation. Blue stars: homoclinic bifurcations or special point on the homoclinic bifurcation curve. Individual behaviors in each zone are commented in appendix C.1. Diagrams obtained MatCont package [Dhooge et al., 2003b, Dhooge et al., 2003a].

saddle-node bifurcations exist. However, as σ is further increased, a homoclinic bifurcation appears yielding zone E. At this point, a saddle-homoclinic bifurcation arising from a forthcoming Bogdanov-Takens bifurcation reaches a saddle-node bifurcation curve, and bifurcates into a saddle-node homoclinic and a saddle-homoclinic curves. This bifurcation separates the family of limit cycles into two distinct families as shown in Figure C.3 presented in the Annex.

As σ keeps increasing, a Bogdanov-Takens bifurcation arises, and the lower branch of cycles disappears. The system is left, in zone F, with two saddle-node bifurcations, a supercritical Hopf bifurcation and a saddle-node homoclinic bifurcation. The supercritical Hopf bifurcation becomes subcritical at a Bautin bifurcation (GH, for Generalized Hopf), yielding a fold of limit cycles in the diagram in zone G. Zone H is characterized by the fact that one of the branches of saddle-node bifurcations undergoes a cusp. As σ is further increased, the fold of limit cycles arising from the Bautin bifurcation bifurcates with a saddle-homoclinic bifurcation that will arise from a Bogdanov-Takens bifurcation corresponding to the extinction of the last Hopf bifurcation (see the zoom at the bottom right of Figure 6.1). At this point, in zone I, the system is left with no stable limit cycles. As σ increases further, the system undergoes a Bogdanov-Takens, then a cusp bifurcations, and is left in zone K with two saddle-node bifurcations. We found numerically this to be the case for all larger values of σ.

This bifurcation diagram also provides very interesting information about the behavior of the system **as a function of the noise level, for fixed values of I_1.** For example, let us fix $I_1 = 0$. For $\sigma = 0$, the system features a single stable equilibrium and two unstable equilibria, therefore all the trajectories converge towards the unique stable fixed point. When σ is increased, a branch of periodic orbit appears through a saddle-homoclinic bifurcation. In a small interval of values of σ, cycles coexist with the stable fixed point. This stable fixed point looses stability, as σ is further increased, through a saddle-node bifurcation, and the system is left with an attractive limit cycle and an unstable fixed point, and hence presents **an oscillatory behavior in a large range of values of σ.** In this range of values, the solutions of the mean-field equations are Gaussian processes with oscillating mean and standard deviation. As σ is further increased, the limit cycles disappear through a supercritical Hopf bifurcation, and the unstable fixed point becomes stable. This corresponds to the fact that in the large noise regime, the solution of the mean-field equation converges towards a stationary Gaussian process with constant mean and standard deviation. **The synaptic noise can therefore**

induce oscillations, oscillations that then disappear for larger noise values (see figure 6.2).

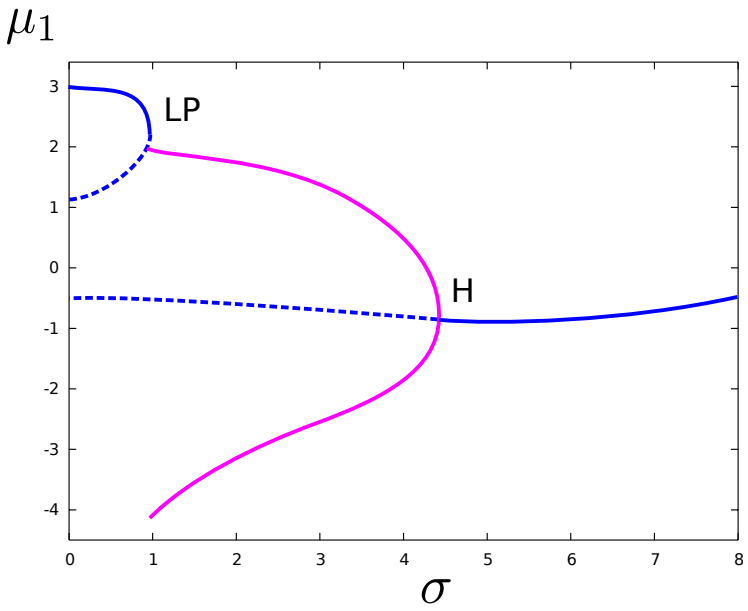

Figure 6.2: Creation and destruction of cycles through variations of the synaptic noise: Codimension one bifurcation diagram with respect to σ of the variable μ_1 for $I_1 = 0$. The diagram presents three bifurcations: a saddle-node bifurcation (or limit point, LP), a Hopf bifurcation (H) and a saddle homoclinic bifurcation accounting for the creation of cycles, separating the behaviors in three different regimes (see text).

As the system studied is more complex it is not a surprise to find that the codimension 2 bifurcation diagram presented in Figure 6.1 is more intricate than the one corresponding to purely additive noise presented in Figure 4.2.

However the same qualitative conclusions can be drawn. First it is possible to separate the diagram in several zones defined by the noise interval, where the codimension 1 bifurcation diagrams as function of I_1 (i.e. the way the system reacts to an external input) are qualitatively the same. As could be expected, we found more zones in the synaptic noise case than in the purely additive noise case, so if we could obtain by an experiment the bifurcation diagram of μ_1 as a function of the external input I_1, it would be possible to guess the level of noise the system is submitted to with a better precision than in the additive noise case.

And, most importantly, as in the case of the additive noise, we observe that the synaptic noise has a strong impact on the behavior of the system, in particular it is able to create or destroy oscillations.

6.3.2 Back to the network dynamics

Thus far, we studied the dynamics of the mean-field equations representing regimes of the network dynamics in the limit where the number of neurons is infinite. We now compare the regimes identified in this analysis with numerical simulations of the finite-size stochastic network and will be particularly interested in finite-size effects. We will perform simulations of the network in two cases: the case where the fluctuations of the weights are modeled by white noise, and the case where the weights are modeled by Ornstein-Uhlenbeck processes.

6.3.2.1 The case of weights modeled by white noise

We start by the case of finite-size networks with noisy synaptic weights whose fluctuations are modeled by white noise. We study the three different regimes observed in diagram 6.2. These regimes are: an equilibrium regime for $\sigma < 0.952$, a bistable regime with very slow oscillations and a stable fixed point for $\sigma \in [0.95, 0.96]$, a purely oscillating regime for $\sigma \in [0.96, 4.40]$, and again an equilibrium regime for $\sigma > 4.40$.

The results of the simulations of a finite network composed of 5 000 neurons in each population are shown in Figure 6.3. For large σ, we used 10 Monte-Carlo simulations to smooth the finite-size effects. In the fixed points regimes (Figure 6.3 (a), (b), (e) and (f)), each neuron ends up stochastically varying around the equilibrium value of the mean-field equation. The empirical mean and standard deviation of each population closely match the solution of the mean-field equations. The oscillatory regimes show an additional effect the additive noise case did not feature. Indeed, in that case the variance variable of the mean-field equations, whose dynamics is nonlinearly coupled to the mean, **oscillates with the same period**. Along these cycles, the variance periodically reaches zero, and is minimal at the switching between the up-state and down-state of the oscillations. This small variance results in the fact that all neurons tend to switch in a very synchronized way, **producing a seemingly sharper synchronization than the purely additive noise** case when comparing Figure 4.6(c) and Figure 6.3(c). Synaptic noise has therefore the effect of producing a better synchronization, which is a very desirable property in a stochastic oscillating system.

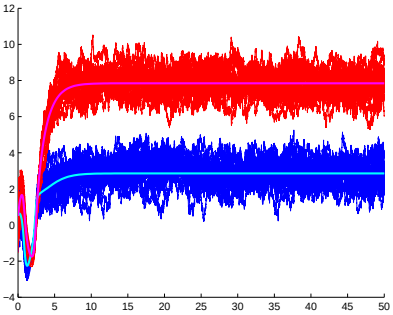

(a) $\sigma = 0.7$. **Fixed-point regime**. Individual trajectories vs mean-field.

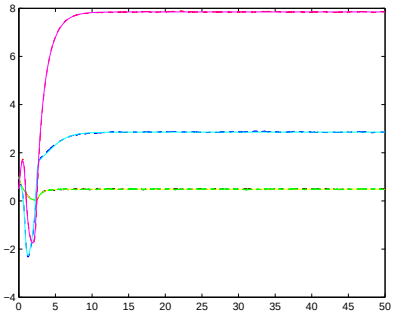

(b) $\sigma = 0.7$. **Fixed-point regime** Empirical network statistics vs mean-field.

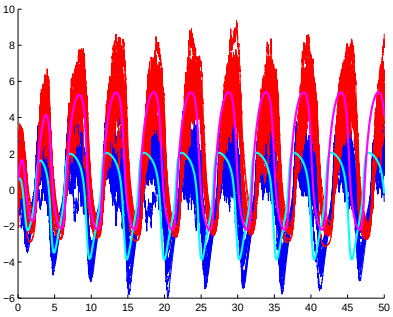

(c) $\sigma = 1.2$. **Oscillatory regime**. Individual trajectories vs mean-field.

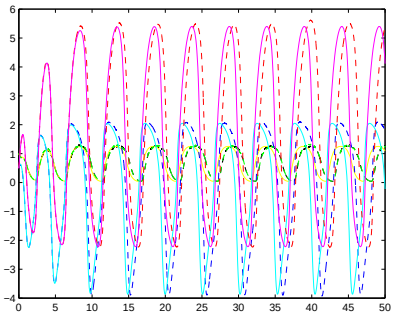

(d) $\sigma = 1.2$. **Oscillatory regime** Empirical network statistics vs mean-field.

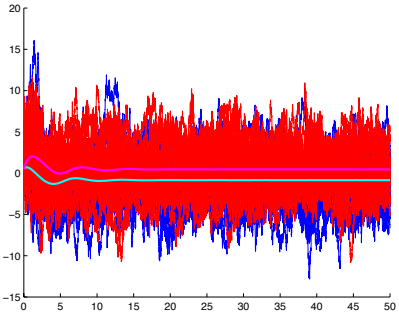

(e) $\sigma = 6$. **Noisy fixed point regime**. Individual trajectories vs mean-field.

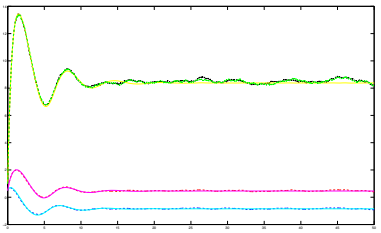

(f) $\sigma = 6$. **Noisy fixed point regime** Empirical network statistics vs mean-field.

Figure 6.3: Solution of the network dynamics for different values of the noise parameter σ in the case of synaptic weights whose fluctuations are modeled by white noise. Same network characteristics, plotted curves and color code as in Figure 4.6.

In order to determine the precise value of σ corresponding to the appearance and to the disappearance of oscillations, we again perform extensive simulations of the network for different values of the synaptic noise parameter σ and computed the Fourier transform of the empirical mean. We recovered in the simulation of the network these different behaviors for very close values of the parameter σ, as explained in Figure 6.4, where we have compared the spectrum of the empirical mean of the network and of the mean of the mean-field solution for different values of σ. Moreover, though the interval corresponding to the bistable regime is rather small, we recovered this bistability in a finite network (similar to the λ case, result not shown).

6.3.2.2 The case of weights modeled by Ornstein-Uhlenbeck processes

We present in this section the simulation of a finite-size stochastic network whose weights are modeled by Ornstein-Uhlenbeck processes of standard deviation σ. Though we have seen that the system 6.7 is not a rigorous description of the network, since Gaussian weights cannot be bounded, we will compare simulations of solutions to the system 6.7 with computations of the empirical mean and the empirical variance of the stochastic network, and observe that the results match relatively well, except for a progressive phase shift and a slight difference in the amplitudes of the oscillations (see Fgure 6.5 (d)). The results of the simulations of a finite network composed of 5 000 neurons in each population are shown in Figure 6.5.

As in the preceding subsection, we have again performed extensive simulations of a stochastic network of 5000 neurons whose synaptic weights are Ornstein-Uhlenbeck processes, for different values of the synaptic noise parameter σ, and computed the Fourier transform of the empirical mean. The results are displayed in Figures 6.6, 6.7, and 6.8.

Eventually there is an interesting phenomenon that discriminates between the three models proposed in this thesis: additive noise, synaptic inhomogeneity and synaptic noise. In the three cases we observed that the noise parameter had similar effects on the dynamics: **compare Figures 4.8, 5.3 and 6.4 where the route to oscillations is almost the same**. Nevertheless in the case of synaptic noise there is a distinctive feature: the amplitude of the Fourier transform presents a clear maximum as a function of the noise level whereas in the additive noise case or synaptic inhomogeneity the corresponding curve is less peaked. We have hence **a resonance phenomenon in the synaptic noise model**.

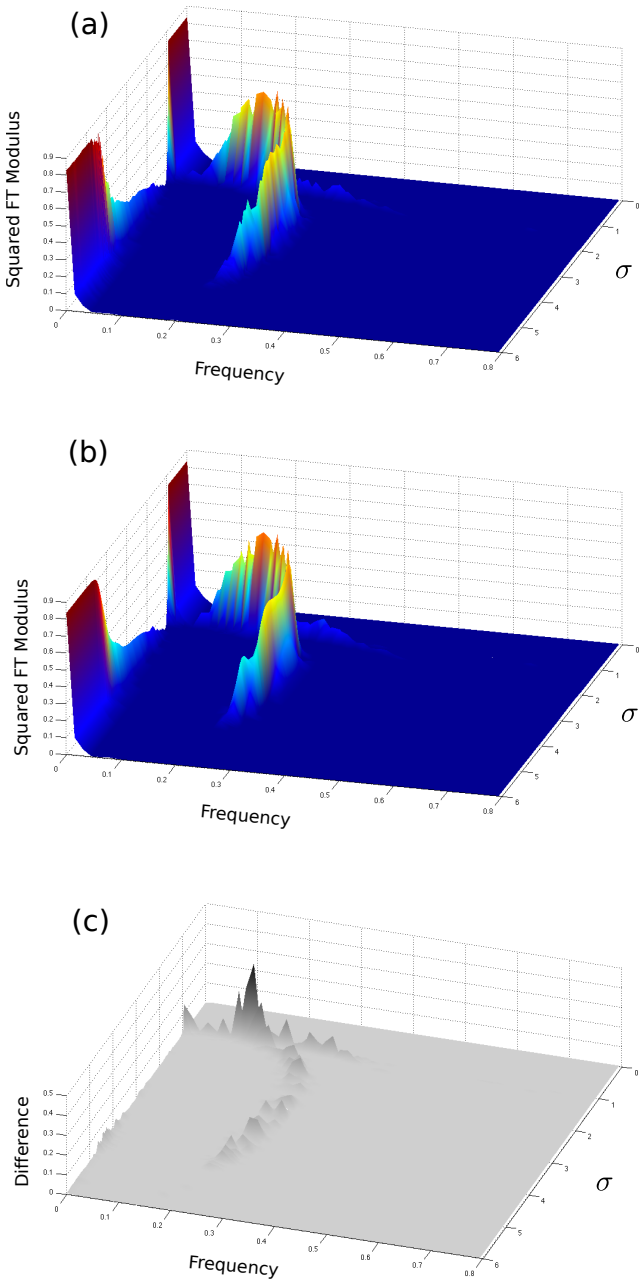

Figure 6.4: Squared modulus of the Fourier transform of the empirical mean for simulations of the network with synaptic weights whose fluctuations are modeled by white noise (a) compared with the mean variable of the solution of the mean-field equations (b), as a function of the frequency (Hz) and the synaptic noise parameter σ. We observe that oscillations in the network appear for the same value of σ as in the mean-field equations (Fig. 6.2), first through a seemingly homoclinic bifurcation (arbitrary small frequencies) and disappear also for the same value of σ through a seemingly Hopf bifurcation (discontinuity in the power spectrum). (c) Absolute difference between the two diagrams: we remark that the frequency distribution is precisely peaked at the same value, and the main differences are observed, as expected, at the bifurcation points.

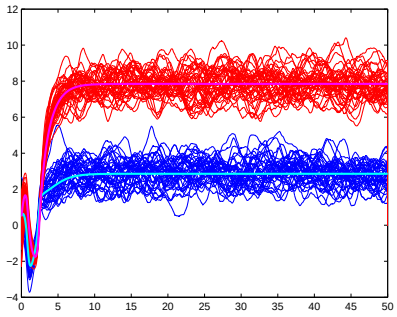

(a) $\sigma = 0.7$. **Fixed-point regime**. Individual trajectories vs solutions of 6.7

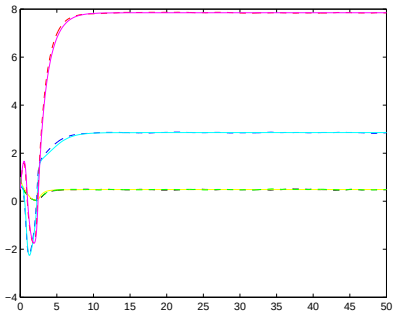

(b) $\sigma = 0.7$. **Fixed-point regime** Empirical network statistics vs solutions 6.7

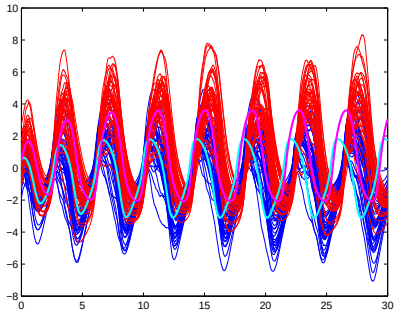

(c) $\sigma = 2$. **Oscillatory regime**. Individual trajectories vs solutions of 6.7

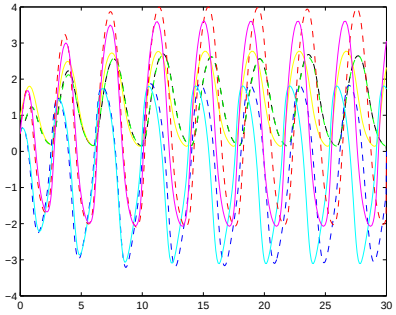

(d) $\sigma = 2$. **Oscillatory regime** Empirical network statistics vs solutions of 6.7

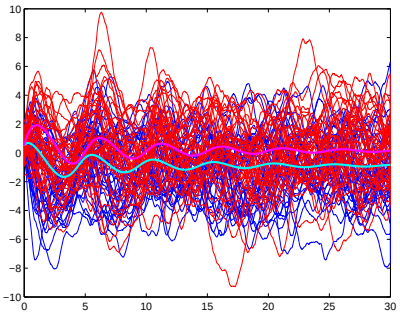

(e) $\sigma = 5$. **Noisy fixed point regime**. Individual trajectories vs solutions of 6.7

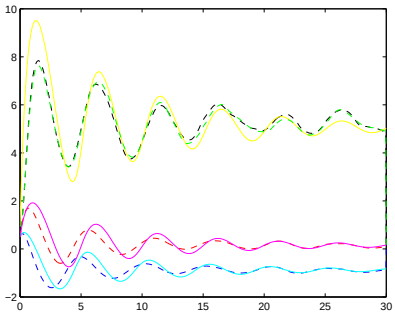

(f) $\sigma = 5$. **Noisy fixed point regime** Empirical network statistics vs solutions of 6.7

Figure 6.5: Solution of the network dynamics for different values of the noise parameter σ in the case of synaptic weights modeled by Ornstein-Uhlenbeck processes. Same network characteristics, plotted curves and color code as in Figure 6.3 except that the cyan and magenta curves are not the mean field solutions, but solutions of the system 6.7.

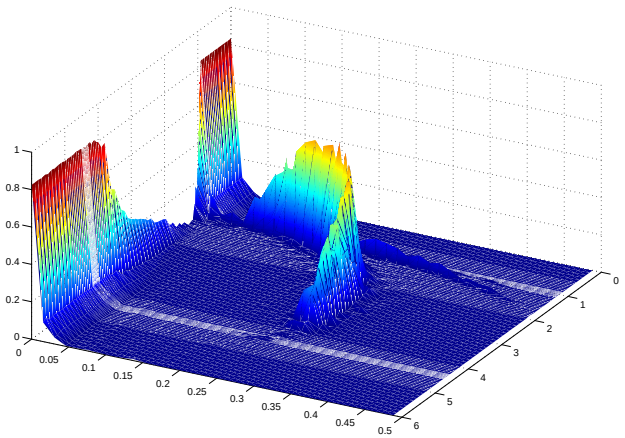

Figure 6.6: Squared modulus of the Fourier transform of the empirical mean for simulations of the network with synaptic weights modeled by Ornstein-Uhlenbeck processes as a function of the frequency (Hz) and the synaptic noise parameter σ.

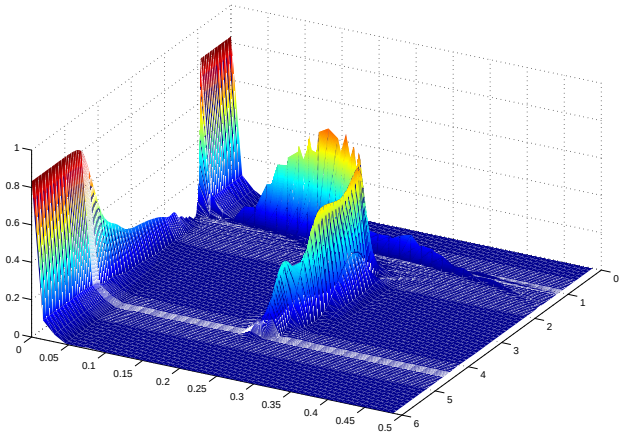

Figure 6.7: Squared modulus of the Fourier transform of the mean for simulations of the system 6.7 as a function of the frequency (Hz) and the synaptic noise parameter σ.

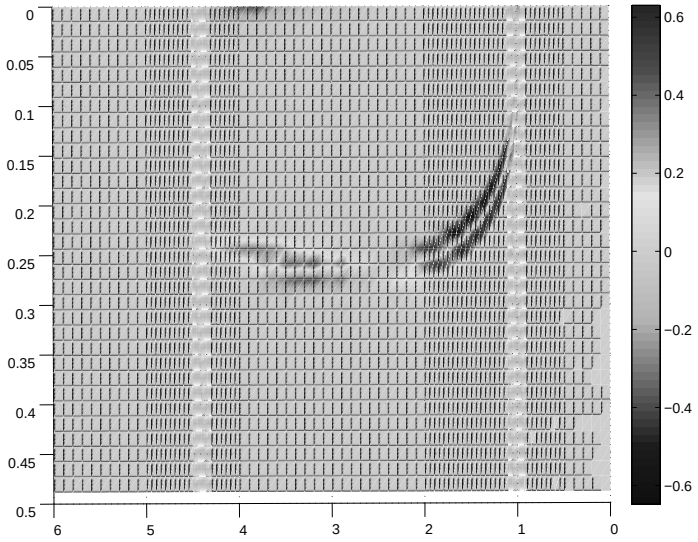

Figure 6.8: Difference between the two diagrams (system 6.7 and network): we remark that the frequency distribution is precisely peaked at the same value, and the main differences are observed, as expected, at the bifurcation points. Though there is a slight phase difference, the oscillations in the network appear for the same value of σ as in the system 6.7, first through a seemingly homoclinic bifurcation (arbitrary small frequencies) and disappear also for the same value of σ through a seemingly Hopf bifurcation (discontinuity in the power spectrum).

6.4 Summary

In this chapter, we have been interested in the large-scale behavior of networks of firing rate neuron models, including models of synaptic noise. Using a probabilistic approach based on the mathematics of interacting particle systems, we derived the equations corresponding to the behavior of a given neuron in the network. In that limit, all neurons behave independently (propagation of chaos property) and satisfy a mean-field equation, whose solutions are Gaussian processes with their mean and variance exactly satisfying a closed set of nonlinear ordinary differential equations, provided that the synaptic weights fluctuations are modeled by white noise.

We then numerically studied the resulting system of equations as a function of the intensity of the synaptic noise σ. A complex codimension two bifurcation diagram was obtained when simultaneously varying an input parameter and the noise intensity. The analysis of this diagram yielded several qualitatively distinct codimension one bifurcation diagrams for different ranges of noise intensity, displayed in Annex C.1.

These classes of behaviors were then compared to simulations of the original finite-size networks. We obtained a very good agreement between simulations of the finite-size system and the mean-field equations. Transitions between different qualitative behaviors of the network matched precisely the related bifurcations of the mean-field equations (see Figure 6.4). Regular oscillations in the mean activity, linked with a synchronization of all neurons in the network, appear in the system for some precise values of the noise. But as the variance is oscillating with the same period than the mean, the synchronization of the neurons in the network is sharper in the case of synaptic noise than in the case of purely additive noise. For weights modeled by Ornstein-Uhlenbeck processes, there was also a good agreement between the network behavior and simulations of 6.7 (see Figure 6.8).

Noise therefore clearly induces transitions in the global behavior of the network, structuring its Gaussian activity by inducing smooth oscillations of its mean and its variance with a sharp synchronization at the network level. These findings have several implications in neuroscience that will be discussed in the conclusion of this thesis (8.2.2).

Part III

Conclusion

Overview

In the fist part of the conclusion (see chapter 7), we present a **summary of the main results** of this thesis, namely the derivation of three different mean field equations, related to three distinct microscopic descriptions of the network, and the study of the dependency of their solutions with respect to the three parameters underlying the microscopic description: **the additive noise, the synaptic inhomogeneity and the synaptic noise**. We also **compare** our results with other usual mean field approaches and underline the specificity of our results. Eventually, we present the **perspectives** opened by our work in chapter 8. First we list several possible extensions of the reference model that lead to new mean field equations. However the precise analysis of their dynamics seems for now mathematically intractable. That's why we stress particularly in our conclusion the biological relevance of the noise-induced phenomena we have been able to evidence in our more simple models, that can serve as **a proof of concept for the functional role of noise** in models more biologically plausible, but much more complex to analyze.

Chapter 7

Summary of the main results

7.1 Summary

The main findings of chapter 4 are presented in an article that has been accepted for publication [Touboul et al., 2011] in the SIAM Journal on Applied Dynamical Systems. We plan to submit soon, as first author, an article comparing the mean field dynamics described in chapter 5 and 6.

7.1.1 The three models exhibit propagation of chaos

In this thesis we have presented three different models of networks of firing-rate neurons. We have used three different versions of "randomness"[1] at the neuronal or synaptic level. First (chapter 4) an **additive noise** that can be best thought as accounting for channel noise. In chapter 5, we have introduced a frozen disorder at the synaptic level, i.e. a degree of **synaptic inhomogeneity** accounting for individual variations in the biological characteristics of synapses. Eventually, in chapter 6, we have modeled the synaptic weights by dynamically evolving stochastic processes in order to include **synaptic noise**.

We were interested in the dynamical properties of these networks in the thermodynamic limit, i.e. when the number of neurons tends to $+\infty$. In simulations we have also checked that the limiting equations, i.e. our **mean field equations**, were a good approximation of the network behavior when the number of neurons is sufficiently large. In the three cases we have stated a **propagation of chaos property**, which means that any finite number of neurons with independent and population-wise identically distributed initial conditions will remain independent during the evolution in the thermodynamic limit and have the same probability distribution (depending only on the population they belong to) solution of an implicit mean field equation.

[1] We use hereafter the term "randomness" in inverted commas, as in the case of synaptic inhomogeneity this term is not well adapted since, if we removed the additive noise source, the microscopic equations for each realization of the J_{ij} would be deterministic. In this case "randomness" refers to the disorder introduced at initial time in the system which accounts for inhomogeneities in the synaptic weights.

7.1.2 The influence of the noise level and of the inhomogeneity level

Our main topic of investigation was to understand the influence of these parameters in the resulting mean field equations. We found **two relatively unexpected results**.

First, we have seen that the presence of noise or inhomogeneity in the system induces different qualitative behaviors. For instance, regular oscillations of the mean firing rate, linked with a synchronization of all neurons in the network, appear in the system at some precise values of the noise parameter, in particular for systems that feature a stable fixed point in a noiseless context. This means that **noise has a strong structuring effect on the global behavior of a cortical assembly**, which is rather a counterintuitive phenomenon, since noise is usually chiefly seen as altering structured responses. Of course, in the additive noise case for example, our mean-field equations form a set of nonlinear ordinary differential equations and as such, oscillations are likely to appear by modifying one of the parameters. However, **when thinking to the underlying microscopic model**, we believe that this is a relatively original and unexpected result: a set of stochastic processes in interaction starts oscillating synchronously for a very specific range of values of the noise. This phenomenon is also rather surprising when thinking at the underlying models corresponding to synaptic inhomogeneity or synaptic noise, all the more that these oscillations are synchronous and regular.

The second relatively unexpected conclusion is that **we have observed the same qualitative behaviors in all our three models**, be the "randomness" modeled by an additive noise, by synaptic inhomogeneity or by synaptic noise. In the first case some analytical results have been obtained (see e.g. sections 4.3.1 and 4.3.2), but in more general cases we relied on numerical computations of bifurcation diagrams. This similarity between the three models is striking when we compare the three Figures 4.8, 5.3 and 6.7 obtained by computing the squared modulus of the Fourier transform of the empirical mean of the network as a function of the frequency and the noise parameter.

We have nevertheless observed **slight differences** in the simulation of these three models. In the additive noise case the variance of the Gaussian process solution of the mean field equation converges to a constant fixed value proportional to the square of the noise parameter. On the contrary in the cases including synaptic inhomogeneity or synaptic noise, the variance is coupled

with the mean and may oscillate synchronously with the mean. Hence, **the synchronization of all the neurons in the network will be sharper** in these two last cases. We also observed by comparing the Figures 4.8, 5.3 and 6.7 that in the last case the modulus of the Fourier transform presents a sharp and clear peak as a function of the synaptic noise parameter. Hence in this last case, there is a **resonance** phenomenon.

These similarities are striking when thinking to the underlying microscopic models which are very different in the three cases and which result in **distinct mean field equations**. This is especially true when we compare the synaptic inhomogeneity case to the two others. Indeed the microscopic model is here, if we except the additive noise source, deterministic [2]. The resulting mean field equation is also non-Markovian. Eventually the case of synaptic noise is more involved than the one of additive noise since, even when we do the simplifying assumption that the weights' fluctuations are modeled by white noise, so that the solution is Gaussian, the resulting system of ordinary differential equations is non-autonomous and couples the variance with the mean, whereas for additive noise the system is autonomous and the variance is not coupled with the mean.

The noise-induced phenomena evidenced in this thesis appear hence quite universal. We think that our results can be seen as a **proof of concept**, and it seems reasonable to extrapolate that such noise-induced transitions will occur in other mean-field equations of more complex, but more biologically plausible systems. The type of extensions that can be envisaged are presented in chapter 8.

7.2 Comparison with other mean field approaches

7.2.1 The balanced state

As pointed out by Haim Sompolinsky, the *chaotic (deterministic)* nature of the balanced state is similar in many respects to the chaotic state of spin-glasses with random asymmetric connections. When the synaptic inhomogeneity σ reaches a threshold, there is a bifurcation from a solution of null variance to a solution with non-zero variance (recall section 5.2.3), corresponding to the chaotic regime defined by Sompolinsky in [Sompolinsky et al., 1988]. As we

[2] The synaptic weights are drawn at the beginning of the evolution in a Gaussian law. But once the synaptic connectivity matrix is set the synaptic weights keep their fixed values and do not evolve stochastically like in the case of synaptic noise.

have already mentioned the mean field equations with synaptic inhomogeneity are rigorously derived only for a non-vanishing additive noise λ. But we can also take a λ arbitrarily small, and in that case, the (deterministic) trajectories will be given by the realization of Gaussian processes whose mean and covariance verify 5.1.2 where λ is set to zero.

7.2.2 Oscillations in one-population networks

The influence of noise in *spiking one-population neural networks* was studied in another context by Pham and collaborators in [Pham et al., 1998] and Brunel and collaborators [Brunel, 2000, Fourcaud and Brunel, 2002]. In [Pham et al., 1998], the authors study randomly or fully connected one-population networks of spiking neurons. They analyze the probability distribution of spike sequences and reduce this analysis to the study of the properties of a certain map under an independence assumption and in the limit where the number of neurons is infinite (which makes the independence assumption particularly relevant).

They show that noise can trigger oscillations for certain values of the total connectivity parameter in a one-population case. They end up with a partition of the parameter space in different zones where the system either shows a single "high" fixed point, a "low" fixed point, oscillations, or multistability between these different attractors. Similar phenomena are shown in the study of sparse randomly connected integrate-and-fire neurons as shown in [Brunel, 2000] where the system can present *synchronous regular regimes*. In the mean field model studied in chapter 4, no oscillatory activity is possible in such one-population systems, since its dynamics can be reduced to a *one-dimensional autonomous dynamical system*. Smooth nonlinearities in the intrinsic dynamics or discontinuities such as the presence of a spiking threshold in [Pham et al., 1998, Brunel, 2000] makes the dynamics of the mean field equations more complex, in particular prevents reduction to a one-dimensional autonomous system governing the mean of the solution. Such intricacies may also be the source of oscillations in one-population systems.

In order to compare our results to these previous results, we adopt the same presentation as in [Pham et al., 1998]. We consider the dynamics of the mean field system presented in chapter 4 as a function of *the connectivity strength j and the noise*, for a fixed value of the currents $I_1 = 0$ and $I_2 = -3$. The total connectivity strength j[3] is a particularly interesting parameter for applica-

[3] the connectivity matrix is taken in the simulations equal to $j \times \begin{pmatrix} 15 & -12 \\ 16 & -5 \end{pmatrix}$

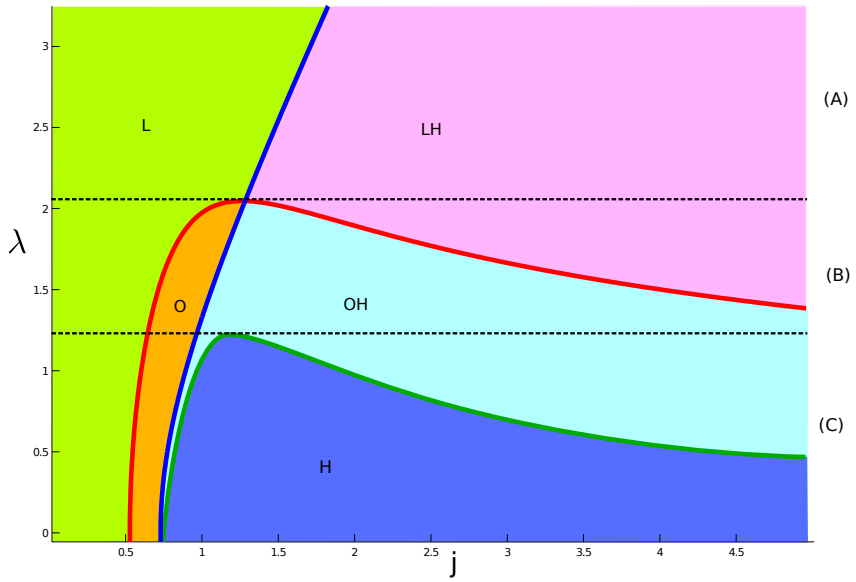

Figure 7.1: Codimension two bifurcation diagram of the mean field system with respect to the noise intensity λ and the total connectivity j. The diagram is partitioned into 5 different zones depending on the number and type of stable attractors: L: Low fixed point, H: High fixed point, O: Oscillations. Transitions between two zones are characterized by codimension one bifurcations: Blue line: saddle-node bifurcation, red: Hopf bifurcation, green: saddle homoclinic bifurcation.

tions, for it can account for such phenomena as the well established fact that functional connectivity is increased in epilepsy (see e.g. [Bettus et al., 2008]).

The *codimension two bifurcation diagram* of our model with respect to j and λ contains manifolds of saddle-node, Hopf and saddle-homoclinic bifurcations, and shows no codimension two bifurcation. The parameter space can be partitioned into five qualitatively different zones where the system either shows a "low" fixed point (L), a "high" fixed point (H), oscillations (O), or multistability between these attractors (see Figure 7.1). The diagram is quite similar to the one found in [Pham et al., 1998]. As in the case discussed in section 4.3, the analysis of this diagram results in defining three regions of values of the noise parameter λ in which the bifurcation diagrams as a function of j are qualitatively identical. These three regions make less sense here as the total connectivity parameter is not easily controllable experimentally, in contrast with the external input parameter I_1.

The resulting diagram has a number of similarities and dissimilarities with the results of Pham and collaborators [Pham et al., 1998, Section V and Fig.11]. Indeed, similarly to the spiking case, we observe that for small values of the connectivity strength j the fully connected system is characterized by a low fixed point, whereas large values of the connectivity parameter chiefly correspond to the presence of a high fixed point, and the overall structure is comparable. One of the main differences is that in our case, a two-population network, the system does present oscillations as the only attractor for some parameter values. Another interesting difference is that for small values of the noise parameter, the spiking system studied in [Pham et al., 1998] never presents oscillations, whereas the diagram 7.1 exhibits an oscillatory region (O) and a bistable region (OH) for arbitrarily small values of the noise parameter. This is due to the fact that their system consists of a unique neural population with purely excitatory interactions, whereas our network models the interaction of an excitatory and an inhibitory populations, and can feature deterministic oscillations.

7.2.3 Stochastic and coherence resonance

The phenomena observed in our analysis of large-scale neuronal networks can be related to the ones of stochastic resonance or coherence resonance well documented in the neuro-computational literature (see e.g. [Lindner et al., 2004] for a review of the effect of noise in excitable systems). These phenomena correspond to the fact that there exists a particular level of noise maximizing the regularity of an oscillatory output related to periodic forcing (stochastic resonance) or maximizing the regularity of an output without any periodic forcing (coherence resonance). Such situations are evidenced through the computation of the maximal value of the Fourier transform of the output. Stochastic resonance was first discovered in cat visual cortex and has attracted a lot of theoretical work (see e.g. [Longtin et al., 1991] and references therein). Several papers have shown that a similar mechanism can lead at the network level to the occurrence of synchronized oscillations. For example in [Yu et al., 2003], the transition between asynchronous and synchronous firing state is studied in a globally coupled stochastic Hodgkin-Huxley neural network and is found to be analogous to a second-order phase transition. In our models, the forcing is not periodic and, as we can see in the Fourier transform plots, the maximal value of the Fourier transform does present a clear peak as a function of the noise level (see Figure 6.7) only in the synaptic noise case, hence the system does exhibit a form of **coherence resonance** in this case. Besides this observation, the regularity of the oscillation can be expected to be relatively high for large networks in our three

frameworks, since the mean activity is asymptotically perfectly periodic.

7.2.4 The Kuramoto model

We can also compare our findings with the Kuramoto model that we introduced in section 3.1. In fact the mean field approach we have presented in chapter 4 applies also to some simple formulations of the Kuramoto models. We can for example consider *neural oscillators*, whose phase θ^i obey the following network equations:

$$d\theta^i(t) = dB^i(t) - \Big[\sum_{j=1}^{N} \frac{K}{N} \sin(\theta^i(t) - \theta^j(t))\Big]dt \tag{7.1}$$

By using a coupling argument, we can show, provided that the $B^i(t)$ are independent Brownian motions, that when $N \to +\infty$, the network is described by the following mean field equation:

$$d\bar{\theta}(t) = dB(t) - K\mathbb{E}_\Gamma[\sin(\bar{\theta}(t) - \Gamma(t))]dt \tag{7.2}$$

where $\Gamma(t)$ is a process independent of $\bar{\theta}(t)$ that has the same law.

One of the main question concerning Kuramoto models is to find regions of parameters (most importantly the coupling constant K) where the neurons will **synchronize** and oscillate in phase. This is usually the case when K is strong enough. However we must emphasize that the synchronization observed in Kuramoto models is rather different from ours since in the case we have studied, neurons in the network may synchronize to produce an oscillatory coherent behavior without the assumption that they are all already on a limit cycle described by a phase variable θ^i. Furthermore, in contrast to many models studying the synchronization of oscillators (see [Ermentrout et al., 2008] for references), in our models the neurons synchronize without requiring that their noisy inputs be correlated.

7.2.5 Specificity of our approach

The type of phenomena we observed is fundamentally related to the randomness we introduced, and will not be observed in particular in the mean field equations of the Markovian approach developed by [Buice and Cowan, 2007, Bressfloff, 2009]. Indeed, apart from the difference inherent to the fact that they consider Markov chains governing the firing of individual neurons as their microscopic model, the randomness and the correlations in the activity is vanishing in the limit $N \to \infty$ yielding the *deterministic* Wilson and Cowan equation.

Another important result of ours is the ability to define classes of parameter ranges attached to a few generic bifurcation diagrams (see the Appendix A.2 and C.1) as functions of the input to a population. This property suggests further some **reverse-engineering** studies allowing to infer from measurements of the system's responses to different stimuli the level of noise it is submitted to.

We eventually emphasize the fact that the noise-induced transitions presented here are related to the nature of the mean-field equations, which is **not a standard stochastic differential equation**. Such phenomena do not generally occur in usual stochastic differential equations with a purely additive noise, as for instance shown in [Horsthemke and Lefever, 1984] (see the Appendix D.3 where we explain that under the approach of Horsthemke and Lefever no transition occur in the additive noise case as there is no change in the extrema of the stationary probability distribution obtained by the Fokker-Planck equation).

Chapter 8

Perspectives

8.1 Mathematical perspectives

Many extensions to the microscopic models we have presented are possible. However as they yield equations all the more involved that the underlying model is sophisticated, it seems rather difficult to reach a mathematical understanding of the solutions, and especially of their dependence on the noise parameter. In this thesis, as we were mainly interested in the *consequences of our work in the fields of neuroscience and cognitive science*, we decided to limit ourselves to models that remained at least partially **mathematically tractable**. The main idea was to show that the solutions were **Gaussian** so we could reduce the mean field dynamics to systems of coupled equations on the mean and covariance.

The first possibility would be to include nonlinear intrinsic dynamics and different ionic populations. For instance mean field equations can also be derived for **spiking neurons**, using the Hodgkin-Huxley model or its simplified version the Fizhugh-Nagumo model. This is what is done in this paper [Baladron et al., 2011], where the authors introduce also a distinction between electrical and chemical synapses and random conductances. We note that we have already presented in chapter 6 a proof close to this general setting since we did not make the assumption of linear intrinsic dynamics. The only necessary assumption on the intrinsic dynamics is that it is given by a Lipschitz function. Concerning the Hodgkin-Huxley model, this is the case and the state variable is of dimension 4. However it is much more complex to study mathematically the behavior of the solutions of the resulting mean field equations since the solutions are not Gaussian. In [Baladron et al., 2011] the authors present simulations indicating that the mean field equations are a good representation of the mean activity of a finite size network, however this requires simulations with elaborated numerical schemes on GPUs.

In two forthcoming papers [Touboul, 2011b, Touboul, 2011a], Jonathan Touboul has also derived and studied mean field equations taking into account the spatial extension of the cortex and the delays resulting from the propagation of neural information. This results in **stochastic neural fields**

equations with delays. They are complex stochastic integro-differential equations. The core idea of the proof to establish a propagation of chaos is the same (to use a coupling argument) but the technical details are more involved than what we presented in this thesis. Furthermore, except in the case of linear intrinsic dynamics, these equations seem very difficult to understand and simulate.

Eventually one last improvement would be to include **learning** in these neural fields equations. Learning is usually modeled in computational neuroscience by laws governing the evolution of the values of synaptic weights, the most famous being Hebb's law. In our chapter 6, we have introduced dynamically evolving synaptic weights. However a new mathematical framework would be necessary to include learning as learning involves a different time scale (i.e. it is much slower than the evolution of the membrane potential). It would then be necessary to develop a mean field theory with time scale separation.

Other refinements to our reference model would consist in introducing colored noise (i.e. correlated noise) and consider a network that is not globally coupled. However, as we have already explained, we consider, *for now*, that the majority of these extensions pertain rather to the mathematical field than to neuroscience. Indeed new and exciting equations can be derived exhibiting likely very rich dynamics. General approaches to study them consist either in studying their properties as random processes, or in describing their probability distribution. In the first case, one is led to investigate an implicit equation in the space of stochastic processes, and in the second case, one is led to study a complex non-local partial differential equation (through Fokker-Planck), as done in a recent paper by Careers and collaborators [Caceres et al., 2011]. But in both cases one faces a difficult challenge, and the **dependency of the solutions with respect to parameters** is extremely hard to describe.

8.2 Implications in neuroscience

8.2.1 Propagation of chaos and correlations

Our propagation of chaos results have two implications. First, as we have already noted, in spite of the asymptotic independence, synchronization effects are possible between individual neurons of the same population *as they are governed asymptotically by the same law*. And the fact that neurons become

asymptotically independent (i.e uncorrelated) does not rule out the fact that they *fluctuate* about their mean value.

Second, one of the specificity of our mean field approach is that it states that any finite number of neurons whose initial conditions are independent **will remain independent**. This is of great importance for the understanding of the neural code, as independent neurons may encode more information than correlated neurons. A recent study published in Science [Ecker et al., 2010] has precisely found that neuronal firing in cortical microcircuits was almost decorrelated *in vivo*. This is in agreement with the propagation property. By contrast, though their influence on the mean vanishes for large N, correlations are present in the mean field model presented by Bressloff [Bressfloff, 2009] (see its equations 3.35 to 3.37).

However there are some limitations to the applicability of the propagation of chaos property. First it is true only for a finite number k of neurons (or at best $k = o(\sqrt{N})$) when N tends to $+\infty$. This property is only asymptotic and may not be checked when we consider small microcircuits. Second the propagation of chaos would not be verified for colored noise, e.g. if the Brownian motions in 4.1 were not assumed independent.

8.2.2 Noise-induced synchronized oscillations

In this last section we wish to emphasize qualitatively the functional relevance of noise-induced transitions. The question of the **functional role of noise in the brain** is indeed widely debated today since noise clearly affects neuronal information processing. A key point is that the presence of noise is not necessarily a problem for neurons: as an example, stochastic resonance helps neurons detecting and transmitting weak subthreshold signals. Furthermore neuronal networks that have evolved in the presence of noise are bound to be more robust and able to explore more states, which is an advantage for learning in a dynamic environment.

The fact that noise can trigger synchronized oscillations at the network level **enriches the possible mechanisms leading to rhythmic oscillations in the brain**, directly relating it to the functional role of noise. Rhythmic patterns are ubiquitous in the brain and take on different functional roles. Among those, we may cite visual feature integration [Singer and Gray, 1995], selective attention, working memory and even consciousness[1].

[1]Indeed some authors have proposed that regular synchronous oscillations in the gamma band may provide a "neural basis" for consciousness. See for example [Llinas, 1998].

Abnormal neural synchronization is present in various brain disorders [Uhlhaas and Singer, 2006]. This means that oscillations themselves can signal a pathological behavior. For instance, epileptic seizures are characterized by the appearance of sudden, collective, slow oscillations of large amplitude, corresponding at the cell level to a synchronization of neurons, and visible at a macroscopic scale through EEG/MEG recordings. This phenomenon is very close to what we observed in our model (as noise is slowly increased, the solutions of the mean field equations undergo a saddle-homoclinic bifurcation abruptly yielding large amplitude and small frequency oscillations). The collective phenomena we described thus resemble the onset of epileptic seizures, that could be triggered by a sudden increase of the noise parameter in epileptic brain areas.

The mean field models we have developed in this thesis, based on relatively simple descriptions of neural activity, are therefore able to account for **complex biologically relevant phenomena**, in a mathematically and computationally tractable way while including noise effects. This observation suggests to use these new models as cortical mass models and compare them to more established cortical column models such as Jansen and Rit's or Wendling and Chauvel's [Touboul et al., 2010, Wendling and Chauvel, 2008, Jansen and Rit., 1995]. Fitting the microscopic model to biological measurements would yield a new neural mass model for large scale areas and we could then study the appearance of stochastic seizures and rhythmic activity in relationship with different parameters of the model.

Though we cannot decide exactly what may be the functional role of the noise-induced oscillations we found, since such regular synchronous oscillations may be as well the signature of a healthy as of a pathological behavior, we underline that **we have integrated the presence of noise in a mathematically and biologically relevant manner.** All these findings point towards the idea that there must be a carefully controlled **optimal level of noise** in the brain.

Part IV

Appendix

Appendix A

A mean field equation with additive noise

A.1 Proof of lemma 4.2.3

In this appendix we prove lemma 4.2.3 stating that in the case where the sigmoidal transforms are of the form $S_\alpha(x) = \mathrm{erf}(g_\alpha x + \gamma_\alpha)$, the functions $f_\alpha(\mu_\alpha, v_\alpha)$ involved in the mean field equations (4.2) with a Gaussian initial condition take the simple form (4.9).

Proof. We have, using the definition of the erf function

$$\begin{aligned}\mathbb{E}\left[S_\alpha(X_\alpha)(t)\right] &= \int_{\mathbb{R}} \mathrm{erf}\left(g_\alpha\left(x\sqrt{v_\alpha(t)} + \mu_\alpha(t)\right) + \gamma_\alpha\right) \frac{e^{-x^2/2}}{\sqrt{2\pi}}\, dx \\ &= \int_{\mathbb{R}} \int_{-\infty}^{g_\alpha\left(x\sqrt{v_\alpha(t)}+\mu_\alpha(t)\right)+\gamma_\alpha} \frac{e^{-(x^2+y^2)/2}}{2\pi} dxdy\end{aligned}$$

This integral is of the form:

$$\int_{\mathbb{R}} \int_{-\infty}^{a\,x+b} \frac{e^{-(x^2+y^2)/2}}{2\pi} dxdy$$

and therefore, the integration domain has an affine shape as plotted in figure A.1. In order to compute this integral, we change variables by a rotation of

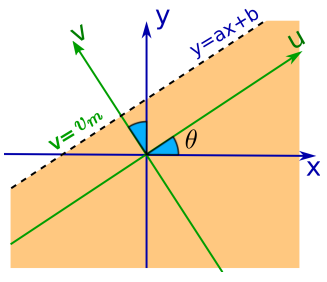

Figure A.1: Change of variable for the erf function.

the axes (x, y) and align the affine boundary of our integration domain with

our new variables (u, v) (see figure A.1). Simple geometric analysis shows that the rotation angle θ for this change of variable is such that $\tan(\theta) = a$. The new integration domain is in the new coordinates given by $v \leq v_m = b\cos(\theta) = \frac{b}{\sqrt{1+a^2}}$:

$$\int_{\mathbb{R}} \int_{-\infty}^{a\,x+b} \frac{e^{-(x^2+y^2)/2}}{2\pi} dxdy = \int_{\mathbb{R}} \int_{-\infty}^{\frac{g\,b}{\sqrt{1+g^2a^2}}} e^{-(u^2+v^2)/2} \frac{1}{2\pi} dudv$$
$$= \operatorname{erf}\left(\frac{gb}{\sqrt{1+g^2a^2}}\right)$$

which reads with the parameters of the model:

$$f_\alpha(\mu, v) = \operatorname{erf}\left(\frac{g_\alpha\,\mu + \gamma_\alpha}{\sqrt{1+g_\alpha^2 v}}\right)$$

□

A.2 Bifurcation Diagrams as a function of λ

In section 4.3, we observed that six different bifurcation diagrams appear as I_1 is varied, depending on the value of λ characterizing the additive noise input. For the particular choice of parameters of that section, the different zones are segmented for values of λ given in table A.1.

Type	C	BT	Hom TP	H TP	C
λ	0.16	2.934	2.948	2.968	3.74

Table A.1: Numerical values of the separation into six λ zones for Figure 4.2. C stands for Cusp, BT: Bogdanov-Takens, Hom TP: turning point of the Homoclinic bifurcations curve, H TP: Hopf bifurcation curve turning point.

In each of these zones, typical codimension 1 bifurcation diagrams as the input I_1 is varied are depicted in figure A.2. We now describe the behavior of the system in each of these zones.

(A) For very small values of λ, the system features four saddle-node bifurcations and one supercritical Hopf bifurcation, associated to the presence of stable limit cycles that disappear through saddle-homoclinic bifurcation arising from the Bogdanov-Takens bifurcation (after the turning point). In an extremely limited range of parameter, the occurrence of two saddle-node bifurcation relates to a bistable regime in that small parameter region.

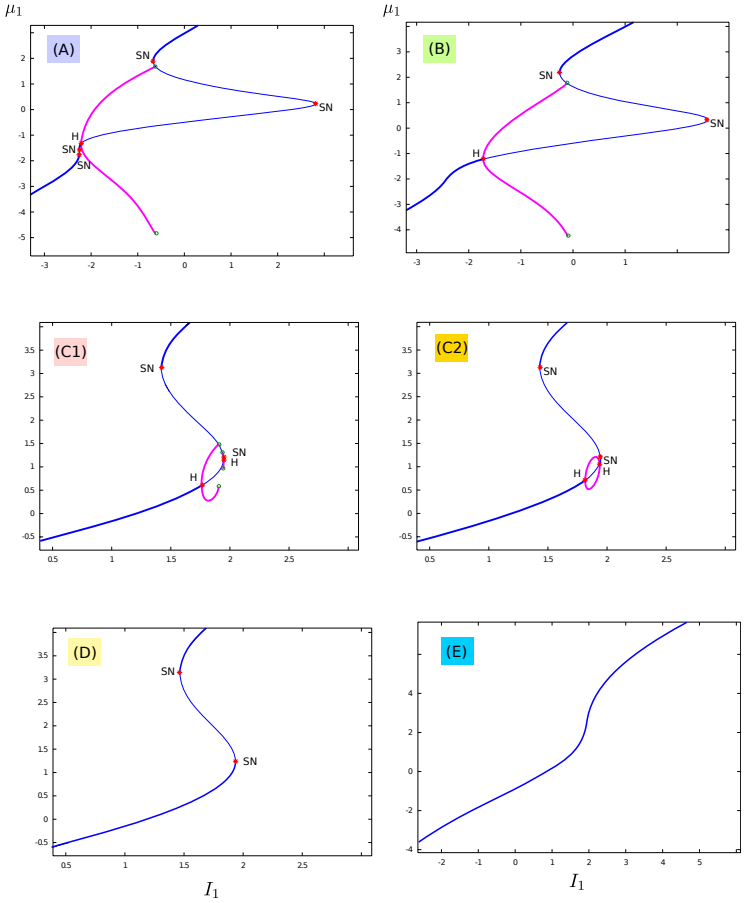

Figure A.2: Typical behavior of the system in each zone (A) through (E). (A): $\lambda = 0$, (B): $\lambda = 1$, (C1): $\lambda = 2.945$, (C2):$\lambda = 2.955$, (D): $\lambda = 3$, (E): $\lambda = 4$. Red stars: bifurcations, SN: Saddle-Node, H: Hopf, green circle: Saddle-Homoclinic bifurcation. Thick blue line: stable fixed point, thin blue line: unstable fixed point, thick pink line: stable cycle. See text for precise description.

(B) In zone (B), the system differs from zone (A) in that the two inferior saddle-node bifurcation disappeared through Cusp bifurcation. Globally the same behavior are observed, except for the bistable behavior commented above (which was not a prominent phenomenon due to the reduced parameter region concerned).

(C1) On the upper branch of saddle nodes, the systems undergoes a Bogdanov-Takens bifurcations, yielding the presence in zone (C1) of a supercritical Hopf bifurcation and of a saddle-homoclinic bifurcation curve. This BT bifurcation accounts for the family of Hopf bifurcations observed in zones (A-B) and for the saddle-homoclinic bifurcations, because of the turning points observed in the full bifurcation diagrams. In region (C1), two families of limit cycles coexist, both arising from supercritical Hopf bifurcation and disappearing through saddle-homoclinic bifurcation.

(C2) Because of the topology of the bifurcation diagram, the turning point of the saddle-homoclinic bifurcations curve occurs before the turning point of the Hopf bifurcations curve. This difference yields zone (C2) between the two turning points. In that zone, we still have two supercritical Hopf bifurcations, but no more homoclinic bifurcation. The families of limit cycles corresponding to each of the Hopf bifurcations are identical.

(D) After the turning point of the Hopf bifurcations manifold, we are left with two saddle-node bifurcations, hence a pure bistable behavior with no cycle.

(E) Both saddle-node bifurcation disappear by merging into a cusp bifurcation. After this cusp, the system has a trivial behavior, i.e. it features a single attractive equilibrium whatever I_1.

Appendix B

A mean field equation with inhomogeneity at the synaptic level

B.1 Reduction to a linear Volterra equation for small σ

We show here how to simplify the system 5.1.2 in the limit of low synaptic inhomogeneity σ. We will show that for small σ, the whole dynamics can be reduced to an integro-differential equation on the mean. We recall that the mean and covariance of the Gaussian process solution of the mean field equations verify the following differential and integral equations:

$\mu_\alpha(t)$ satisfies the differential equation:

$$\frac{d\mu_\alpha(t)}{dt} = -\frac{\mu_\alpha(t)}{\tau_\alpha} + \sum_{\beta=1}^{P} J_{\alpha\beta} m_\beta(t) + I_\alpha(t),$$

with

$$m_\beta(t) = \int_{\mathbb{R}} S_\beta\left(x\sqrt{C_\beta(t,t)} + \mu_\beta(t)\right) Dx.$$

The covariance $C_\alpha(t,s)$ obeys:

$$C_\alpha(t,s) = e^{-(t+s)/\tau_\alpha}\Big[C_\alpha(0,0) + \frac{\tau_\alpha\lambda_\alpha^2}{2}\left(e^{2(t\wedge s)/\tau_\alpha} - 1\right) + \sum_{\beta=1}^{P}\sigma_{\alpha\beta}^2\int_0^t\int_0^s e^{(u+v)/\tau_\alpha}\Delta_\beta(u,v)dudv\Big],$$

where Δ_β is given by

$$\Delta_\beta(u,v) = \int_{\mathbb{R}}\int_{\mathbb{R}} S_\beta\left(\frac{\sqrt{C_\beta(u,u)C_\beta(v,v) - C_\beta(u,v)^2}}{\sqrt{C_\beta(u,u)}}x + \frac{C_\beta(u,v)}{\sqrt{C_\beta(u,u)}}y + \mu_\beta(v)\right) S_\beta\left(y\sqrt{C_\beta(u,u)} + \mu_\beta(u)\right) Dx\, Dy.$$

In the sequel we set $\sigma_{\alpha,\beta} = \varepsilon \times \widehat{\sigma}_{\alpha,\beta}$, where ε is a scaling factor, and we take also into account a very small additive noise[1] of the same order $\lambda_\alpha = \varepsilon\widehat{\lambda}_\alpha$. We analyze the dynamical mean-field equations when ε is varying from $\varepsilon = 0$ to some positive value. Consider first the case $\varepsilon = 0$. Then $\sigma^2_{\alpha,\beta} = 0$ and the covariance reads:

$$C_\alpha(t,s) = e^{-(t+s)/\tau_\alpha} C_\alpha(0,0)$$

If we take $C_\alpha(0,0) = 0$, $C_\alpha(t,t) = 0$, we get:

$$m_\beta(t) = \int_{\mathbb{R}} S_\beta(\mu_\beta(t))\, Dx = S_\beta(\mu_\beta(t))$$

The mean-field equations reduce then to a set of differential equations on the mean $\mu_\alpha(t)$ of the Wilson-Cowan type.

$$\frac{d\mu_\alpha(t)}{dt} = -\frac{\mu_\alpha(t)}{\tau_\alpha} + \sum_{\beta=1}^{P} J_{\alpha\beta} S_\beta(\mu_\beta(t)) + I_\alpha(t)$$

B.1.1 Perturbation expansion about $\varepsilon = 0$

Here we set $C_\alpha(0,0) = 0$ and consider a very small additive noise of order ε. Concerning the covariance, we have:

$$C_\alpha(t,s) = e^{-(t+s)/\tau_\alpha}\varepsilon^2 \frac{\tau_\alpha \widehat{\lambda}^2_\alpha}{2}\left(e^{2(t\wedge s)/\tau_\alpha} - 1\right) + e^{-(t+s)/\tau_\alpha}\varepsilon^2 \sum_{\beta=1}^{P} \widehat{\sigma}^2_{\alpha,\beta} \int_0^t \int_0^s e^{(u+v)/\tau_\alpha} \Delta_\beta(u,v) du dv,$$

so we can pose:

$$C_\alpha(t,s) = \varepsilon^2 \times \widehat{C}_\alpha(t,s).$$

We write the function $\Delta_\beta(u,v)$ in the following form:

$$\Delta_\beta(u,v) = \int_{\mathbb{R}^2} S_\beta\Big(Ax + By + \mu_\beta(v)\Big) S_\beta\left(Cy + \mu_\beta(u)\right) Dx\, Dy. \tag{B.1}$$

with: $A = \frac{\sqrt{C_\beta(u,u)C_\beta(v,v) - C_\beta(u,v)^2}}{\sqrt{C_\beta(u,u)}}$

$B = \frac{C_\beta(u,v)}{\sqrt{C_\beta(u,u)}}$

[1] We can do all the computation with $\lambda_\alpha = 0$, but this would correspond to a degenerate case as the presence of this noise term is necessary to establish the mean field equations, even if it is arbitrary small.

$C = \sqrt{C_\beta(u,u)}$
Having introduced the parameter ε, we see that we have:

$$A = \frac{\sqrt{\varepsilon^4\widehat{C_\beta}(u,u)\widehat{C_\beta}(v,v) - \varepsilon^4\widehat{C_\beta}(u,v)^2}}{\sqrt{\varepsilon^2\widehat{C_\beta}(u,u)}} = \varepsilon\times\frac{\sqrt{\widehat{C_\beta}(u,u)\widehat{C_\beta}(v,v) - \widehat{C_\beta}(u,v)^2}}{\sqrt{\widehat{C_\beta}(u,u)}} = \varepsilon\times\widehat{A}.$$

Similarly we have $B = \varepsilon \times \widehat{B}$ and $C = \varepsilon \times \widehat{C}$ with $\widehat{B} = \frac{\widehat{C_\beta}(u,v)}{\sqrt{\widehat{C_\beta}(u,u)}}$ and $\widehat{C} = \sqrt{\widehat{C_\beta}(u,u)}$. Now we can *expand S_β in series at μ_β*. For $m_\beta(t)$, we have to expand[2] $S_\beta\left(Cx + \mu_\beta(t)\right)$.

$$S_\beta\left(Cx + \mu_\beta(t)\right) = \sum_{n=0}^{+\infty} \frac{S_\beta^{(n)}(\mu_\beta(t))}{n!} C^n x^n$$

where $S_\beta^{(n)}$ is the n-th derivative of S_β Hence:

$$m_\beta(t) = \int_{\mathbb{R}} S_\beta\left(x\sqrt{C_\beta(t,t)} + \mu_\beta(t)\right) Dx = \sum_{n=0}^{+\infty} \frac{S_\beta^{(n)}(\mu_\beta(t))}{n!} C^n \int_{\mathbb{R}} x^n Dx$$

But the moments of a gaussian are well-known: if we put $M_k = \int_{\mathbb{R}} x^k Dx$, we have:

$$M_{2k+1} = 0$$
$$M_{2k} = \frac{(2k)!}{2^k k!}$$

So

$$m_\beta(t) = \sum_{k=0}^{+\infty} \frac{S_\beta^{(2k)}(\mu_\beta(t))}{(2k)!} C^{2k} \frac{(2k)!}{2^k k!} = \sum_{k=0}^{+\infty} \frac{S_\beta^{(2k)}(\mu_\beta(t))}{2^k k!} C_\beta^k(t,t).$$

Eventually we get for the development in power of epsilon:

$$m_\beta(t) = \sum_{k=0}^{+\infty} \varepsilon^{2k} \frac{S_\beta^{(2k)}(\mu_\beta(t))}{2^k k!} \widehat{C}_\beta^k(t,t). \tag{B.2}$$

For $\Delta_\beta(u,v)$, we have to extend $S_\beta(Ax + By + \mu_\beta(v)) \times S_\beta(Cy + \mu_\beta(u))$

$$\Delta_\beta(u,v) = \sum_{n=0}^{+\infty}\sum_{m=0}^{+\infty} \frac{S_\beta^{(n)}(\mu_\beta(v)) S_\beta^{(m)}(\mu_\beta(u))}{n!m!} \int_{\mathbb{R}}\int_{\mathbb{R}} (Ax + By)^n (Cy)^m DxDy$$

$$= \sum_{n=0}^{+\infty}\sum_{m=0}^{+\infty} \frac{S_\beta^{(n)}(\mu_\beta(v)) S_\beta^{(m)}(\mu_\beta(u))}{n!m!} \sum_{\substack{n_1, n_2 = 0 \\ n_1 + n_2 = n}}^{n} \frac{n!}{n_1! n_2!} A^{n_1} B^{n_2} C^m \int_{\mathbb{R}}\int_{\mathbb{R}} x^{n_1} y^{n_2+m} DxDy.$$

[2] the whole series is written formally, but we will care only on the first terms.

Since x, y are independent under $DxDy$ we obtain:

$$\Delta_\beta(u,v) = \sum_{n=0}^{+\infty}\sum_{m=0}^{+\infty} \frac{S_\beta^{(n)}(\mu_\beta(v))S_\beta^{(m)}(\mu_\beta(u))}{m!} \sum_{\substack{n_1,\, n_2 \,=\, 0 \\ n_1+n_2=n}}^{n} \frac{A^{n_1}B^{n_2}C^m}{n_1!n_2!} M_{n_1}M_{n_2+m}.$$

Therefore, in the series expansion of Δ, only terms such that $n_1 = 2k_1, k_1 \geq 0$, $n_2 + m = 2k_2, k_2 \geq \frac{m}{2}$ are non zero. Since $n_1 + n_2 = n$ in the sum above, one has $k_1 + k_2 = \frac{n+m}{2}$, requiring that n, m have the same parity. Denoting by $\sum_{n,m=0}^{+\infty,*} \equiv \sum_{n=0}^{+\infty}\sum_{m=0}^{+\infty}$, where n, m have the same parity, we finally obtain:

$$\Delta_\beta(u,v) = \sum_{n,m=0}^{+\infty,*} \frac{S_\beta^{(n)}(\mu_\beta(v))S_\beta^{(m)}(\mu_\beta(u))}{m!} C^m \sum_{\substack{k_1 \geq 0 \\ k_2 \geq \frac{m}{2} \\ k_1+k_2=\frac{n+m}{2}}}^{n} \frac{A^{2k_1}B^{2k_2-m}}{(2k_1)!(2k_2-m)!} M_{2k_1}M_{2k_2}.$$

Eventually we get for the development in power of epsilon:

$$\Delta_\beta(u,v) = \sum_{n,m=0}^{+\infty,*} \varepsilon^{n+m} \frac{S_\beta^{(n)}(\mu_\beta(v))S_\beta^{(m)}(\mu_\beta(u))}{m!} \widehat{C}^m \sum_{\substack{k_1 \geq 0 \\ k_2 \geq \frac{m}{2} \\ k_1+k_2=\frac{n+m}{2}}}^{n} \frac{\widehat{A}^{2k_1}\widehat{B}^{2k_2-m}}{(2k_1)!(2k_2-m)!} M_{2k_1}M_{2k_2}. \tag{B.3}$$

Let's now keep only the lowest order in ε. For $m_\beta(t)$ we get according to (B.2):

$$m_\beta(t) = S_\beta(\mu_\beta(t)) + \varepsilon^2 \frac{S_\beta^{(2)}(\mu_\beta(t))}{2} \widehat{C}_\beta(t,t) = S_\beta(\mu_\beta(t)) + \frac{S_\beta^{(2)}(\mu_\beta(t))}{2} C_\beta(t,t). \tag{B.4}$$

For $\Delta_\beta(u,v)$ we get according to (B.3) only the terms such that $n = m = 0$ and $n = m = 1$, the second condition implying $k_1 = 0$ and $k_2 = 1$. Hence at this order the equation is:

$$\Delta_\beta(u,v) = S_\beta(\mu_\beta(u))S_\beta(\mu_\beta(v)) + \varepsilon^2 S_\beta^{(1)}(\mu_\beta(u))S_\beta^{(1)}(\mu_\beta(v))\widehat{B}\widehat{C}M_2$$

Remembering the definition of $\widehat{B}$ and $\widehat{C}$, we have:

$$\Delta_\beta(u,v) = S_\beta(\mu_\beta(u))S_\beta(\mu_\beta(v)) + S_\beta^{(1)}(\mu_\beta(u))S_\beta^{(1)}(\mu_\beta(v))C_\beta(u,v).$$

We can now write an equation for the covariance:

$$C_\alpha(t,s) = e^{-(t+s)/\tau_\alpha}\frac{\tau_\alpha\lambda_\alpha^2}{2}\left(e^{2(t\wedge s)/\tau_\alpha}-1\right)+ e^{-(t+s)/\tau_\alpha}\sum_{\beta=1}^{P}\sigma_{\alpha,\beta}^2\int_0^t\int_0^s e^{(u+v)/\tau_\alpha}[S_\beta(\mu_\beta(u))S_\beta(\mu_\beta(v))+ S_\beta^{(1)}(\mu_\beta(u))S_\beta^{(1)}(\mu_\beta(v))C_\beta(u,v)]dudv \quad \text{(B.5)}$$

B.1.2 Reduction to an integro-differential equation on the mean

For σ small, we have hence reduced the integral equation giving the covariance to a **linear Volterra equation.** This will allow us to **reduce the whole dynamics to a unique integro-differential equation on the mean** μ. Let's consider for the sake of simplicity that we have only one population.

We can write the equation on $C(t,s)$ as follows:

$$C(t,s) = \sigma^2 f(t,s) + \sigma^2\int_0^t\int_0^s K(t,s,u,v)C(u,v)dudv$$

where:

$$f(t,s) = e^{-(t+s)/\tau}\frac{\tau\lambda^2}{2\sigma^2}\left(e^{2(t\wedge s)/\tau}-1\right)+e^{-(t+s)/\tau}\int_0^t\int_0^s e^{(u+v)/\tau}[S(\mu(u))S(\mu(v))]dudv$$

where $\frac{\lambda^2}{\sigma^2} = \frac{\varepsilon^2\widehat{\lambda}}{\varepsilon^2\widehat{\sigma}} = (\frac{\widehat{\lambda}}{\widehat{\sigma}})^2$ is of order 0 and gives the relative intensity of the two parameters, and the kernel K is given by:

$$K(t,s,u,v) = e^{((u+v)-(t+s))/\tau}S^{(1)}(\mu(u))S^{(1)}(\mu(v))$$

We consider the inhomogeneous integral Volterra equation of the second kind (with two state variables):

$$C(t,s) = \theta\int_0^t\int_0^s K(t,s,u,v)C(u,v)dudv + \theta f(t,s)$$

with $\theta = \sigma^2 = \varepsilon^2\hat{\sigma}^2$, an infinitely small of order 2.

We know (see [Tricomi, 1957]) that the Volterra integral equation of the second kind $\Phi(x) - \theta\int_0^x K(x,y)\Phi(y)dy = f(x)$ for $0 \leqq x \leqq h$ has one and essentially one solution in the class L_2 when the kernel $K(x,y)$ and the function $f(x)$ belong to the class L_2.

The solution is given by the formula $\Phi(x) = f(x) - \theta \int_0^x H(x,y;\theta) f(y) dy$ where $H(x,y;\theta)$, the *resolvent kernel*, is given by the series (converging almost everywhere) of iterated kernels:

$$-H(x,y;\theta) = \sum_{\nu=0}^{\infty} \theta^\nu K_{\nu+1}(x,y)$$

and the iterated kernels are defined by: $K_1(x,y) = K(x,y)$ and $K_{n+1}(x,y) = \int_0^x K(x,z) K_n(z,y) dz$ for $n \geqq 1$.

In our case, we can extrapolate the above formulas to functions of two variables:

$$C(t,s) = \theta f(t,s) - \theta^2 \int_0^t \int_0^s H(t,s,u,v;\theta) f(u,v) du dv$$

with $H(t,s,u,v;\theta) = -\sum_{\nu=0}^{\infty} \theta^\nu K_{\nu+1}(t,s,u,v)$, the iterated kernels being defined by:

$$K_1(t,s,u,v) = K(t,s,u,v)$$

and

$$K_{n+1}(t,s,u,v) = \int_0^t \int_0^s K(t,s,u',v') K_n(u',v',u,v) du' dv'$$

Hence if we consider only the lowest order, we have $C(t,s) = \theta f(t,s)$. The mean μ is therefore the solution of the following **integro-differential equation**:

$$\frac{d\mu}{dt} = -\frac{\mu}{\tau} + J\Big[S(\mu(t)) + \frac{S^{(2)}(\mu(t))}{2} C(t,t)\Big] =$$
$$= -\frac{\mu}{\tau} + JS(\mu(t)) + J\frac{S^{(2)}(\mu(t))}{2}\Big[\frac{\tau\lambda^2}{2\sigma^2}\left(1 - e^{-2t/\tau}\right) + \sigma^2 \int_0^t \int_0^t e^{\frac{(u+v)-2t}{\tau}} S(\mu(u)) S(\mu(v)) du dv\Big]$$

If λ is infinitely smaller than σ, we can study separately the influence of the parameter σ on the mean field dynamics by looking at the following equation:

$$\frac{d\mu}{dt} = -\frac{\mu}{\tau} + JS(\mu(t)) + \sigma^2 J \frac{S^{(2)}(\mu(t))}{2} \int_0^t \int_0^t e^{\frac{(u+v)-2t}{\tau}} S(\mu(u)) S(\mu(v)) du dv$$

The perturbative calculus that we have presented can of course be extended at **higher orders**. The first corrections to B.4 and B.5 are given below, without going into the details of the computation. Concerning the mean we have:

$$m_\beta(t) = S_\beta(\mu_\beta(t)) + \frac{S_\beta^{(2)}(\mu_\beta(t))}{2} C_\beta(t,t) + \frac{S_\beta^{(4)}(\mu_\beta(t))}{8} C_\beta^2(t,t).$$

And the equation for the covariance $C_\alpha(t,s)$ reads:

$$C_\alpha(t,s) = e^{-(t+s)/\tau_\alpha}\frac{\tau_\alpha\lambda_\alpha^2}{2}\left(e^{2(t\wedge s)/\tau_\alpha}-1\right)+$$
$$\sum_{\beta=1}^{P}\sigma_{\alpha,\beta}^2\int_0^t\int_0^s e^{(u-t+v-s)/\tau_\alpha}\Big[S_\beta(\mu_\beta(u))S_\beta(\mu_\beta(v))+S_\beta^{(1)}(\mu_\beta(u))S_\beta^{(1)}(\mu_\beta(v))C_\beta(u,v)+$$
$$\frac{S_\beta^{(2)}(\mu_\beta(u))S_\beta^{(2)}(\mu_\beta(v))}{2}\Big(C_\beta^2(u,v)+\frac{1}{2}C_\beta(u,u)C_\beta(v,v)\Big)\Big]dudv$$

This time it is not anymore a linear Volterra equation due to terms like $C_\beta(u,v)^2$.

Appendix C

A mean field equation with synaptic noise

C.1 Bifurcation Diagrams as a function of σ

In section 6.3, we observed that when $\lambda = 0$, varying σ yielded eleven different behaviors, each one therefore characteristic of the level of synaptic noise. For the particular choice of parameters chosen in that section, the different zones are segmented for values of σ given in table C.1.

In each of these zones, typical behaviors are depicted in the two following figures: figure C.1 and figure C.2. They show all the different codimension one bifurcation diagrams, obtained when varying the external input, corresponding to the eleven zones highlighted. We will now give a precise description of all these behaviors.

Type	BT	Hom TP	CP	G1	BT	GH	CP	G2	BT	CP
σ	2.464	2.545	2.908	7.482	9.111	~ 10.3	13.789	13.915	14.796	15.133

Table C.1: Numerical values of the separation into eleven σ zones for diagram 6.1. C stands for Cusp, BT: Bogdanov-Takens, Hom TP: turning point of the Homoclinic bifurcations curve,GH: generalized Hopf.

(A). In the **region (A)**, for $0 < \sigma < \sigma_{BT_1,}$, the system undergoes four saddle-node bifurcations and one Hopf bifurcation. There is a very small input interval where the system presents bistability. Indeed after the first saddle-node the equilibrium loses stability and regains stability at the second saddle-node until the Hopf. Hence in the input space, there is a small region where two stable equilibria coexist. Depending on the initial condition, the system will either converge to one or another fixed point. Away from this region, the system either converges to a stable fixed point or presents a stable cycle. This cycle appears through the Hopf bifurcation and disappears via a saddle-homoclinic bifurcation.

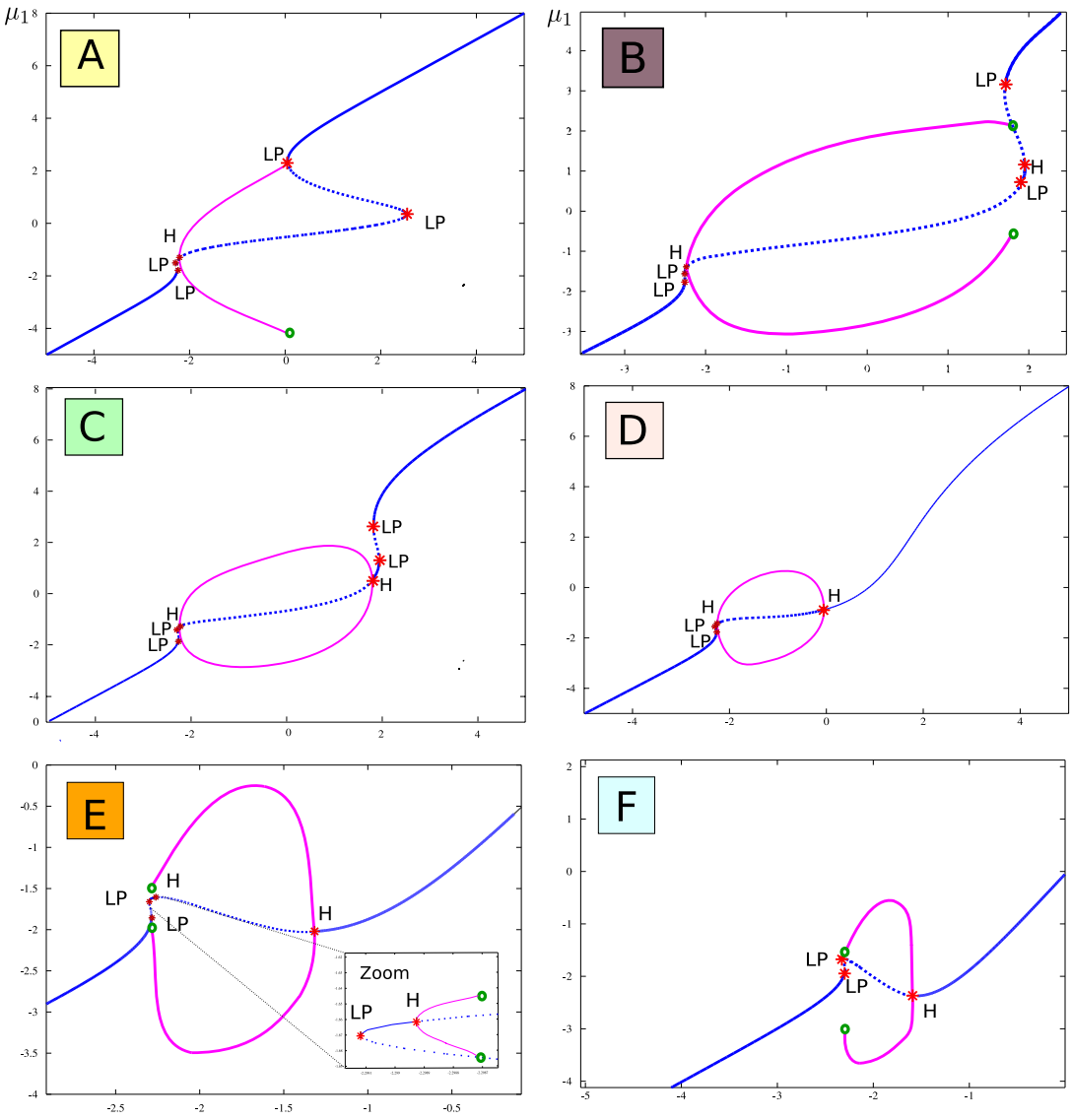

Figure C.1: Typical behavior of the system in each zone (A) through (F). (A): $\sigma = 0$, (B): $\sigma = 2.52$, (C): $\sigma = 2.7$, (D):$\sigma = 4.5$, (E): $\sigma = 8.6$, (F): $\sigma = 10$. LP stands for Limit Point bifurcation (also called fold or saddle-node bifurcation). H: Hopf bifurcation. Plain blue: stable equilibria. Dashed blue: unstable equilibria. Plain pink: stable cycles. Dashed pink: unstable. Green circles: homoclinic orbits. See text for precise description.

(B). In the **region (B)**, for $\sigma_{BT_1} < \sigma < \sigma_{Global_1}$, the system undergoes four saddle-node bifurcations and two Hopf bifurcations. There is one new Hopf bifurcation compared to region (A): this manifold of supercritical Hopf bifurcations appears through the Bogdanov-Takens bifurcation

BT_1. This Bogdanov-Takens bifurcation gives also birth to one curve of saddle-homoclinic bifurcations and zone (B) is then also characterized by the presence of two saddle-homoclinic bifurcations.

(C). In the **region (C)**, for $\sigma_{Global_1} < \sigma < \sigma_{CP_1}$, the system undergoes four saddle-node bifurcations and two Hopf bifurcations . The difference with the preceding case is the disappearance of the saddle-homoclinic bifurcation at the turning point of the homoclinic bifurcation curve. There are two small regions for the input I_1 where the system presents bistability. Otherwise the system either converges to a stable fixed point or presents a stable cycle, depending on the value of I_1.

(D). In the **region (D)**, for $\sigma_{CP_1} < \sigma < \sigma_{Global_2}$, the system undergoes two saddle-node bifurcations and two Hopf bifurcations . Compared to the preceding case, two saddle-node bifurcations vanished at the Cusp point CP_1. Once again, there is a very small input interval where the system presents bistability. Otherwise the system either converges to a stable fixed point or presents a stable cycle, depending on the value of I_1.

(E). In the **region (E)**, for $\sigma_{Global_2} < \sigma < \sigma_{BT_2}$, the system undergoes two saddle-node bifurcations and two Hopf bifurcations . Compared to the preceding case, a global codimension two bifurcation, that we may call saddle saddle-node homoclinic, leads to the appearance of two homoclinic orbits (one where the orbit joins a saddle point and the other where the orbit joins a saddle-node). There are two stable cycles, however they do not coexist for a given I_1 as can be seen on figure 6.1. The mechanism by which the stable cycle of region (D) gives birth to two stable cycles is illustrated in figure. Once again, there is a very small input interval where the system presents bistability. Otherwise the system either converges to a stable fixed point or presents a stable cycle, depending on the value of I_1.

(F). In the **region (F)**, for $\sigma_{BT_2} < \sigma < \sigma_{GH}$, the system undergoes two saddle-node bifurcations and one Hopf bifurcations. Compared to the preceding case, one Hopf bifurcation disappeared at the Bogdanov-Takens BT_2 bifurcation. There is no more bistability as the equilibrium loses stability at the first saddle-node and remains unstable at the second saddle-node to regain stability only at the Hopf bifurcation. Hence the system either converges to a stable fixed point or presents a stable cycle, depending on the value of I_1.

(G). In the **region (G)**, for $\sigma_{GH} < \sigma < \sigma_{CP_2}$, the system undergoes two saddle-node bifurcations and one Hopf bifurcation. Compared to the

preceding case, the supercritical Hopf bifurcation becomes subcritical at the generalized Hopf GH bifurcation. Hence the cycles emerging from this Hopf are unstable. They meet stable cycles to form a fold of limit cycles. The system does not present bistability. There is a small input interval where unstable cycles coexist with stable cycles but the system will either converge to a stable fixed point or present stable cycles.

(H). In the **region (H)**, for $\sigma_{CP_2} < \sigma < \sigma_{Global_3}$, the system undergoes four saddle-node bifurcations and one Hopf bifurcation. Compared to the preceding case, two saddle-node appear through the Cusp point CP_2 but the behavior of the system is the same as in region (G).

(I). In the **region (I)**, for $\sigma_{Global_3} < \sigma < \sigma_{BT_3}$, the system undergoes four saddle-node bifurcations and one Hopf bifurcation. Compared to the preceding case, the stable cycles disappear with the fold of limit cycles ++at the third global bifurcation point, that we may call saddle-fold. Hence only the unstable cycles remain. The system has either one stable fixed point or two stable fixed points. No more oscillations can be observed and input interval corresponding to bistability is larger than in the previous cases.

(J). In the **region (J)**, for $\sigma_{BT_3} < \sigma < \sigma_{CP_3}$, the system undergoes four saddle-node bifurcations. Compared to the preceding case, the Hopf bifurcation disappears at the Bogdanov-Takens BT_3. There is no more cycles, even unstable. The system presents the same behavior as in region (I).

(K). In the **region (K)**, for $\sigma_{CP_3} < \sigma$, the system undergoes two saddle-node bifurcations. Compared to the preceding case, two saddle-node bifurcation vanish at the cusp CP_3. The system presents the same behavior as in region (J): it either converges to a stable fixed point or presents bistability.

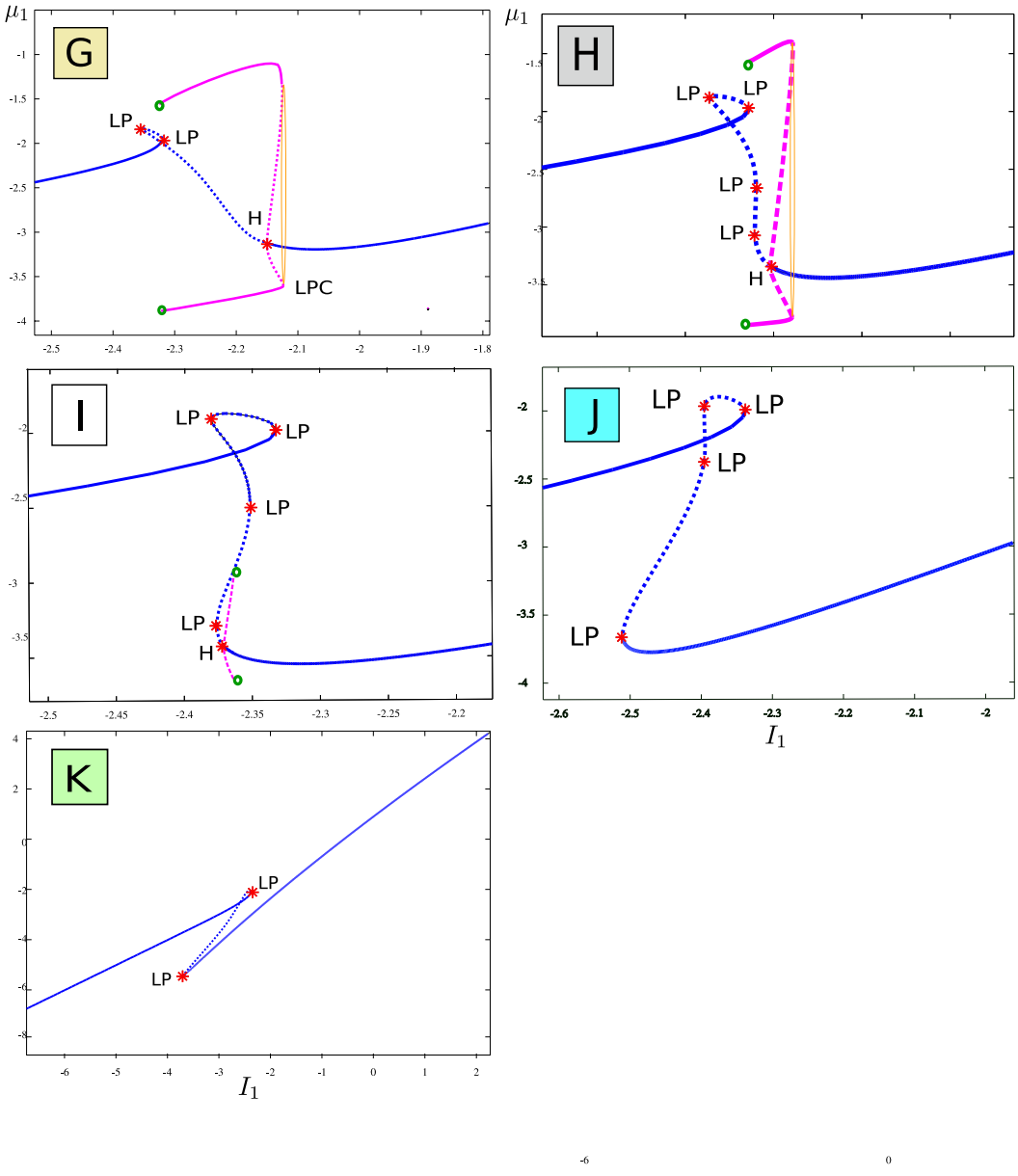

Figure C.2: Typical behavior of the system in each zone (G) through (K). (G): $\sigma = 11.3$, (H): $\sigma = 13.84$, (I): $\sigma = 14.2$, (J):$\sigma = 14.95$, (K): $\sigma = 20$. LP: Limit Point bifurcation (also called fold or saddle-node bifurcation). H: Hopf bifurcation. Plain blue: stable equilibria. Dashed blue: unstable equilibria. Plain pink: stable cycles. Dashed pink: unstable. Green circles: homoclinic orbits. Orange oval: fold of limit cycles.

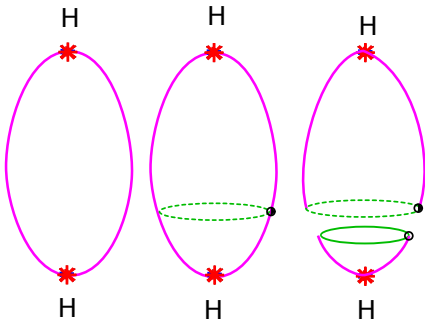

Figure C.3: The cycles at the transition from region (D) to region (E). Left image: there is a family of stable cycles delimited by two Hopf bifurcations in region (D). Center image: at the transition a saddle-node homoclinic orbit appears. Right image: One saddle-node homoclinic bifurcation and one saddle-homoclinic bifurcation have given birth to two families of stable cycles in region (E).

Appendix D

Introduction to stochastic bifurcations

In this thesis we have shown that noise at the microscopic level can induce global coherent phenomena at the system level. These transition phenomena present a fascinating subject of investigation since, contrary to all intuition, the environmental randomness induces a more structured behavior of the system. Our strategy in this thesis to unravel these kinds of transitions was first to derive mean field equations summing up the behavior of the system, and then to study the bifurcation diagrams as the noise parameter was varied, when the mean field dynamics could be reduced to ordinary differential equations.

In this chapter we will present several results concerning *stochastic bifurcations*[1]. First we will review the different definitions of **stochastic stability**, and show how noise can stabilize fixed points. This is based on the book [Mao, 2008] by Xuerong Mao. We will then study in details the effect of a **multiplicative noise on a pitchfork bifurcation**. We present two theorems that we have derived with Jonathan Touboul. Eventually we present the approach to noise-induced transition by Horsthemke and Lefever [Horsthemke and Lefever, 1984], based on the study of the **Fokker-Planck equation** related to the stochastic differential equation describing the system. We emphasize the crucial difference between **additive** and **multiplicative** noise.

D.1 Stochastic stabilization or destabilization

In this section we present, following Mao [Mao, 2008] the definitions of stochastic stability. We present a proof showing that noise can stabilize a system, for example a neural network.

[1] The formal definition of a random dynamical system can be found in [Arnold, 1998].

- *Stability of ordinary differential equations.* We study the d-dimentional ordinary differential equation on $t \geq t_0$:

$$x'(t) = f(x(t), t) \tag{D.1}$$

We assume that for every initial value $x(t_0) = x_0 \in R^d$, there exits a unique global solution which is denoted by $x(t; t_0, x_0)$. We assume furthermore that $f(0, t) = 0$ for all $t \geq t_0$. So the differential equation has the solution $x(t) = 0$ corresponding to the initial value $x(t_0) = 0$. This solution is called the trivial solution or **equilibrium** position.

The trivial solution is said to be **stable** if, for every $\varepsilon > 0$, there exits a $\delta = \delta(\varepsilon, t_0)$ such that $|x(t; t_0, x_0)| < \varepsilon$ for all $t > t_0$ whenever $|x_0| < \delta$. Otherwise, it is said to be unstable.

If there exits a positive-definite function $V(x, t) \in C^{2,1}(\mathbb{R}^d \times [t_0, \infty), R_+)$ such that $V_t(x(t), t) + V_x(x(t), t) * f(x(t), t) \leq 0$ for all $(x, t) \in \mathbb{R}^d \times [t_0, \infty)$, then the trivial solution of eq D.1 is stable.(A continuous function $V(x, t)$ is positive-definite if $V(x, t) > \mu(|x|)$ for μ a positive nondecreasing function such that $\mu(0) = 0$ and $\mu(r) > 0$ for $r > 0$). Such a V is called a *Lyapunov function.*

- *Stability in probability.* From now on we shall consider the stochastic differential equation on $t > t_0$ given by:

$$dx(t) = f(x(t), t)dt + g(x(t), t)dB(t) \tag{D.2}$$

The trivial solution is said to be **stochastically stable** or stable in probability if for every pair of $\varepsilon \in]0, 1[$ and $r > 0$, there exists a $\delta = \delta(\varepsilon, r, t_0) > 0$ such that, $P(|x(t; t_0, x_0)| < r \text{ for all } t \geq t_0) \geq 1 - \varepsilon$ whenever $|x_0| < \delta$. Otherwise, it is said to be stochastically unstable. The trivial solution is said to be **stochastically asymptotically stable** if it is stochastically stable and, moreover, for every $\varepsilon \in]0, 1[$, there exits a $\delta_0 = \delta_0(\varepsilon, t_0) > 0$ such that $P(\lim_{t \to +\infty} x(t; t_0, x_0) = 0) \geq 1 - \varepsilon$ whenever $|x_0| < \delta_0$.

- *A Lyapunov type theorem.* What conditions should a stochastic Lyapunov function satisfy?

Define L by:

$$LV(x,t) = V_t(x(t),t)+V_x(x(t),t)*f(x(t),t)+\frac{1}{2}tr(g^T(x,t)V_{xx}(x,t)g(x,t))$$

If there exits a positive-definite function $V(x,t) \in C^{2,1}(\mathbb{R}^d \times [t_0,\infty), R_+)$ such that $LV(x,t) \leq 0$ for all $(x,t) \in \mathbb{R}^d \times [t_0,\infty)$, then the trivial solution of equation D.2 is stochastically stable.

Proof. Itô formula gives:

$$dV(x(t)),t) = LV(x(t),t)dt + V_x(x(t),t)g(x(t),t)dB(t)$$

Let $\varepsilon \in]0,1[$ and $r > 0$ be arbitrary (without loss of generality we may assume that $r < h$.) By the continuity of $V(x,t)$ and the fact that $V(0,t_0) = 0$, we can find a $\delta = \delta(\varepsilon, r, t_0) > 0$ such that:

$$\frac{1}{\varepsilon} * \sup_{x \in S_\delta} V(x,t_0) \leq \mu(r)$$

where $S_h = \{x \in R^d; |x| < h\}$. It is easy to see that $\delta < r$. Now fix the initial value $x_0 \in S_\delta$ arbitrarily and write $x(t;t_0,x_0) = x(t)$ simply. Let τ be the first exit time of $x(t)$ from S_r, that is $\tau = \inf\{t \geq t_0 : x(t) \notin S_r\}$. For all $t \geq t_0$ $V(x(t \wedge \tau), t \wedge \tau) =$

$$V(x_0,t_0) + \underbrace{\int_{t_0}^{t\wedge\tau} LV(x(s),s)ds}_{\leq 0} + \underbrace{\int_{t_0}^{t\wedge\tau} V_x(x(s),s) * g(x(s),s)dB(s)}_{Expectation=0}$$

By taking the Expectation on both sides, we have $\mathbb{E}[V(x(t\wedge\tau), t\wedge\tau)] \leq V(x_0,t_0)$. If $\tau \leq t$ $|x(t\wedge\tau)| = |x(\tau)| = r$ Hence, since $V(x(t\wedge\tau), t\wedge\tau) = \mathbb{1}_{\tau\leq t} \times V(x(\tau),\tau) + \mathbb{1}_{\tau>t} \times V(x(t),t)$

$$\mathbb{E}[V(x(t\wedge\tau), t\wedge\tau)] \geq \mathbb{E}[1_{\tau\leq t} \times \underbrace{V(x(\tau),\tau)]}_{\geq\mu(|x(\tau)|)=\mu(r)} \geq \mu(r) \times P(\tau \leq t)$$

Hence, $V(x_0,t_0) \geq \mathbb{E}[V(x(t\wedge\tau), t\wedge\tau)] \geq$

$$\frac{1}{\varepsilon} \times \sup_{x\in S_\delta} V(x,t_0) \times P(\tau \leq t) \geq \frac{1}{\varepsilon} \times V(x_0,t_0) \times P(\tau \leq t)$$

We conclude that $P(\tau \leq t) \leq \varepsilon$ so $P(\tau < \infty) \leq \varepsilon$ which means: $P(|x(t)| < r \text{ for all } t \geq t_0) \geq 1 - \varepsilon$. □

- *Moment exponential stability.* The trivial solution of equation D.2 is said to be **pth moment exponentially stable** if there is a pair of positive constants λ and C such that $\mathbb{E}[|x(t;t_0,x_0)|^p] \leq C|x_0|^p e^{-\lambda(t-t_0)}$ on $t \geq t_0$ for all $x_0 \in R^d$. When p=2, it is usually said to be exponentially stable in mean square.

- *Almost sure exponential stability.* The trivial solution of equation D.2 is said to be almost surely exponentially stable if

$$\limsup_{t\to+\infty}\frac{1}{t}\log|x(t;t_0,x_0)|<0$$

a.s. for all $x_0\in R^d$. Almost all sample paths of the solution will tend to the equilibrium position x=0 exponentially fast.

Theorem D.1.1. *Assume that there exits a function* $V\in C^{2,1}(\mathbb{R}^d\times[t_0,\infty),R_+)$ *and constants* $p>0$, $c_1>0$, $c_2\in R$ *and* $c_3\geq 0$, *such that for all* $x\neq 0$ *and* $t\geq_0$

$$(i)c_1|x|^p\leq V(x,t)$$

$$(ii)LV(x,t)\leq c_2V(x,t)$$

$$(iii)|V_x(x,t)g(x,t)|^2\geq c_3V^2(x,t)$$

Then

$$\limsup_{t\to+\infty}\frac{1}{t}\log|x(t;t_0,x_0)|\leq-\frac{c_3-2c_2}{2p}$$

a.s.for all $x_0\in R^d$. *In particular, if* $c_3>2c_2$, *the trivial solution of equation D.2 is almost surely exponentially stable.*

Proof. We give here a sketch of the proof. First we apply Itô formula to get:

$$d\log V(x(t),t)=\frac{LV(x(t),t)}{V(x(t),t)}dt+\frac{V_x(x(t),t)g(x,t)}{V(x(t),t)}dB_t-\frac{1}{2}\frac{|V_x(x(t),t)g(x,t)|^2}{V(x(t),t)^2}dt$$

Then we use the *exponential martingale inequality* applied to:

$$M(t)=\int_{t_0}^{t}\frac{V_x(x(s),s)g(x(s),s)}{V(x(s),s)}dB_s=\int_{t_0}^{t}h(s)dB_s$$

which states that:

$$P(\sup_{0\leq t\leq T}[\int_0^t h(s)dB_s-\frac{\alpha}{2}\int_0^t|h(s)|^2ds]>\beta)\leq e^{-\alpha\beta}$$

And we conclude with Borel-Cantelli Lemma. □

- *Stochastic stabilization and destabilization.* It is not surprising that noise can destabilize a system but we will see in the following that **multiplicative noise** can also **stabilize** a system.

The general set up is the following. We consider the system:

$$y'(t) = f(y(t), t)$$

with f locally Lipschitz continuous such that for all $(x, t) \in R^d \times R_+$:

$$|f(x,t)| \leq K|x| \tag{D.3}$$

we use an m-dim Brownian motion such that:

$$dx(t) = f(x(t), t)dt + \sum_{i=1}^{m} G_i x(t) dB_i(t) \tag{D.4}$$

where G_i are all $d \times d$ matrices.

Theorem D.1.2. *Let D.3 hold. Assume that there are two constants $\lambda > 0$ and $\rho \geq 0$ such that $\sum_{i=1}^m |G_i x|^2 \leq \lambda |x|^2$ and $\sum_i^m |x^T G_i x|^2 \geq \rho |x|^4$ for all $x \in R^d$.*

Then:

$$\limsup_{t \to +\infty} \frac{1}{t} \log |x(t; t_0, x_0)| \leq -(\rho - K - \frac{\lambda}{2})$$

a.s. for all $x_0 \in R^d$. In particular, if $\rho > K + \frac{\lambda}{2}$, the trivial solution of equation D.4 is almost surely exponentially stable.

Proof. Take $V(x,t) = |x|^2$.

$$LV(x,t) = 2x^T f(x,t) + \sum_{i=1}^{m} |G_i x|^2 \leq (2K + \lambda)|x|^2$$

Since $g(x,t) = (G_1 x, ..., G_m x)$ we have the upperbound:

$$|V_x(x,t) g(x,t)|^2 = 4 \sum_{i=1}^{m} |x^T G_i x|^2 \geq 4\rho x^4$$

We apply Theorem D.1.1 to conclude. □

Therefore any nonlinear system satisfying D.3 can be stabilized by a (scalar) Brownian motion. It suffices to take $m = 1$ and $G_1 = \sigma_1 Id$. We have $\sum_{i=1}^m |G_i x|^2 = \sigma_1^2 |x|^2$ and $\sum_{i=1}^m |x^T G_i x|^2 = \sigma_1^2 |x|^4$. By Theorem D.1.2 we have:

$$\limsup_{t \to +\infty} \frac{1}{t} \log |x(t; t_0, x_0)| \leq -(\frac{1}{2}\sigma_1^2 - K)$$

.

We can stabilize the system by a **strong enough multiplicative perturbation**.

- We now consider an *application to neural networks*. We are interested in the equation:

$$dx(t) = [-Bx(t) + Ag(x(t))]dt + \sum_{i=1}^{m} \sigma_i x(t) dB_i(t) \tag{D.5}$$

where $B = diag(b_1, ..., b_d)$, A is a $d \times d$ matrix and $g(x) = (g_1(x_1)), ..., g_d(x_d))^T$ with g_i sigmoidal such that: $xg_i(x) \geq 0$ and $|g_i(x)| \leq 1 \wedge \beta_i$ where β_i is the slope of the sigmoid at 0.

Now let us see how we can stabilize this neural network. By taking $m = 1$ and $V(x) = |x|^2$, we see that if

$$2x^T[-Bx + Ag(x)] + \sigma_1^2|x|^2 \leq \mu|x|^2$$

$$\limsup_{t \to +\infty} \frac{1}{t} \log |x(t; t_0, x_0)| \leq -(\sigma_1^2 - \frac{\mu}{2})$$

(see D.1.1).

But we have $2x^T Ag(x) \leq 2|x|||A|||g(x)| \leq 2\beta||A|||x|^2$ where $\beta = \max_k \beta_k$. So $2x^T[-Bx + Ag(x)] \leq 2(\beta||A|| - b)|x|^2$ where $b = \min_k b_k$. Hence we can take $\mu = 2(\beta||A|| - b) + \sigma_1^2$ and the system is stable provided $\sigma_1^2 > 2(\beta||A|| - b)$.

D.2 Effect of multiplicative noise on a pitchfork bifurcation

In this section we deal with the stability of the fixed point 0 in the stochastic pitchfork normal form equation. The deterministic normal form of the pitchfork bifurcation reads:

$$\frac{\mathrm{d}x}{\mathrm{d}t} = \lambda x + \varepsilon x^3 \tag{D.6}$$

where λ is a real parameter and $\varepsilon = \pm 1$. The solution $x = 0$ is a stable fixed point for all $\lambda < 0$, and is unstable for $\lambda > 0$. If $\varepsilon = 1$ (supercritical pitchfork bifurcation), two stable equilibria $\pm\sqrt{\lambda}$ exist for $\lambda > 0$ and for $\varepsilon = 1$ the two unstable fixed $\pm\sqrt{-\lambda}$.

From now on, we consider $W = \left(W_t\right)_{t\geq 0}$ a standard Brownian motion defined on a complete probability space $(\Omega, \mathcal{F}, \mathbb{P})$ endowed with the natural filtration $\left(\mathcal{F}_t\right)_t$ of the Brownian motion W. We are interested here in the stability of the fixed point 0 for the stochastic pitchfork equation with **multiplicative noise**:

$$dX_t = (\lambda X_t + \varepsilon X_t^3)\, dt + \sigma X_t\, dW_t \tag{D.7}$$

with initial condition X_0 at $t = 0$, and where σ is a constant non-negative parameter. This equation clearly has a unique strong solution since the functions are locally Lipschitz-continuous (see e.g.[Karatzas and Shreve, 1998]).

The null process $X_t(\omega) = 0$ for all $t \geq 0$ for (almost) all $\omega \in \Omega$ constitutes a solution of the stochastic pitchfork equation. We are interested in the stochastic stability of this solution as a function of the parameters $(\lambda,\ \sigma)$.

We will address two notions of stability: the *almost sure exponential stability*, defined by the property $\text{limsup}_{t\to\infty} \frac{1}{t} \log|X(t)| < 0$ almost surely for any initial condition $X_0 \in \mathbb{R}$ and *almost surely exponential instability* defined by the property $\text{liminf}_{t\to\infty} \frac{1}{t} \log|X(t)| > 0$ almost surely for any initial condition $X_0 \in \mathbb{R}$ (see e.g. [Mao, 2008] and the preceding section D.1). This definition is quite strong.

We will also be interested in the weaker notion of (asymptotic) stability and instability *in probability* (a.k.a. stochastic stability), defined by the property that for all $\mu \in]0, 1[$ and $r > 0$ there exists δ depending on μ and r such that $\mathbb{P}\{|X_t| < r \quad \forall t \geq 0\} \geq 1 - \mu$ whenever $|X_0| < \mu$. Otherwise it is said to be unstable in probability. The solution 0 is stochastically (or in probability) *asymptotically* stable if it is stable and for every $\mu \in]0, 1[$ there exists δ_0 depending on μ such that $\mathbb{P}(\lim_{t\to\infty} X_t = 0) \geq 1 - \mu$ whenever $|X_0| < \delta_0$

In order to show the stability or instability of the origin in the stochastic system, we make use of the *stochastic Lyapunov theory*. We denote by $\mathcal{L}$ the differential operator associated with Itô's representation of the supercritical pitchfork bifurcation ($\varepsilon = -1$) acting on twice differentiable functions $V \in C^2(\mathbb{R}, \mathbb{R})$:

$$\mathcal{L}V(x) = (\lambda x - x^3)\, V'(x) + \frac{\sigma^2}{2} x^2 V''(x).$$

and we will make use of the Lyapunov function $V(x) = x^2$ which will simplify all the calculations.

Theorem D.2.1. *The solution* 0 *of the equation* (D.7) *is almost surely exponentially stable if* $\lambda < \frac{\sigma^2}{2}$. *If* $\lambda > \frac{\sigma^2}{2}$ *the solution is asymptotically unstable in probability.*

Proof. The proof of this theorem is based on the application of the stability theorem D.1.1 (Theorem 3.3 of [Mao, 2008]) using the aforementioned function $V : x \mapsto x^2$. The map V satisfies:

i. $V(x) = x^2$,

ii. $\mathcal{L}V\ (x) = (2\lambda + \sigma^2)x^2 - 2\,x^4 \leq (2\lambda + \sigma^2)V(x)$,

iii. $|V'(x)\sigma\ x|^2 = |2\sigma x^2|^2 = 4\sigma^2 V(x)$

Using the stochastic stability theorem D.1.1, we conclude that:

$$\limsup_{t\to\infty} \frac{1}{t} \log|X(t)| \leq -\frac{4\sigma^2 - 2(2\lambda + \sigma^2)}{4} = \lambda - \frac{\sigma^2}{2} \qquad \text{almost surely.}$$

By definition of the almost sure exponential stability, we conclude that the solution 0 is almost surely exponentially stable for any $\lambda < \frac{\sigma^2}{2}$.

Let us now assume that $\lambda > \frac{\sigma^2}{2}$. In that case, $\mathcal{L}V(x) = (2\lambda + \sigma^2)x^2 - x^4$ is positive definite and decrescent for all $|x| < \sqrt{2\lambda + \sigma^2}$. Therefore the positive function V satisfies the property that there exists a neighborhood of the origin where $\mathcal{L}V > 0$, which implies that the origin is asymptotically unstable in probability (by application of a corollary of e.g. [Mao, 2008, Theorem 2.2]). □

In the case of the subcritical stochastic pitchfork bifurcation, we show the following:

Theorem D.2.2. *The fixed point* 0 *of the subcritical stochastic pitchfork equation is almost surely exponentially unstable for* $\lambda > \frac{\sigma^2}{2}$, *asymptotically unstable in probability for* $\lambda > -\frac{\sigma^2}{2}$ *and asymptotically stable in probability if* $\lambda < -\frac{\sigma^2}{2}$.

Proof. We use here the same function $V(x) = x^2$ and $\mathcal{L}_s$ the differential operator associated with the subcritical pitchfork bifurcation ($\varepsilon = 1$). We have:

$$\mathcal{L}_s V(x) = (\lambda\, x + x^3)\, 2x + \sigma^2\, x^2 = (2\lambda + \sigma^2)\, x^2 + 2x^4 \geq (2\lambda + \sigma^2)V(x)$$

and $|V'(x)\sigma x|^2 = 4\sigma^2 V(x)^2$. Therefore by application of [Mao, 2008, Theorem 3.5], we have:

$$\liminf_{t\to\infty} \frac{1}{t} \log|X(t)| \geq \frac{2\,(2\lambda + \sigma^2) - 4\sigma^2}{4} = \lambda - \frac{\sigma^2}{2} \qquad \text{almost surely}$$

which proves the fact that 0 is almost surely exponentially unstable for $\lambda > \frac{\sigma^2}{2}$. Moreover, if $\lambda > -\frac{\sigma^2}{2}$, then we have $\mathcal{L}_s V \geq 0$ and positive-definite for all $x \in \mathbb{R}$ which implies that the origin is stochastically unstable.

Let us now assume that $\lambda < -\frac{\sigma^2}{2}$. In that case, for all $|x| \leq \sqrt{-(2\lambda + \sigma^2)}$, we have $\mathcal{L}_s V < 0$ and V decrescent which implies that the origin is asymptotically stable in probability (see e.g. [Mao, 2008, Theorem 2.2]). □

D.3 Noise-induced transitions in SDEs according to the study of Fokker-Planck equations

We present here the approach by Horsthemke and Lefever [Horsthemke and Lefever, 1984], based on **Fokker-Planck equations**.

We consider systems that can be modeled by a phenomenological equation of the type: $\frac{dX}{dt} = f_{\lambda_t}(x)$, where $\lambda_t = \lambda + \sigma\xi_t$, ξ_t being a white noise. If we suppose that $f_{\lambda_t} = h + \lambda_t g$ is linear in the external parameter, the system is described by the stochastic differential equation:

$$dX_t = [h(X_t) + \lambda g(X_t)]dt + \sigma g(X_t)dW_t = f_\lambda(X_t)dt + \sigma g(X_t)dW_t \qquad \text{(D.8)}$$

and the corresponding Fokker-Planck equation governing the evolution of the transition probability $p(y, t|x)$ is:

$$\partial_t p(y,t|x) = -\partial_y[f_\lambda(y)p(y,t|x)] + \frac{\sigma^2}{2}\partial_{yy}[g^2(y)p(y,t|x)]$$

Since the random fluctuations have been modeled by a stationary random process, we expect that for a sufficiently long time the system will also reach a stationary behavior defined by the stationary probability density $p_{stat}(x)$ solution of the stationary Fokker-Planck equation:

$$\partial_x J_{stat}(x) = 0,$$

where the probability current is given by $J_{stat} = f_\lambda(x)p_{stat}(x) - \frac{\sigma^2}{2}\partial_x[g^2(x)p_{stat}(x)]$. Note that the state of the system in the stationary regime does still fluctuate, but in a way such that X_t and $X_{t+\tau}$ have the same probability density.

The stationary solution is given by:

$$p_{stat}(x) = \frac{N}{g^2(x)} \exp\left[\frac{2}{\sigma^2}\int^x \frac{f_\lambda(u)}{g^2(u)}du\right]$$

In [Horsthemke and Lefever, 1984], the authors then develop an argument to explain why a study of noise-induced phenomena must focus on the *extrema of* $p_{stat}(x)$. As a consequence additive and multiplicative noise will not have the same effect.

In the case of **additive noise**, the influence of the environment random fluctuations does not depend on the state of the system. We can set $g(x) = c$ where c is a constant. The extrema of $p_{stat}(x)$ will coincide with the deterministic steady states. Indeed the highest maximum of

$$U(x) = \int^x \frac{f_\lambda(u)}{g^2(u)} du = \int^x \frac{f_\lambda(u)}{c^2} du$$

and hence of the stationary density:

$$p_{stat}(x) = \frac{N}{c^2} \exp\left[\frac{2}{\sigma^2} U(x)\right]$$

coincide for all σ with the position of the deepest deterministic potential well, which is given by the value of x minimizing:

$$V_\lambda(x) = -\int^x f_\lambda(u) du = \int^x [h(u) + \lambda g(u)] du$$

In the additive noise case, the potential is not qualitatively modified and no shift occurs in the most likely value of x. The additive noise term has only a disorganizing effect.

In the **multiplicative case** the picture is totally different. Indeed, as $U(x) \neq -\frac{1}{c^2} V_\lambda(x)$, the highest maximum of the probability density $p_{stat}(x)$ **does not necessarily coincide** with the deterministic steady state. For small values of σ the potential does not change qualitatively but the stability may change. However when σ is increased, the extrema of $p_{stat}(x)$ can be essentially different in number and position from the deterministic case. External multiplicative noise, by creating new potential wells, can therefore induce new transitions.

To conclude we emphasize the fact that, in this thesis, **we have found noise-induced transitions in the additive noise case**, in the equation 4.2.1. But this is due to the fact that our equation was precisely not an ordinary stochastic differential equation like the one in D.8. Indeed our mean field equation, even in the simplest case of a purely additive noise, is not an ordinary stochastic differential equation, as the right hand side depends on the law of the solution. This is why the study of their dynamics is so rich, but it is also what precludes a thorough analytical study in more complicated cases.

Bibliography

[Abbott and van Vreeswijk, 1993] Abbott, L. and van Vreeswijk, C. (1993). Asynchronous states in networks of pulse-coupled oscillators. *Physical Review E*, 48:1483–1490. 34

[Amari, 1972] Amari, S.-I. (1972). Characteristics of random nets of analog neuron-like elements. *Systems, Man and Cybernetics*, 2(5):643–657. 33

[Amari, 1977] Amari, S.-I. (1977). Dynamics of pattern formation in lateral inhibition type neural fields. *Biological Cybernetics*, 27:77–87. 33

[Amari et al., 1977] Amari, S.-I., Yoshida, K., and Kanatani, K.-I. (1977). A mathematical foundation for statistical neurodynamics. *SIAM Journal on Applied Mathematics*, 33(1):95–126. 38

[Amit and Brunel, 1997] Amit, D. and Brunel, N. (1997). Model of global spontaneous activity and local structured delay activity during delay periods in the cerebral cortex. *Cerebral Cortex*, 7:237–252. 34

[Arbib, 1964] Arbib, M. (1964). *Brains, Machines and Mathematics*. McGraw-Hill Book Company. 4

[Arnold, 1998] Arnold, L. (1998). *Random Dynamical Systems*. Springer. 58, 157

[Arous and Guionnet, 1995] Arous, G. B. and Guionnet, A. (1995). Large deviations for langevin spin glass dynamics. *Probability Theory and Related Fields*, 102(4):455–509. 37, 38, 80

[Arous and Guionnet, 1997] Arous, G. B. and Guionnet, A. (1997). Symmetric langevin spin glass dynamics. *The Annals of Probability*, 25(3):1367–1422. 80

[Azevedol et al., 2009] Azevedol, F., Carvalho, L., Grinberg, L., Farfel, J., Ferretti, R., Filho, R. L. W. J., Lent, R., and Herculano-Houzel, S. (2009). Equal numbers of neuronal and nonneuronal cells make the human brain an isometrically scaled-up primate brain. *The Journal of Comparative Neurology*, 513(5):532â–541. 12

[Baladron et al., 2011] Baladron, J., Fasoli, D., Faugeras, O., and Touboul, J. (2011). Mean field description of and propagation of chaos in recurrent multipopulation networks of hodgkin-huxley and fitzhugh-nagumo neurons. *Arxiv preprint*. 133

[Benayoun et al., 2010] Benayoun, M., Cowan, J., van Drongelen, W., and Wallace, E. (2010). Avalanches in a stochastic model of spiking neurons. *PLoS Computanional Biology*, 6(7). 34

[Bernard, 1966] Bernard, C. (1966). *Introduction à l'étude de la médecine expérimentale*. Ãditions Garnier-Flammarion. 15

[Bettus et al., 2008] Bettus, G., Wendling, F., Guye, M., Valton, L., Régis, J., Chauvel, P., and Bartolomei, F. (2008). Enhanced eeg functional connectivity in mesial temporal lobe epilepsy. *Epilepsy research*, 81:58–68. 129

[Bressfloff, 2009] Bressfloff, P. (2009). Stochastic neural field theory and the system-size expansion. *SIAM Journal on Applied Mathematics*, 70(5):1488–1521. 34, 39, 40, 131, 135

[Bressloff, 2010] Bressloff, P. (2010). Metastable states and quasicycles in a stochastic wilson–cowan model. *Physical Review E*, 82. 34

[Bressloff et al., 2002] Bressloff, P., Cowan, J., Golubitsky, M., Thomas, P., and Wiener, M. (2002). What geometric visual hallucinations tell us about the visual cortex. *Neural Computation*, 14:473–491. 33

[Brewer, 1978] Brewer, J. (1978). Kronecker products and matrix calculus in system theory. *IEEE Transactions on Circuits and Systems*. 60

[Brunel, 2000] Brunel, N. (2000). Dynamics of sparsely connected networks of excitatory and inhibitory spiking neurons. *Journal of Computational Neuroscience*, 8:183–208. 36, 128

[Brunel and Hakim, 1999] Brunel, N. and Hakim, V. (1999). Fast global oscillations in networks of integrate-and-fire neurons with low firing rates. *Neural Computation*, 11:1621–1671. 34, 45

[Buice and Cowan, 2007] Buice, M. and Cowan, J. (2007). Field-theoretic approach to fluctuation effects in neural networks. *Physical Review E*, 75. 34, 39, 40, 45, 131

[Buice and Cowan, 2009] Buice, M. and Cowan, J. (2009). Statistical mechanics of the neocortex. *Progress in Biophysics and Molecular Biology*, 99:53–86. 39, 40

[Buice et al., 2010] Buice, M., Cowan, J., and Chow, C. (2010). Systematic fluctuation expansion for neural network activity equations. *Neural computation*, 22:377–426. 39, 40

[Burton, 2005] Burton, T. (2005). *Volterra integral and differential equations*. Elsevier. 84, 91

[Caceres et al., 2011] Caceres, M., Carrillo, J. A., and Perthame, B. (2011). Analysis of nonlinear noisy integrate and fire neuron models: blow-up and steady states. *Journal of Mathematical Neuroscience*, 1. 134

[Cai et al., 2004] Cai, D., Tao, L., Shelley, M., and McLaughlin, D. (2004). An effective kinetic representation of fluctuation-driven neuronal networks with application to simple and complex cells in visual cortex. *Proceedings of the National Academy of Sciences of the USA*, 101:7757–7762. 34

[Cattiaux et al., 2008] Cattiaux, P., Guillin, A., and Malrieu, F. (2008). Probabilistic approach for granular media equations in the non-uniformly convex case. *Probability Theory and Related Fields*, 140:19–40. 49

[Cessac et al., 1994] Cessac, B., Doyon, B., Quoy, M., and Samuelides, M. (1994). Mean field equations, bifurcation map and route to chaos in discrete time neural networks. *Physica D*, 74:24–44. 39

[Coombes and Owen, 2005] Coombes, S. and Owen, M. (2005). Bumps, breathers, and waves in a neural network with spike frequency adaptation. *Physical Review Letters*, 94(14). 33

[Crisanti and Sompolinsky, 1987] Crisanti, A. and Sompolinsky, H. (1987). Dynamics of spin systems with randomly asymmetric bonds: Langevin dynamics and a spherical model. *Physical Review A*, 36:4922–4939. 37, 38

[Dayan and Abbott, 2001] Dayan, P. and Abbott, L. (2001). *Theoretical Neuroscience: Computational and Mathematical Modeling of Neural Systems*. MIT Press. 7, 14, 15, 46

[Deco et al., 2009] Deco, G., Rolls, E., and Romo, R. (2009). Stochastic dynamics as a principle of brain function. *Progress in Neurobiology*, 88:1–16. 18, 21

[Destexhe, 2008] Destexhe, A. (2008). Self-sustained asynchronous irregular states and up/down states in thalamic, cortical and thalamocortical networks of nonlinear integrate-and-fire neurons. *Journal of Computational Neuroscience*, 27:493–506. 34

[Destexhe and Paré, 1999] Destexhe, A. and Paré, A. (1999). Impact of network activity on the integrative properties of neocortical pyramidal neurons in vivo. *Journal of Neurophysiology*, 81:1531–1547. 16, 36

[Dhooge et al., 2003a] Dhooge, A., Govaerts, W., and Kuznetsov, Y. (2003a). Numerical continuation of fold bifurcations of limit cycles in matcont. In *Proceedings of the ICCS*, pages 701–710. 63, 110

[Dhooge et al., 2003b] Dhooge, A., Govaerts, W., and Kuznetsov, Y. A. (2003b). Matcont: A matlab package for numerical bifurcation analysis of odes. *ACM Transactions on Mathematica Software*, 29:141–164. 63, 110

[Dobrushin, 1970] Dobrushin, R. (1970). Prescribing a system of random variables by conditional distributions. *Theory of Probability and its Applications*, 15. 45, 49

[Ecker et al., 2010] Ecker, A., Berens, P., Keliris, G., Bethge, M., Logothetis, N., and Tolias, A. (2010). Decorrelated neuronal firing in cortical microcircuits. *Science*, 327:584–587. 135

[El-Boustani and Destexhe, 2009a] El-Boustani, S. and Destexhe, A. (2009a). Brain dynamics at multiple scales: can one reconcile the apparent low-dimensional chaos of macroscoic variables with the seemingly stochastic behavior of single neurons? *International Journal of Bifurcation and Chaos*. 17

[El-Boustani and Destexhe, 2009b] El-Boustani, S. and Destexhe, A. (2009b). A master equation formalism for macroscopic modeling of asynchronous irregular activity states. *Neural Computation*, 21:46–100. 34, 39

[Engel et al., 1999] Engel, A., Engel, A., Fries, P., Konig, P., Brecht, M., and Singer, W. (1999). Temporal binding, binocular rivalry and consciousness. *Consciousness and Cognition*, 8:128–151. 19

[Ermentrout, 1998] Ermentrout, G. (1998). Neural networks as spatio-temporal pattern-forming systems. *Reports on Progress in Physics*, 61:353–430. 33

[Ermentrout, 2002] Ermentrout, G. (2002). Simulating, analyzing, and animating dynamical systems: A guide to xppaut for researchers and students. *Society for Industrial Mathematics*. 63

[Ermentrout and Cowan, 1979] Ermentrout, G. and Cowan, J. (1979). A mathematical theory of visual hallucination patterns. *Biological Cybernetics*, 34:137–150. 33

[Ermentrout et al., 2008] Ermentrout, G., Galan, R., and Urban, N. (2008). Reliability, synchrony and noise. *Trends in Neuroscience*, 31(8):428–434. 15, 18, 19, 131

[Ermentrout and Terman, 2010] Ermentrout, G. and Terman, D. (2010). *Mathematical Foundations of Neuroscience*. Springer. 7

[Faisal et al., 2008] Faisal, A. A., Selen, L., and Wolpert, D. (2008). Noise in the nervous system. *Nature Review Neuroscience*, 9:292–303. 15, 17, 18, 47

[Fatt and Katz, 1952] Fatt, P. and Katz, B. (1952). Spontaneous subthreshold activity at motor nerve endings. *Journal of Physiology*, 117:109–128. 18, 97

[Faugeras et al., 2009] Faugeras, O., Touboul, J., and Cessac, B. (2009). A constructive mean field analysis of multi-population neural networks with random synaptic weights and stochastic inputs. *Frontiers in Computational Neuroscience*, 3. 77, 80

[Faure et al., 2000] Faure, P., Kaplan, D., and Korn, H. (2000). Synaptic efficacy and the transmission of complex firing patterns between neurons. *Journal of Neurophysiology*, 84:3010–3025. 16

[Fourcaud and Brunel, 2002] Fourcaud, N. and Brunel, N. (2002). Dynamics of the firing probability of noisy integrate-and-fire neurons. *Neural Computation*, 14:2057–2110. 36, 128

[Galán et al., 2006] Galán, R., Fourcaud-Trocmé, N., Ermentrout, G., and Urban, N. (2006). Correlation-induced synchronization of oscillations in olfactory bulb neurons. *Journal of Neuroscience*, 26:3646–3655. 19

[Gerstner and Kistler, 2002] Gerstner, W. and Kistler, W. (2002). *Spiking Neuron Models*. Cambridge University Press. 7, 15, 46

[Giacomin et al., 2011] Giacomin, G., Pakdaman, K., and Pellegrin, X. (2011). Global attractor and asymptotic dynamics in the kuramoto model for coupled noisy phase oscillators. *Arxiv preprint*. 35

[Goldwyn and Shea-Brown, 2011] Goldwyn, J. and Shea-Brown, E. (2011). The what and where of adding channel noise to the hodgkin-huxley equations. *ArXiv:1104.4823v1 [q-bio.NC], submitted*. 17

[Gourine et al., 2010] Gourine, A., Kasymov, V., Marina, N., Tang, F., Figueiredo, M., Lane, S., Teschemacher, A., Spyer, K., Deisseroth, K., and Kasparov, S. (2010). Astrocytes control breathing through ph-dependent release of atp. *Science*, 329(5991):571–575. 9

[Guckenheimer and Holmes, 1990] Guckenheimer, J. and Holmes, P. (1990). *Nonlinear Oscillations, Dynamical Systems and Bifurcations of Vector Fields*. Springer. 60

[Guionnet, 1997] Guionnet, A. (1997). Averaged and quenched propagation of chaos for spin glass dynamics. *Probability Theory and Related Fields*, 109:183–215. 38, 80

[Herrmann and Tugaut, 2010] Herrmann, S. and Tugaut, J. (2010). Non uniqueness of stationary measures for self-stabilizing diffusions. *Stochastic Processes and their Applications*, 120:1210–1246. 45

[Horsthemke and Lefever, 1984] Horsthemke, W. and Lefever, R. (1984). *Noise-induced Transitions*. Springer-Verlag. 132, 157, 165, 166

[Hubel and Wiesel, 1962] Hubel, D. and Wiesel, T. (1962). Receptive fields, binocular interaction and functional architecture in the cat's visual cortex. *Journal of Physiology*, 160:106–154. 12

[Jansen and Rit., 1995] Jansen, B. and Rit., V. (1995). Electroencephalogram and visual evoked potential generation in a mathematical model of coupled cortical columns. *Biological Cybernetics*, 73:357–366. 136

[Karatzas and Shreve, 1998] Karatzas, I. and Shreve, S. (1998). *Brownian Motion and Stochastic Calculus*. Springer. 163

[Krogh and Hertz, 1992] Krogh, A. and Hertz, J. (1992). Generalization in a linear perceptron in the presence of noise. *Journal of Physics A: Mathematical and Theoretical*, 25:1135–1147. 21

[Kuramoto and Nishikawa, 1987] Kuramoto, K. and Nishikawa, I. (1987). Statistical macrodynamics of large dynamical systems. case of a phase transition in oscillator communities. *Journal of Statistical Physics*, 49(3/4):569–605. 35

[Lindner et al., 2004] Lindner, B., Garcia-Ojalvo, J., Neiman, A., and Schimansky-Geier, L. (2004). Effects of noise in excitable systems. *Physics Report*, 392:321–424. 18, 130

[Llinas, 1998] Llinas, R. (1998). The neuronal basis for consciousness. *Philosophical Transactions of the Royal Society of London B*, 353:1841–1849. 135

[Longtin et al., 1991] Longtin, A., Bulsara, A., and Moss, F. (1991). Time-interval sequences in bistable systems and the noise-induced transmission of information by sensory neurons. *Physical Review Letters*, 67:656–659. 130

[Ly and Tranchina, 2007] Ly, C. and Tranchina, D. (2007). Critical analysis of dimension reduction by a moment closure method in a population density approach to neural network modeling. *Neural Computation*, 19:2032–2092. 34

[Mainen and Sejnowski, 1995] Mainen, Z. and Sejnowski, T. (1995). Reliability of spike timing in neocortical neurons. *Science*, 268:1503–1506. 19, 20

[Mao, 2008] Mao, X. (2008). *Stochastic Differential Equations and Applications*. Horwood publishing. 58, 65, 157, 163, 164, 165

[Maruyama, 1955] Maruyama, G. (1955). On the poisson distribution derived from independent random walks. *Natural Science Report Ochanomizu University*, 6(1):1–6. 65

[McKean, 1966] McKean, H. (1966). A class of markov processes associated with nonlinear parabolic equations. *Proceedings of the National Academy of Sciences of the USA*, 56(6):1907–1911. 45, 47

[Mischler et al., 2011] Mischler, S., Mouhot, C., and Wennberg, B. (2011). A new approach to quantitative chaos propagation estimates for drift, diffusion and jump processes. *Arxiv Preprint, arXiv:1101.4727*. 49

[Moynot and Samuelides, 2002] Moynot, O. and Samuelides, M. (2002). Large deviations and mean field theory for asymmetric random reccurent neural networks. *Probability Theory and Related Fields*, 123(1):41–75. 39

[Neudecker, 1969] Neudecker, H. (1969). Some theorems on matrix differentiation with special reference to kronecker matrix products. *Journal of the American Statistical Association*, 64:953–963. 60

[Ohira and Cowan, 1993] Ohira, T. and Cowan, J. (1993). Master-equation approach to stochastic neurodynamics. *Physical Review E*, 48:2259–2266. 34

[Pakdaman et al., 2001] Pakdaman, K., Tanabe, S., and Shimokawa, T. (2001). Coherence resonance and discharge time reliability in neurons and neuronal models. *Neural Networks*, 14:895–905. 19

[Penrose, 1989] Penrose, R. (1989). *The Emperor's New Mind: Concerning Computers, Minds and The Laws of Physics*. Oxford University Press. 16

[Petitot, 2008] Petitot, J. (2008). *Neurogéométrie de la vision*. Les Editions de l'Ecole Polytechnique. 4, 7

[Pham et al., 1998] Pham, J., Pakdaman, K., and Vibert, J. (1998). Noise-induced coherent oscilations in randomly connected neural networks. *Physical Review E*, 58(3):3610–3622. 128, 129, 130

[Rolls and Deco, 2010] Rolls, E. and Deco, G. (2010). *The Noisy Brain: Stochastic Dynamics as a Principle of Brain Function*. Oxford University Press. 34

[Rosenblum et al., 1996] Rosenblum, M., Pikovsky, A., and Kurths, J. (1996). Phase synchronization of chaotic oscillators. *Physical Review Letter*, 76:1804–1807. 19

[Singer and Gray, 1995] Singer, H. and Gray, C. (1995). Visual feature integration and the temporal correlation hypothesis. *Annual Review of Neuroscience*, 18:555–586. 135

[Softy and Koch, 1993] Softy, W. and Koch, C. (1993). The highly irregular firing of cortical cells is inconsistent with temporal integration of random epsps. *Journal of Neuroscience*, 13:334–350. 16

[Sompolinsky et al., 1988] Sompolinsky, H., Crisanti, A., and Sommers, H. (1988). Chaos in random neural networks. *Physical Review Letters*, 61(3):259–262. 37, 38, 45, 87, 92, 127

[Sulzer and Rayport, 2000] Sulzer, D. and Rayport, S. (2000). Dale's principle and glutamate corelease from ventral midbrain dopamine neurons. *Amino Acids*, 19(1):45–52. 10

[Sznitman, 1984a] Sznitman, A.-S. (1984a). Equations de type de boltzmann, spatialement homogènes. *Probability Theory and Related Fields*, 66:559–592. 45

[Sznitman, 1984b] Sznitman, A.-S. (1984b). Nonlinear reflecting diffusion process, and the propagation of chaos and fluctuations associated. *Journal of Functional Analysis*, 56:311–336. 37, 45

[Sznitman, 1986] Sznitman, A.-S. (1986). A propagation of chaos result for burgers' equation. *Probability Theory and Related Fields*, 71:581–613. 45

[Sznitman, 1989] Sznitman, A.-S. (1989). Topics in propagation of chaos. *Ecole d'Eté de Probabilités de Saint-Flour XIX*, pages 165–25. 45, 47, 49

[Tanaka, 1978] Tanaka, H. (1978). Probabilistic treatment of the boltzmann equation of maxwellian molecules. *Probability Theory and Related Fields*, 46:67–105. 45, 47

[Tanaka, 1983] Tanaka, H. (1983). Some probabilistic problems in the spatially homogeneous boltzmann equation. *Theory and Application of Random Fields*, pages 258–267. 47

[Tanaka, 1984] Tanaka, H. (1984). *Limit theorems for certain diffusion processes with interaction*, volume 32. North-Holland Mathematical Library. 45

[Thom, 2009] Thom, R. (2009). *Prédire n'est pas expliquer*. Flammarion. 4

[Touboul, 2011a] Touboul, J. (2011a). On the dynamics of mean field equations for stochastic neural fields with delays. *Arxiv:1108.2407, submitted*. 133

[Touboul, 2011b] Touboul, J. (2011b). The propagation of chaos in neural fields. *Arxiv:1108.2414, submitted*. 133

[Touboul and Ermentrout, 2011] Touboul, J. and Ermentrout, G. (2011). Finite-size and correlation-induced effects in mean field dynamics. *Journal of Computational Neuroscience*. 35, 40

[Touboul et al., 2011] Touboul, J., Hermann, G., and Faugeras, O. (2011). Noise-induced behaviors in neural mean-field dynamics. *accepted for publication in SIADS*. 43, 125

[Touboul et al., 2010] Touboul, J., Wendling, F., Chauvel, P., and Faugeras, O. (2010). Neural mass activity, bifurcations, and epilepsy. *submitted*. 64, 136

[Tricomi, 1957] Tricomi, F. (1957). *Integral Equations*. Interscience Publishers. 147

[Uhlhaas and Singer, 2006] Uhlhaas, P. and Singer, W. (2006). Neural synchrony in brain disorders: relevance for cognitive dysfunctions and pathophysiology. *Neuron*, 52:155–168. 136

[van Vreeswijk and Sompolinsky, 1996] van Vreeswijk, C. and Sompolinsky, H. (1996). Chaos in neuronal networks with balanced excitatory and inhibitory activity. *Science*, 274(5293):1724–1726. 35

[Varela et al., 1993] Varela, F., Thompson, E., and Rosch, E. (1993). *L'inscription corporelle de l'esprit, sciences cognitives et expérience humaine*. Seuil. 5

[Villani, 2001] Villani, C. (2001). Limite de champ moyen. Cours de DEA 2001-2002. 49

[Wainrib, 2010] Wainrib, G. (2010). *Randomness in neurons: a multiscale probabilistic analysis*. PhD thesis, Ecole doctorale de l'Ecole Polytechnique. 17

[Wendling and Chauvel, 2008] Wendling, F. and Chauvel, P. (2008). *Computational Neuroscience in Epilepsy*, chapter Transition to Ictal Activity in Temporal Lobe Epilepsy: Insights from Macroscopic Models. Stolesz and Staley Ed. 136

[White et al., 2000] White, J., Rubinstein, J., and Kay, A. (2000). Channel noise in neurons. *Trends in Neurosciences*, 23:131–137. 47

[Wiesenfeld and Moss, 1995] Wiesenfeld, K. and Moss, F. (1995). Stochastic resonance and the benefits of noise: from ice ages to crayfish and squids. *Nature*, 373:33–36. 19

[Wilson and Cowan, 1972] Wilson, H. and Cowan, J. (1972). Excitatory and inhibitory interactions in localized populations of model neurons. *Biophysical Journal*, 12:1–24. 33

[Wilson and Cowan, 1973] Wilson, H. and Cowan, J. (1973). A mathematical theory of the functional dynamics of cortical and thalamic nervous tissue. *Biological Cybernetics*, 13:55–80. 33

[Yarom and Hounsgaard, 2011] Yarom, Y. and Hounsgaard, J. (2011). Voltage fluctuations in neurons: signal or noise? *Physiological Review*, 91:917–929. 15, 18, 19

[Yu et al., 2003] Yu, Y., Liu, F., and Wang, W. (2003). Synchronized rythmic oscillations in a noisy neural network. *Journal of the Physical Society of Japan*, 72(12):3291–3296. 130